SYNTHESIS AND MOLECULAR EVALUATION OF 15-DEOXY-$\Delta^{12,14}$-PROSTAMIDE J_2 AS A NOVEL ANTI-SKIN CANCER AGENT

By

Daniel A. Ladin

August, 2017

Director of Dissertation: Dr. Rukiyah Van Dross

Department of Pharmacology and Toxicology, The Brody School of Medicine, East Carolina University

Skin cancers including non-melanoma skin cancer (NMSC) and melanoma are the most common form of cancer in the United States and thus represent a substantial burden to the health care system. Current chemotherapeutic treatments for skin cancer cause harmful side effects due to lack of tumor-cell selectivity. Our group previously found that the endocannabinoid, arachidonoyl-ethanolamide (AEA), induces apoptosis in tumor but not non-tumor cell lines through its metabolism to novel J-series prostaglandin-ethanolamides (prostamides). Therefore, the goal of this study was to synthesize the novel prostamide, 15-deoxy-$\Delta^{12,14}$-prostamide J_2 (15d-PMJ_2) and determine the molecular mechanism of its antineoplastic activity. To our knowledge, we are the first group to successfully synthesize and biologically characterize a J-series prostamide. 15d-PMJ_2 exhibited potent and selective apoptotic properties in both non-melanoma and melanoma skin cancers. Furthermore, 15d-PMJ_2 was a potent inducer of tumor cell apoptosis *in vivo*. Induction of endoplasmic reticulum (ER) stress was required for 15d-PMJ_2 –mediated

cancer cell death and was an important determinant of selective toxicity. This project also conducted a targeted structure-activity assessment of the electrophilic double bond, definitively showing this moiety as the molecular “warhead” necessary for the cytotoxic activity. Taken together, these data provide sound evidence that 15d-PMJ_2 may provide a clinical alternative for treatment of non-melanoma and melanoma skin cancer with less adverse effects.

SYNTHESIS AND MOLECULAR EVALUATION OF 15-DEOXY-$\Delta^{12,14}$-PROSTAMIDE J_2 AS A NOVEL ANTI-SKIN CANCER AGENT

A Dissertation

Presented To

The Faculty of the Department of Pharmacology and Toxicology

The Brody School of Medicine

East Carolina University

In Partial Fulfillment

Of the Requirements for the Degree of

Doctor of Philosophy in Pharmacology and Toxicology

By

Daniel A. Ladin

August, 2017

SYNTHESIS AND MOLECULAR EVALUATION OF 15-DEOXY-$\Delta^{12,14}$-PROSTAMIDE J_2 AS A NOVEL ANTI-SKIN CANCER AGENT

By

Daniel A Ladin

APPROVED BY:

DIRECTOR OF
DISSERTATION:_____

(Rukiyah Van Dross-Anderson, Ph.D.)

COMMITTEE MEMBER:_____

(Colin Burns, Ph.D.)

COMMITTEE MEMBER:_____

(Jacques Robidoux, Ph.D.)

COMMITTEE MEMBER:_____

(Li V. Yang, Ph.D.)

COMMITTEE MEMBER:_____

(Latoya Griffin, Ph.D.)

CHAIR OF THE DEPARTMENT
OF **(**Pharmacology and Toxicology):_____

(David Taylor Ph.D.)

DEAN OF THE
GRADUATE SCHOOL:_____

(Paul J. Gemperline Ph.D.)

DEDICATED

To

My Mother and Father

Your love and unwavering support have been essential for my success. You instilled within me the virtues of perseverance and commitment

AND

My Best Friend and Beautiful Fiancé Emily

Your love and devotion have been with me through every adventure, especially this one.

TABLE OF CONTENTS

LIST OF FIGURES

LIST OF SYMBOLS OR ABBREVIATIONS

2-APB	2-Aminoethoxydiphenyl borate
15d-PGJ_2	15-deoxy-$\Delta^{12,14}$-prostaglandin J_2
15d-PMJ_2	15-deoxy-$\Delta^{12,14}$-prostamide J_2
4-PBA	4-phenylbutrate
AA	Arachidonic acid
ACN	Acetonitrile
AEA	Arachidonoyl-ethanolamide (also known as anandamide)
ALM	Acral lentiginous melanoma
ANOVA	Analysis of Variance
ATF	Activated transcription factor
BAP31	B-cell receptor associated protein 31
BAX	B-cell-associated X protein
BCC	Basal cell carcinoma
Bcl-2	B-cell lymphoma 2
BiP/GRP78	Binding immunoglobulin protein/ 78kDa glucose-regulated protein
$CDCL_3$	Deuterated chloroform
CDIP1	Cell death inducer p53 target 1
C/EBP	CCAAT/Enhancer-binding protein
CHOP10	C/EBP homologous protein
CM-H_2DCFDA	Chloromethyl-2', 7' dichlorodihydrofluorescein diacetate
CNX	Calnexin
CRT	Calreticulin
CTLA4	Cytotoxic T-lymphocyte-associated protein 4
DAMP	Damage associated molecular patterns
DCM	Dichloromethane
DIC	Diisopropylcarbodiimide

DIEA	N,N-diisopropylethlyamine
DMBA	7, 12-Dimethylbenz(a)anthracene
DMF	Dimethylformamide
DMSO	Dimethyl sulfoxide
DP1	D-series prostanoid receptor type 1
DP2	D-series prostanoid receptor type 2
DR5	Death receptor 5
ECS	Endocannabinoid system
EDTA	Ethylenediaminetetraacetic acid
eIF2α	Eukaryotic initiation factor -2 alpha
ELISA	Enzyme-linked immunosorbant assay
EP	E-series prostaglandin receptor
ER	Endoplasmic reticulum
ERO1α	ER oxidoreductase 1 alpha
ERp44	Endoplasmic reticulum protein-44
ESI	Electrospray ionization
ETOH	Ethanol
FAAH	Fatty amide acid hydrolase
FBS	Fetal bovine serum
GADD	Growth arrest and DNA damage-inducible protein
GAPDH	Glyceraldehyde 3-phosphate dehydrogenase
GSH	Glutathione
HBTU	O-(benzotriazol-1-yl)-N,N,N’,N’,-tetramethyluronium hexafluoroborate
HDA	Heptadecanoic acid
HOBt	Hydroxybenzotriazole
HNE	4-Hydroxy-2-nonenal
^{1}H-NMR	Proton nuclear magnetic resonance
HPLC	High performance liquid chromatography

ICD	Immunogenic cell death
IHC	Immunohistochemistry
IP_3R	Inositol 1,4,5-triphosphate receptor
IRE1	Inositol requiring kinase-1
LC_{50}	Lethal concentration in 50% of cells
LC-MS	Liquid chromatography mass spectrometry
m/z	Mass to charge ratio
MAM	Mitochondrial-associated ER membrane
MAPK	Mitogen activated protein kinase
MCU	Mitochondrial calcium uniporter
mPTP	Mitochondrial permeability transition pore
MTS	(3-(4,5-dimethylthiazol-2-yl)-5-(3carboxymethoxyphenyl)-2-(4-Sulfophenyl)-2H-tetrazolium
NAC	N-acetyl cysteine
NAPE	N-arachidonyl-phosphatidylethanolamide
NAT	N-acyltransferase
NF-κB	Nuclear factor-kappa beta
NMSC	Non-melanoma skin cancer
NOX	NADPH-oxidase
PARP	Poly (ADP-ribose) polymerase
PBS	Phosphate buffered saline
PDI	Protein disulfide isomerase
PERK	Double-stranded RNA-activated protein kinase (PKR)-like endoplasmic Reticulum kinase
PG	Prostaglandin
PGA_2	Prostaglandin A_2
PGD_2	Prostaglandin D_2
PGDS	Prostaglandin D synthase

PGES	Prostaglandin E synthase
PGFS	Prostaglandin F synthase
PGJ_2	Prostaglandin J_2
PM	Prostamides
PMD_2	Prostamide D_2
PME_2	Prostamide E_2
$PMF_{2\alpha}$	Prostamide $F_{2\alpha}$
PMH_2	Prostamide H_2
PKA	Protein kinase A
PKC	Protein kinase C
PP1	Protein phosphatase 1
PPAR	Peroxisome proliferator-activated receptor
P-PERK	Phosphorylated PERK
ROS	Reactive oxygen species
RR	Ruthenium Red
RXR	Retinoic acid receptor
RyR	Ryanodine receptor
SCC	Squamous cell carcinoma
SERCA	Sarco/endoplasmic reticulum Ca^{2+}-ATPase
SEM	Standard error of the mean
Sig-1R	Sigma-1 receptor
SSM	Superficial spreading melanoma
TBTU	O-(benzotriazol-1-yl)-N,N,N’,N’,-tetramethyluronium tetrafluoroborate
TLR	Toll like receptors
TPA	12-O-Tetradecanoyl-phorbol-13-acetate
TRPV1	Transient potential vanilloid receptor 1
TUNEL	Terminal deoxynucleotidyl transferase dUDP nick-end labeling
UPR	Unfolded protein response

UV	Ultraviolet
VDAC	Voltage-dependent anion-selective channel
VEGF	Vascular endothelial growth factor
XBP-1	X box-binding protein 1

CHAPTER ONE: GENERAL INTRODUCTION

1.1 Cancer

Cancer is the second leading cause of death in the United States and is characterized by the uncontrolled proliferation of malignant cells [1]. These autonomously expanding cells invade nearby tissues, promote angiogenesis and migrate throughout the body (metastasis). The process of tumor formation is known as carcinogenesis and consists of three distinct phases. Initiation occurs when a carcinogen causes irreversible DNA alterations within oncogenes or tumor suppressor genes of a cell. Oncogenes encode proteins that promote cell proliferation, growth, and cell cycle progression while tumor suppressor genes typically regulate cell death and cell cycle arrest. The subsequent phase of carcinogenesis is known as promotion, which occurs when an initiated cell undergoes clonal expansion and is amplified into a benign tumor. Finally, progression is the last phase of carcinogenesis and results in autonomous and unregulated malignant cell growth. While cancerous cells can develop from any tissue type within the body, some cancers occur more frequently than others.

1.1.1 Non-Melanoma Skin Cancer

Non-melanoma skin cancer (NMSC) is the most frequently diagnosed cancer in the United States with over 5 million new lesions diagnosed annually [2]. The direct cost of NMSC treatment was estimated to be 4.8 billion dollars, representing a significant financial cost to the United States health care system [3]. Basal cell carcinoma (BCC) is the most common form of NMSC and arises from basal layer cells of the epidermis. The majority of BCCs occur due to exposure to natural and artificial sources of ultraviolet (UV) light and are commonly found on sun-exposed areas of

the body including the face, ears, neck, and the backs of the hands [4]. Squamous cell carcinoma (SCC) on the other hand, is the second most common form of NMSC, originating from squamous layer keratinocytes of the epidermis [4]. Like BCC, exposure to UV light is the most common cause of SCC, however, exposure to chemical carcinogens such as arsenic and polycyclic-aromatic hydrocarbons also contribute to SCC incidence. Other risk factors for developing these skin cancers include poor immune function or rare genetic defects (such as in xeroderma pigmentosum). Typical treatments for NMSC include surgical removal and topical therapy with 5-fluorouracil (5-FU) or imiquimod [5]. While the mortality rate for NMSC is low, the high recurrence rate and detrimental side effects associated with current topical treatments indicate the need for novel NMSC chemotherapeutic agents.

1.1.2 Melanoma Skin Cancer

Melanoma is the most aggressive and deadly form of skin cancer in the United States. It is estimated that more than 76,000 new cases of melanoma will be diagnosed and that over 10,000 of these individuals will succumb to the disease each year [6]. Like NMSC, UV radiation exposure is a primary risk factor for developing melanoma, and individuals with family history, poor immune function or xeroderma pigmentosum may also be at increased risk of developing this malignancy [7]. Unlike other forms of skin cancer, melanoma is especially dangerous due to its highly metastatic nature and resistance to chemotherapy. Melanoma is known to progress in three distinct stages: the radial stage in which melanoma cell proliferation occurs locally within the epidermis, the vertical stage in which melanoma cells invades the dermis layer, and the metastatic stage which occurs when melanoma cells disseminate into peripheral tissues. Treatment of melanoma skin cancer includes surgical excision followed by chemotherapy and radiation therapy. Melanoma is resistant to most chemotherapeutic agents, however, positive clinical outcomes have

been observed with immunotherapeutics and small molecule inhibitors of the MAPK pathway. Immunotherapeutic agents such as the checkpoint inhibitors block cytotoxic T-lymphocyte-associated protein 4 (CTLA4) thereby triggering immune-mediated tumor cell destruction. Several studies report that checkpoint inhibitors increase patient survival rates [8]. In addition, the mitogen activated protein kinase (MAPK) pathway is an important driver for melanoma proliferation and includes several important targets including BRAF and ERK [9]. Downstream signaling of the MAPK pathway has been demonstrated to be hyperactive in up to 90% of human melanoma cases [9]. Thus, treatments with BRAF inhibitors including vemurafenib and dabrafenib significantly decrease tumor growth and are currently being utilized clinically [9]. Recently, melanomas found to possess aberrant signaling of this MAPK pathway have been demonstrated to persistently express heightened levels of pro-survival endoplasmic reticulum stress activation [10;11]. This suggests that agents which propagate endoplasmic reticulum stress may provide a novel therapeutic approach to combating BRAF overexpressing melanoma skin cancer.

1.1.3 Mouse Models for Skin Cancer

Mouse tumor models have become a mainstay for preclinical cancer research due to their ability to produce predictable tumor growth while in specific models maintaining the tumor microenvironment. The most common model used to study NMSC development is the two-staged chemical carcinogenesis model. This model employs two carcinogens (e.g. DMBA and TPA) or one complete carcinogen (e.g. UVB-light) that have the ability to initiate and promote tumorigenesis. For NMSC, DMBA is topically applied as an initiator followed by subsequent repeated doses of TPA used as a promoter. The two-staged chemical carcinogenesis model is particularly useful for testing the preventative and therapeutic properties of antineoplastic. The drawbacks of this model is that tumors are of murine origin and tumor formation can take upwards

of six months. Distinct from NMSC, implantable or grafted tumor models are the most commonly used method to examine melanoma skin cancer. The two major subtypes of these models are the syngeneic (allograft model), in which tumor cell lines of host origin are subcutaneously injected into immune-competent animal and the xenograft model, where cells distinct from the implantation host are subcutaneously injected or grafted into immune-deficient mice [12]. Allograft models provide the advantage of evaluating the immunogenic effects of anti-cancer agents while xenograft models provide an opportunity to evaluate efficacy of anti-cancer agents on a patient-derived tumor [12]. The advantage of the classic B16F10 model include the rapid time period of tumor growth (1 to 2 weeks) and the ability to monitor immunogenic endpoints. In this dissertation, B16F10 melanoma cells will be subcutaneously inoculated into the flank region of C57BL/6 mice [12].

1.2 The Role of Prostaglandins in Cancer

Cyclooxygenase-2 (COX-2) is a 73 kDa protein which is overexpressed in many cancers including NMSC and melanoma [13-15]. COX-2 converts arachidonic acid, a long chain polyunsaturated fatty acid, to prostaglandin G_2 and then to prostaglandin H_2 (PGH_2) [16;17]. PGH_2 then serves as a substrate for a variety of prostaglandin isomerases including prostaglandin E synthase (PGES), prostaglandin F synthase (PGFS) and prostaglandin D synthase (PGDS) which metabolize PGH_2 to PGE_2, $PGF_{2\alpha}$, and PGD_2, respectively [18]. Non-enzymatic dehydration of prostaglandin D yields the pro-apoptotic J-series prostaglandins [19].

1.2.1 E-series Prostaglandins in Cancer

The upregulation of COX-2 in many types of epithelial tumors is accompanied by a high level of prostaglandin synthesis. Most notably, prostaglandin E_2 (PGE_2) has been shown to be

important for tumor development in many cell types including skin cancer, colorectal cancer and breast cancer [13;20]. PGE_2 elicits its activity by binding to four distinct G-protein coupled receptors referred to as EP_1, EP_2, EP_3, and EP_4 [21]. EP_1 receptor activation increases intracellular calcium and protein kinase C (PKC) activation while EP_2 and EP_4 signaling results in increased cyclic AMP and activation of protein kinase A (PKA) [21]. Downstream of the EP receptor, a variety of signal transduction proteins are stimulated that are associated with tumorigenesis including AKT (cell survival), VEGF receptor transactivation (angiogenesis), NF-κB/COX-2 (inflammation) and Cyclin D1 (cell proliferation) [20]. Thus, COX-2 mediated production of E-series prostaglandins is a key driver of tumor proliferation in COX-2 overexpressing cancers such as colorectal, NMSC, and melanoma.

1.2.2 D-series prostaglandins

Similar to other prostaglandin subtypes, the physiological effects of the D-series prostaglandins are mediated through cell surface receptors. DP1 receptors are G-s protein coupled receptors found mostly in epithelial cells and eosinophils while DP2 receptors are G-i protein coupled receptors found in eosinophils and Th2-type lymphocytes [22;23]. DP receptor activation modulates numerous immune responses including eosinophil activation and Th2 mediated cytokine production [24;25]. In cancer, some groups reported that DP1 and DP2 receptor upregulation is associated with tumor invasion and metastasis, while others showed that DP receptor signaling exerts a suppressive effect on tumor growth [26]. These discrepancies may be due to the fact that PGD_2 is non-enzymatically dehydrated to J-series prostaglandins including PGJ_2, Δ^{12}-PGJ_2, and 15-deoxy-$\Delta^{12,14}$-PGJ_2 [27;28]. Because it is currently not possible to block the conversion of D-series prostaglandins to J-series prostaglandins, the role of PGD_2-mediated DP receptor signaling on tumor development remains unclear [29].

1.2.3 The Cytotoxic Effects of J-series Prostaglandins

J-series prostaglandins such as prostaglandin J_2 (PGJ_2), Δ^{12}-prostaglandin J_2 and 15-deoxy-$\Delta^{12,14}$-prostaglandin J_2 (15d-PGJ_2) are naturally occurring derivatives of prostaglandin D_2 [27]. It has been reported by our group and numerous others that J-series prostaglandins are potent inducers of tumor cell apoptosis [30-33]. Additionally, some groups have reported that 15d-PGJ_2 markedly reduces tumor cell growth and causes tumor cell apoptosis *in vivo* [33;34]. Unlike other classes of eicosanoids, these chemically distinct lipids possess an electrophilic α,β-unsaturated carbonyl group on the cyclopentenone ring which can readily react by Michael addition with free sulfhydryls of cellular proteins [27;35;36]. This reactive cyclopentenone ring is suggested to cause tumor cell apoptosis and initiate a variety of biological effects including the generation of endoplasmic reticulum stress and oxidative stress [37;38]

1.2.4 Ethanolamide Conjugated Prostaglandins (Prostamides)

COX-2 has been implicated in metabolizing endogenous cannabinoids (endocannabinoids) to prostaglandins [39]. Specifically, arachidonyl ethanolamide (AEA), is converted to prostamide H_2 (PMH_2) by COX-2 and upon subsequent reaction with prostaglandin synthases, ethanolamide-conjugated prostaglandins (prostamides [PMs]) are produced (Figure 1.1) [40-42]. As such, COX-2 mediated metabolism of AEA leads to production of prostamide D_2 (PMD_2), prostamide E_2 (PME_2), and prostamide $F_{2\alpha}$ ($PMF_{2\alpha}$). Our laboratory demonstrated by mass spectral analysis that conversion of PMH_2 to PMD_2 by prostaglandin D synthase PGDS results in the formation of prostamide J_2, Δ^{12} prostamide J_2, and the terminal cytotoxic product, 15-deoxy- $\Delta^{12,14}$-prostamide J_2 (15d-PMJ_2) (Figure 1.1) [43]. Although structurally similar to arachidonic acid-derived prostaglandins, prostamides possess unique pharmacology and biological activity compared to their non-ethanolamide counterparts [44]. This is due to the fact that prostamides do not bind to

traditional prostaglandin receptors and many groups have suggested the existence of distinct prostamide receptors [44;45]. In most cases the biological activity of prostamides has yet to be elucidated, especially in tumor cells, where prostaglandin signaling has a major impact on tumor growth.

Figure 1.1: COX-2-mediated metabolism of arachidonoyl-ethanolamide to prostamides

Arachidonoyl-ethanolamide is converted to prostamide H_2 by COX-2 followed subsequent metabolism by prostaglandin F synthase (PGFS), prostaglandin D synthase (PGDS) and prostaglandin E synthase (PGES) to prostamide $F_{2\alpha}$, prostamide D_2, and prostamide E_2, respectively. Prostamide D_2 then undergoes spontaneous dehydration and isomerization to prostamide J_2, Δ^{12}-prostamide J_2 and 15-deoxy-$\Delta^{12,14}$-prostamide J_2.

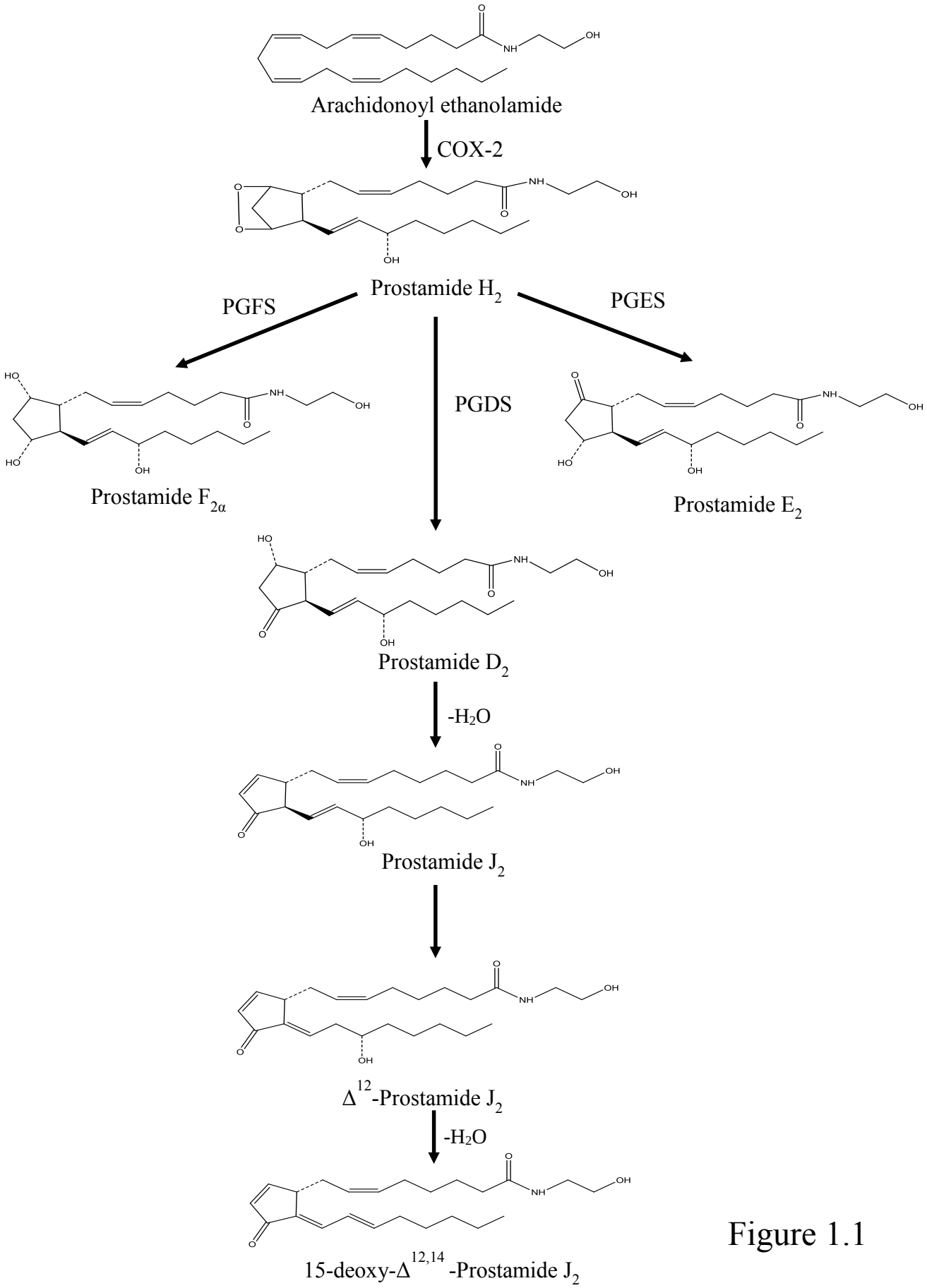
Arachidonoyl ethanolamide
COX-2
Prostamide H2
PGFS
PGES
PGDS
Prostamide F2α
Prostamide E2
Prostamide D2
-H2O
Prostamide J2
Δ12-Prostamide J2
-H2O
15-deoxy-Δ12,14-Prostamide J2

Figure 1.1

1.3 Endoplasmic Reticulum Stress

Endoplasmic reticulum (ER)-stress occurs when normal protein folding efficiency is compromised, causing a buildup of unfolded proteins and eliciting what is known as the unfolded protein response (UPR) [46;47]. Eukaryotic cells are equipped with specific stress response pathways, designed to recognize the accumulation of misfolded or unfolded proteins in order to restore homeostasis. The presence of unfolded proteins in the ER increases the recruitment of protein folding chaperones, including HSP70/GRP78 (BiP) to the nascent, unfolded peptides. Sequestration of BiP results in the liberation of the three ER-localized UPR sensors, PERK, ATF6, and IRE1 to propagate their signals [48]. Homodimerization and auto-phosphorylation of RNA-dependent protein kinase (PKR)-like ER kinase (PERK) attenuates general protein synthesis. PERK mediated phosphorylation of the eukaryotic translation initiation factor, eiF2α, results in selective translation of activated transcription factor 4 (ATF4) [47]. On the other hand, dissociation of BiP from activated transcription factor 6 (ATF6) leads to its translocation to the Golgi-apparatus where it is cleaved to its active form [49]. In the third arm of the ER-stress pathway, IRE1 is activated by autophosphorylation and homodimerization, and then catalyzes the splicing of X-box binding protein 1 (XBP1) mRNA. The XBP-1 protein product then binds to promoters of several genes involved in restoring protein homeostasis [48]. Two known ER-stress inducing agents are thapsigargin and tunicamycin which exert their effects by inhibiting Ca^{2+} channels and blocking N-linked glycosylation, respectively.

Depending on intensity and duration of the ER-stress signal, tumor cells can undergo either pro-survival or pro-apoptotic signaling. In the survival pathway, IRE1, ATF4 and ATF6 induce expression of proteins involved in peptide folding, anti-oxidant responses and protein degradation with the goal of resolving the stockpile of unfolded proteins [49]. Upon activation of the death

pathway, these sensors upregulate the expression of transcriptional factor C/EBP homologous protein (CHOP10)/growth arrest and DNA damage inducible 153 (GADD153), thereby triggering apoptosis through direct inhibition of Bcl-2 transcription, activation of death receptors (DR5) and induction of endoplasmic reticulum oxioreductase-1 (ERO1α) [46-49]).

1.3.1 The Role of CDIP1 in ER-stress

Cell death inducer p53 target 1 (CDIP1) is a 21 kDa protein which is found to be upregulated during DNA damage and acts as a p53-mediated apoptotic initiator. Moreover, CDIP1 was recently found to be a key regulator of ER-stress mediated apoptosis, with knockdown of CDIP1 preventing ER-stress-apoptosis mediated by tunicamycin and thapsigargin *in vitro* and *in vivo* [50]. During ER-stress, CDIP1 translocates to the ER and complexes with B-cell receptor associated protein 31 (BAP31) resulting in the formation of a CDIP1-BAP31 complex [50]. This CDIP1-BAP31 complex triggers the cleavage of BAP31 by caspase-8 into the p20-BAP31 fragment, possesses pro-apoptotic function. The complexation of CDIP1 and BAP31 causes oligomerization of BAX proteins, a member of the BH3 protein group which migrate to the ER and mitochondrial membranes. These BAX proteins then undergo conformational changes, resulting in the formation of homodimeric clusters and the formation of oligomeric pores leading to release of apoptotic factors including cytochrome c [51]. The complexation between CDIP1 and BAP31 was found to be required for BAX oligomerization and genetic knockdown of CDIP completely abrogated this effect [50]. Collectively, these findings suggest that CDIP1 plays an important in regulating the crosstalk between the ER and mitochondria during ER-stress mediated cell death.

1.3.2 Regulation of ER calcium homeostasis during ER-stress

The ER serves as a major Ca^{2+} storage and buffering organelle, providing an ideal environment for Ca^{2+} handling, protein-folding chaperones [52]. The ER achieves large luminal Ca^{2+} concentrations compared to the cytosol by operating the transmembrane ER calcium pump known as the sarco/endoplasmic reticulum Ca^{2+}-ATPase (SERCA). Once inside the ER, Ca^{2+} can be stored and ultimately utilized by binding to ER-resident chaperone proteins including BiP (GRP78), calreticulin (CRT), calnexin (CNX), and protein disulfide isomerase (PDI) [53]. Outflow of Ca^{2+} from the ER is primarily mediated by the ryanodine (RyR) and inositol 1,4,5-triphosphate receptors (IP_3R). As such, significant fluctuations in ER Ca^{2+} levels have been shown to be the cause and consequence of ER-stress induction. Indeed, the ER-stress inducing agent thapsigargin exerts its activity by interrupting SERCA mediated Ca^{2+} uptake, which is crucial for protein folding [54]. Regulation of Ca^{2+} trafficking during ER-stress is considered biphasic in nature, where low levels of unfolded protein result in endoplasmic reticulum protein-44 (ERp44)-mediated protection of Ca^{2+} store depletion, whereas, bouts of prolonged UPR and ER-stress, lead to PERK and BAP31-mediated induction of IP_3R-mediated bolus Ca^{2+} release [55;56].

1.3.3 Mitochondria/ER calcium signaling during cell death

Similar to the ER, the presence of Ca^{2+} within the mitochondria aids in critical organelle functions. Mitochondrial Ca^{2+} levels play a vital role in bioenergetic processes including ATP synthesis. Mitochondrial Ca^{2+} is pumped from the cytosol into the outer mitochondrial membrane through the voltage-dependent anion-selective channel (VDAC) and subsequently into the mitochondrial lumen through the mitochondrial calcium uniporter (MCU). The Ca^{2+} flux between the ER and mitochondria occur at locations recognized as mitochondrial-associated ER membranes (MAMs), a unique locality where endoplasmic IP_3 receptors are tethered to

mitochondrial VDACs [57]. Indeed, the ebb and flow of Ca^{2+} between these organelles plays a homeostatic role in the maintenance of metabolic and protein folding functions. Conversely, perturbations in Ca^{2+} signaling can become propagated during altered ER protein folding and redox status [56]. Specifically, ER-stress causes sustained IP_3 receptor mediated mitochondrial Ca^{2+} uptake, known to activate the intrinsic apoptotic pathway by opening the mitochondrial permeability transition pore (mPTP) [57;58]. The resulting effect is the release of cytochrome c, a factor which activates the executioner caspase cascade, causing apoptotic cell death.

1.3.4 ER-stress Induction as a Chemotherapeutic Avenue

Studies have revealed that agents capable of targeting ER-stress can selectively inhibit proliferation or cause tumor cell apoptosis. Agents with tumor cell selective characteristics are preferred as they are associated with fewer adverse effects. It is well established that basal levels of ER-stress are heightened in cancer cells as a result of the increased protein demand during uncontrolled cell proliferation [49]. In addition, hypoxic conditions within most tumors impairs ATP production and leads to the accumulation of unfolded proteins [49] In contrast, ER-stress is typically inactive in normal cells. These observations provide a basis for selective toxicity, the ability to target tumor cells, while causing limited harm to normal cells, thus minimizing side-effects. As such, antineoplastic agents are currently being utilized to modulate the ER-stress pathway as a therapeutic target [59]. Clinically available agents that target the UPR include irestatin, which inhibits the UPR sensor IRE1α, thereby inhibiting cell proliferation and bortezomib, which exacerbates ER-stress mediated death by blocking proteasome activity [60]. Furthermore, non-melanoma and melanoma skin cancers have demonstrated susceptibility to these agents, suggesting that ER-stress induction may be useful tool for treating skin cancer.

CHAPTER TWO: MATERIALS AND METHODS

2.1 Antibodies and Reagents

15-deoxy, $\Delta^{12,14}$-prostaglandin J_2 and 9,10-dihydro-prostaglandin J_2 were purchased from Cayman Chemical company (Ann Arbor, MI). TBTU, ethanolamine, diispropylethylamine, acetonitrile (ACN), deuterated chloroform ($CDCl_3$), and the antibody for β-actin were purchased from Sigma-Aldrich (St. Louis, MO). Antibodies directed toward full length/cleaved caspase-3, full length/cleaved PARP, full length/cleaved caspase-8, full length caspase 4, P-PERK and total-PERK were from Cell Signaling Technologies (Beverley, MA). Cleaved caspase-4 was from Invitrogen (Grand Island, NY), Anti-CHOP10 and anti-BAP31 antibodies were from Santa Cruz Biotechnology (Santa Cruz, CA), anti-GAPDH was from Millipore (Billerica, MA) and anti-CDIP1 was from Novus Biologicals (Littleton, CO). Anti-rabbit 800CW and anti-mouse 680RD secondary antibody IRDyes were from Li-cor Biosciences (Lincoln, NE). Anti-rabbit Alexafluor 555 was from Invitrogen (Grand Island, NY) while anti-rat Alexafluor was from Jackson Immunoresearch (West Grove, PA). Caspase-Glo® 3/7 assays and MTS reagent were from Promega Life Sciences (Madison, WI).

2.2 Synthesis of Novel Prostamides (Chapter 3)

15-deoxy-$\Delta^{12,14}$-prostaglandin J_2 or 9,10-dihydro-prostaglandin J_2 (Cayman Chemical, Ann Arbor, MI.) was dissolved in a small volume (10mL) of acetonitrile, approximately 1.5 mole equivalent of O-(Benzotriazol-1-yl)-N,N,N′,N′-tetramethyluronium tetrafluoroborate (TBTU), and 2 mole equivalents of diisopropylethylamine were added. The solution was stirred for approximately 60 minutes and 2 mole equivalents of ethanolamine were added. The reaction solution was stirred for 24 hours and the solvent removed by vacuum distillation to yield the

crude product. This product was re-dissolved into 1:1 ACN:H_2O and purified by HPLC (spectroscopic yield 99%), which was characterized by ^1H NMR (400MHz, $CDCl_3$): 0.921 (t, 3H); 1.340 (m, 4H); 1.482 (m, 2H); 1.706 (q, 2H); 2.053 (q, 3H); 2.177 (t, 2H); 2.258 (q, 2H); 2.372 (m, 1H); 2.592 (m, 1H); 3.439 (q, 2H); 3.634 (m, 1H); 3.744 (t, 2H); 5.365 (m, 1H); 5.472 (m, 1H); 5.953 (s, 1H); 6.311 (m, 3H); 6.965 (d, 1H); 7.510 (m, 1H); and ESI-MS: $[M+H]^+$ 360.2270. Patent # 9,328,060.

2.3 Cell Lines and Cell Culture

Non-tumorigenic HaCaT keratinocytes (purchased from Cell Line Service, Eppelheim, Germany), human squamous carcinoma cell line A431 (purchased from ATCC, Manassas, VA) and mouse B16F10 melanoma cells (a kind gift from Dr. Li Yang, East Carolina University) were cultured in Dulbecco's Modified Eagle Medium (Invitrogen, Carlsbad, CA) containing 10% heat inactivated fetal bovine serum (FBS), penicillin (100 mg/mL), streptomycin (100mg/mL), sodium pyruvate, and glutamine. The murine melanocyte Melan-A cell line was purchased from the Bennett-Sviderskaya laboratory (Molecular Cell Sciences Research Centre, St. George's, University of London, UK) and cultured in Roswell Park Memorial Institute (RPMI)-1630 medium supplemented with 10% fetal calf serum, penicillin (100mg/mL), streptomycin (100mg/mL), glutamine and tetradecanoylphorbol acetate (200 nM). Patient melanoma tissue (acquired from Dr. Timothy Fitzgerald ECU, Dept. of Surgery) was washed and dissociated using collagenase type 4 (Worthington Biochemical Corporation, Lakewood, NJ) then cultured in Mel 2% medium containing MCDB 153/Leibovitz L-15 medium (80%/20%), 2% heat inactivated FBS, insulin (5µg/mL), calcium chloride (1.68mM) and bovine pituitary extract (15 µg/mL). The identity of the primary melanoma cells were verified by measuring tyrosinase levels via confocal microscopy. The murine squamous carcinoma cell line, JWF2, was cultured in Eagle's Minimal Essential

Medium (US Biological, Swampscott, MS) containing 5% heat inactivated FBS, penicillin (100 mg/mL), streptomycin (100 mg/mL), nonessential amino acids and glutamine. JWF2 cells were a kind gift from Dr. Susan Fischer (University of Texas, MD Anderson Cancer Center, Smithville, TX).

2.4 Cell Viability Assays

A431, HaCaT, B16F10, Melan-A, JWF2 or primary melanoma cells were plated in 96-well dishes and cultured for 48hrs. Serum-free medium containing different concentrations of 15d-PMJ_2, 15d-PGJ_2 or other agents were then added to the cells. Twenty microliters of MTS reagent were added to each well after 12-24 hours of incubation and absorbance was measured at 495nm as directed by the manufacturer (Promega, Madison, WI). LC_{50} (concentration required to kill 50% of the cell population) values were determined using GraphPad software.

2.5 Caspase-3/7 Activity Assay

Cells were plated in white-walled 96-well plates and cultured for 48 hours. Medium containing the appropriate agents were added to the cells for the indicated amount of time. One hundred microliters of Caspase-Glo 3/7 reagent was then added to each well as directed by the manufacturer and luminescence was measured using a Tecan luminometer.

2.6 E- and J-series Prostaglandin ELISA Assay

Culture medium collected from JWF2 and HaCaT cells was assayed for E- and J-series prostaglandins using ELISA kits according to the manufactures' use protocol as described previously [43].

2.7 Western blot Analysis

All cell lines were incubated in medium containing the indicated agents. Plates were subsequently scraped and protein concentration of the cell lysates was determined with BCA reagents (Pierce, Rockford, IL). Equal concentrations of each sample were loaded onto SDS-PAGE gels and protein bands transferred to nitrocellulose membranes (GE Healthcare Life Sciences, Piscataway, NJ). Blocked membranes were incubated with Peirce Protein Free Blocking Buffer (Thermo Scientific, Waltham, MA) containing full length (FL)/cleaved caspase-3 (1:1000), full length (FL)/cleaved caspase-4 (1:1000), full length (FL)/cleaved caspase-8 (1:1000) FL/cleaved PARP (1:1000), anti-P-PERK (1:500), anti-t-PERK (1:500), anti-CHOP10 (1:1000), anti-β-actin (1:5000), anti-GAPDH (1:5000), or anti-CDIP1 (1:1000) antibodies. Protein bands were visualized using the Li-cor system (Lincoln, NE) and digitized images were quantified using ImageJ software (https://imagej.nih.gov/ij).

2.8 Oxidative stress measurement

The oxidative stress in JWF2 and B16F10 cells was measured using the probe chloromethyl-2,7 dichlorodihydrofluorescein diacetate (CM-H_2DCFDA, Molecular Probes, Invitrogen). Cells were treated with appropriate drugs using phenol red-free, serum-free medium for the indicated time followed by incubation with PBS solution supplemented with magnesium and calcium containing CM-H_2DCFDA. Cells were then dissociated from the culture dish using Hank's Enzyme free dissociation buffer and re-suspended in phenol red-free serum-containing media. Mean fluorescence was measured using an Accuri C6 flow cytometer (BD Accuri Cytometers, Ann Arbor, MI, USA) at an excitation wavelength of 488nm and an emission filter of 533 ± 33nm.

2.9 Intracellular [Ca^{2+}] measurements

To measure intracellular [Ca^{2+}], treated cells were incubated with Fluo-4-NW at 37ºC for 30 minutes in HBSS (without Mg^{2+} or Ca^{2+}). Mean fluorescence was measured using a Tecan Infinite Pro M200 plate reader (Mannedorf, Switzerland) at an excitation wavelength of 493 nm and an emission filter of 513 ± 33nm.

2.10 Mitochondrial [Ca^{2+}] measurements

To measure mitochondrial [Ca^{2+}] levels, treated cells were incubated with Rhod-2 (1mM) at 37ºC for 30 minutes in PBS (without Mg^{2+} or Ca^{2+}). Mean fluorescence was measured using an Accuri C6 flow cytometer (BD Accuri Cytometers, Ann Arbor, MI, USA) at an excitation wavelength of 533 nm and an emission filter of 614 ± 33nm.

2.11 Immunocytochemistry

A431 cells were grown on culture slides followed by incubation in medium containing the indicated agents. Cells were then fixed with methanol, incubated with permeabilization buffer (0.1% Triton X-100 in PBS) for 10 minutes, and blocked with blocking buffer (PBS + 3% FBS + 0.5% Tween20) for 1 hour. Blocked cells were then incubated with indicated primary antibodies and the appropriate immunofluorescence-tagged secondary antibodies. Images were acquired and analyzed by confocal laser microscopy (Zeiss LSM 700 confocal microscope system). Fluorescence intensity was quantified using Zen Blue software.

2.12 B16F10 Allograft Studies

All experiments were approved and conducted in accordance with East Carolina University IACUC guidelines. C57BL/6 female mice (7-week old animals) were purchased from Jackson Laboratories (Bar Harbor, ME). The flank region was shaved and tumors established by inoculating 2 x 10^5 B16F10 cells subcutaneously as previously described [61].When tumors

became palpable (7 - 10 days post implantation), mice were either given daily peritumor injections (0.5 mg/kg 15d-PMJ_2 or PBS as vehicle) or left untreated as a control for 5 days. Animal body weights were measured and recorded daily. The length and width of the tumors were measured daily with calipers (daily tumor volume was calculated as: $Volume = Length^2 \; x \; Width \; x \; (\pi/6)$). After mouse euthanasia, tumors were dissected, blotted dry and weighed at the end of the study.

2.13 Immunohistochemistry

Tumors and livers were formalin-fixed, paraffin-embedded and sectioned at 5µm thickness. Sections were deparaffinized and rehydrated with a series of ethanol solutions and water. Endogenous peroxidase activity was blocked with 3.0% hydrogen peroxide for 30 minutes at room temperature. Sections were then incubated overnight with primary antibody followed by secondary antibody for 30 minutes. Preliminary experiments were conducted to optimize conditions for primary and secondary antibody. Staining was visualized using the Superpicture 3rd GEN IHC Detection Kit (ThermoFisher, Waltham, MA) then counterstained in Harris' hematoxylin. Terminal deoxynucleotidyl transferase deoxyuridine triphosphate nick-end labeling (TUNEL) staining of paraffin-embedded tumor and liver sections was performed according to standard protocols provided by the manufacturer (Roche Diagnostics, Mannheim Germany). Four fields were evaluated per section with a minimum of twelve sections examined per tumor.

2.14 Statistical Analysis

Data are representative of three independent experiments unless otherwise indicated. Data are presented as mean ± standard error of the mean (SEM). Student's *t*-test, one- and two-way ANOVA followed by Tukey's post-hoc analysis were carried out using GraphPad Prism and Microsoft Excel.

CHAPTER THREE: SYNTHESIS AND VERIFICATION OF NOVEL J-SERIES PROSTAMIDES

3.1 ABSTRACT

Our previous data showed that AEA-induced apoptosis in a COX-2-dependent manner. Subsequent findings also showed that AEA was metabolized by COX-2 and mass spectral analysis demonstrated that the novel prostamide, 15-deoxy-$\Delta^{12,14}$ prostamide J_2 (15d-PMJ_2) was a primary metabolic product. As such, this study sought to synthesize 15d-PMJ_2 to determine if the cytotoxic activity of AEA was mediated by this J-series metabolic product. 15d-PMJ_2 was synthesized by using a coupling reagent in the presence of N,N-diisoproylethylamine (DIEA) and ethanolamine. The uronium salt TBTU was chosen as the most appropriate coupling reagent as HBTU possessed limited solubility while removal of byproducts of carbodiimides such as DIC poses a difficulty. The model compound linoleoyl-ethanolamide was synthesized and verified by ^{1}H-NMR following liquid/liquid extraction work-up with diethyl-ether. Recovery and yield were reported to be 88% and 95% respectively. To determine the effect on lipids containing double bonds, the model compound AEA was synthesized from arachidonic acid and verified by ^{1}H-NMR and ESI-MS. Recovery and yield were found to be comparable to linoleoyl-ethanolamide. The cytotoxicity of synthetic AEA in COX-2 overexpressing tumorigenic keratinocytes was found to be by 43% at 20 µM and 92% at 30 µM, respectively. The cytotoxicity of synthesized AEA was found to be similar but slightly higher than commercially available AEA. Finally, 15d-PMJ_2 was synthesized from 15d-PGJ_2 in the presence of TBTU and ethanolamine. High performance liquid chromatography was chosen to purify 15d-PMJ_2, thereby significantly increasing recovery. The identity, purity and reaction yield of 15d-PMJ_2 was verified by ^{1}H-NMR and ESI-MS.

3.1 INTRODUCTION

Our laboratory previously established that AEA potently and selectively induced apoptotic cell death in COX-2 overexpressing tumorigenic keratinocytes [31]. Furthermore, mass spectral analysis indicated the presence of a novel J-series prostamide as a primary COX-2 metabolite. Thus, we hypothesized that the cytotoxic activity of AEA was mediated by this J-series prostamide. To investigate the anti-tumor activity of 15d-PMJ_2, an approach was developed to synthesize 15d-PMJ_2, as this molecule is not commercially available. Specifically, this approach involved the attachment of an ethanolamine group via formation of an amide bond by using a coupling reagent and reacting the commercially available carboxylic acid containing J-series prostaglandin (15-deoxy $\Delta^{12,14}$ prostaglandin J_2) with ethanolamine to form the J-series prostaglandin-ethanolamide (prostamide) product. The collective strategy for optimizing yield and recovery was to first begin by producing ethanolamide conjugates using inexpensive and readily available saturated fatty acid compounds then transitioning to polyunsaturated fatty acids and finally to the J-series prostaglandin (figure 3.1).

The amide moiety is a common feature found in many classes of natural molecules, including proteins, lipids, and carbohydrates. In nature, the process of amide bond formation is very complex and requires specialized coordination of many macromolecules including enzymes, ribosomes, mRNAs, and tRNAs. In lipids and endocannabinoids such as AEA, the amide-ethanolamine group is produced in a two-step process. First, the arachidonic acid component is transferred from arachidonoyl-phosphatidylcholine (PC) to phosphatidylethanolamine (PE) by N-acyltransferase (NAT). Next, N-arachidonoyl-phosphatidylethanolamine (NAPE) is cleaved by NAPE-specific phospholipase D (NAPE-PLD), to generate AEA and phosphatidic acid. Liberation

of arachidonic acid from the ethanolamide group is carried out by fatty acid amide hydrolase (FAAH).

In the laboratory setting, amide bond formation is carried out by a coupling reaction which typically involves the following steps: activation of a carboxylic acid, attachment of a leaving group to the acyl carbon of the acid, and attack of the amino group. In general, a multitude of different strategies using different coupling reagents has been developed aimed at fulfilling unique synthetic goals such as optimizing yield, ease of final purification, avoidance of racemic mixtures or economical scalability. As such, our synthetic goals regarding 15d-PMJ_2 were specifically aimed at utilizing a "one pot" synthetic approach, using mild conditions to preserve the activity of the cyclopentenone ring while simultaneously maximizing yield since the cost of starting material is prohibitive.

To fulfill our synthetic requirements and utilize a "one pot" reaction approach, a class of reagents known as uronium coupling reagents were chosen as the best synthetic candidate. Two popular coupling reagents utilized for this synthesis were O-(Benzotriazol-1-yl)-N,N,N',N'-tetramethyluronium hexafluorophosphate (HBTU) and O-(Benzotriazol-1-yl)- N,N,N',N'-tetramethyluronium tetrafluoroborate (TBTU). These coupling reagents were developed for their extremely efficient amide bond coupling and are now an industry standard for peptide synthesis. Coupling reactions using these reagents occur in as little as six minutes and when 1-hydroxybenzotriazole (HOBt) is added, racemization can be reduced to insignificant levels [62]. Additionally, these reagents are also particularly useful in our case as by-products from the coupling reaction are soluble in aqueous solutions, allowing for separation by liquid-liquid extraction or HPLC. The coupling reaction begins by deprotonation of the carboxylic acid with base followed by reaction with the uronium ion to form an activated ester and a tetramethylurea

by-product (Figure 3.2). Next, the activated ester is subjected to nucleophilic attack by the amino group of ethanolamine to give the final amidated product (Figure 3.2). The final ionic product, HOBt, which is formed from the uronium salt is aqueous soluble and thus can be readily separated by extraction.

Figure 3.1: Optimization strategy for synthesizing 15d-PMJ_2

To maximize reaction yield and recovery, the conjugation of ethanolamide was optimized and carried out using heptadecanoic acid C17:0, linoleic acid C18:2, and arachidonic acid C20:4 to form heptadecanoyl ethanolamide, linoleoyl ethanolamide, and arachidonoyl ethanolamide respectively.

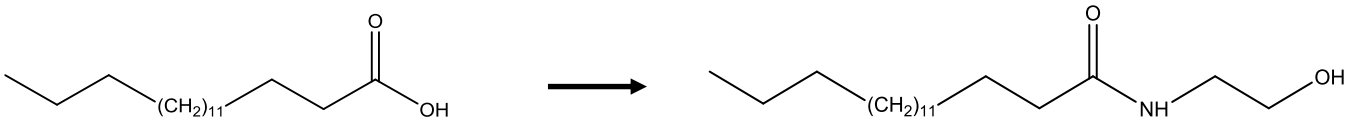

Heptadecanoic Acid C17:0

Heptadecanoyl ethanolamide

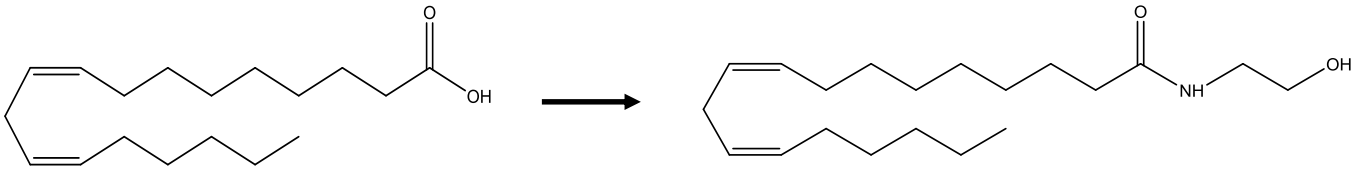

Linoleic Acid C18:2

Linoleoyl ethanolamide

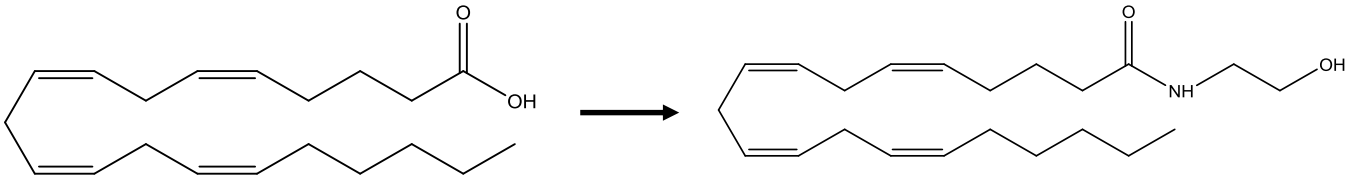

Arachidonic Acid C20:4

Arachidonoyl ethanolamide

Figure 3.2: Mechanism of amide bond coupling by uronium salt

Amide bond coupling begins by deprotonating the carboxylic acid with base followed by formation of the activated ester and tetramethylurea. Lastly, the activated ester is attached at the amino group leading to the formation of the amide bond.

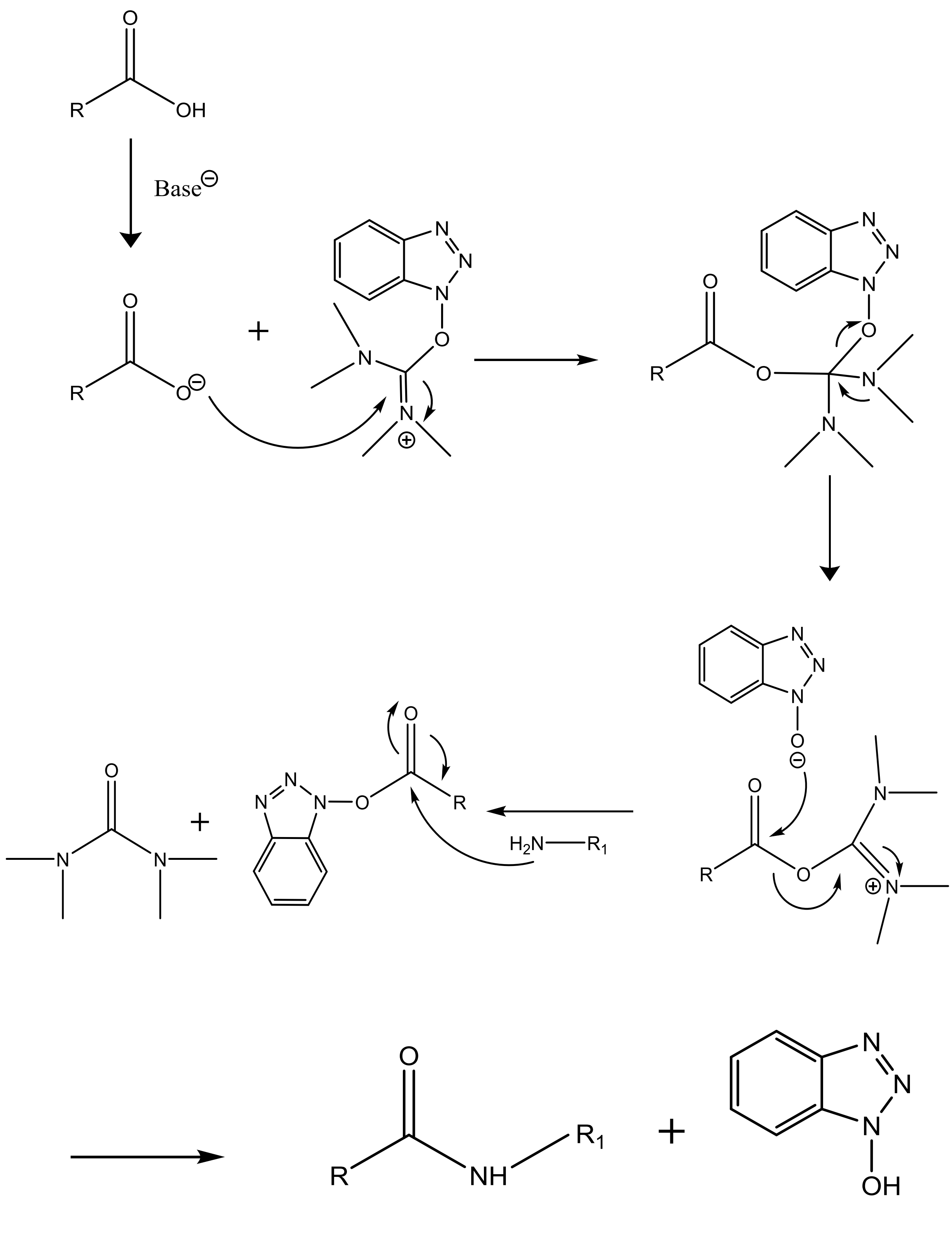
Base$^{\ominus}$
H_2N—R_1

3.2 RESULTS

3.2.1 Synthesis of heptadecanoyl-ethanolamide

A comprehensive study was carried out to determine the appropriate solvent conditions for dissolving the coupling reagent, HBTU, and heptadecanoic acid (HDA) within the same solution. The best solvent balance was found to be 88% dimethylformamide (DMF) and 12% dichloromethane. Changes in percentages of these solvents resulted in the precipitation of HBTU or HDA. To a solution containing 50 mg HDA, 1.1 molar equivalents HBTU, 2 molar equivalents of N,N-diisoproylethylamine (DIEA) followed by 2 molar equivalents ethanolamine were added. HBTU is not added in excess as it can react with double bonds and unprotected N groups. The contents were allowed to mix for 3 hours and then poured into a separatory funnel containing 50 mL dichloromethane. A thick emulsion formed when diH_2O was added, therefore, 3 extractions were performed with 20 mL brine solution followed by 3 extractions with diH_2O. The organic layer was collected and dried using 25 mg sodium sulfate, then filtered using 24/40 Whatman filter paper. The final solution was rotary evaporated under medium heat to yield a white solid. Residual dimethylformamide following rotary evaporation would require subsequent extractions using ethyl acetate followed by overnight vacuum distillation. This reaction was performed a total of three times with the average recovery yield of 75%.

Analytical verification of heptadecanoyl-ethanolamide was performed by ^{1}H-NMR (Figure 3.3). The peaks found at ~3.45 ppm and ~3.75 ppm corresponded to the successful addition of the ethanolamide group and comparison of integration values corresponding to these peaks with that of 0.9 ppm (terminal carbon corresponding to 3 protons) indicated a ~95% conversion. The 1.65 ppm peak which showed a broad base is indicative of H_2O (Figure 3.3).

3.2.2 Synthesis and optimization of linoleoyl-ethanolamide

The synthesis of linoleoyl-ethanolamide was attempted using the same procedure as heptadecanoyl-ethanolamide, however due to the high aqueous partition of DMF, contamination with this solvent occurred at higher frequency. This required additional extraction steps which drastically decreased product recovery. Any attempt to remove DMF using vacuum distillation under moderate heat resulted in complete oxidation of double bonds of linoleic acid. As such, we sought to remove DMF from the synthetic scheme by replacing the coupling reagent with one which possessed greater solvent flexibility. The uronium salt TBTU was found to be an appropriate alternative, with at least one group reporting moderate solubility in ethyl acetate [63]. Under our experimental conditions, however, TBTU was found to be soluble in acetonitrile, but not ethyl acetate. The majority of fatty acids and prostaglandins are readily soluble in acetonitrile (ACN) and as such, all following synthetic reactions were carried out using TBTU in 100% acetonitrile.

Linoleic acid, N'N-diisopropylethylamine and TBTU were dissolved in acetonitrile, which upon mixing, changed the solution from clear to faint pink to copper. This color transition is most likely the result of chelation of the activated carboxyl group. Once ethanolamine was added to the reaction mixture, the solution turned yellow and formed a white, shimmery precipitate. The crude product was then vacuum filtered, re-dissolved in 30mL DCM and extracted 3 times with diH_2O. Rotary evaporation produced a faint yellow oil. Recovery from this method was reported to be greater than 100% and analysis of ^{1}H-NMR spectra revealed a prominent peak at ~2.75 ppm. The impurity associated with this peak was determined to be tetramethylurea, which has been reportedly removed by using ether or heptanes as organic extraction solvents [64]. The subsequent reaction was performed identically but extracted with diethyl ether instead of DCM. Rotary evaporation left behind a clear oil with recovery greater than 88%. Analysis of ^{1}H-NMR spectra

showed 95% reaction yield with no presence of the previous impurity, tetramethylurea (Figure 3.4).

3.2.3 Synthesis and optimization of arachidonoyl-ethanolamide (AEA)

Preliminary synthesis of AEA using the same method to produce linoleoyl-ethanolamide was successful, however, slight oxidation of double bonds was apparent from analysis of ^{1}H-NMR spectrum. The presence of four labile double bonds urged the use of inert atmosphere and as such, all following reactions were carried out under nitrogen gas using a Schlenk line apparatus in dark conditions. Unlike reaction solutions containing linoleic acid, solutions with arachidonic acid underwent no color changes upon addition of DIEA and only a white precipitate formed following the addition of ethanolamine. Work up was identical to that of linoleoyl-ethanolamide, with the exception that rotary evaporation was performed at low temperature to yield a clear oily product.

Analysis of ^{1}H-NMR indicated a 99% reaction yield with all double bonds intact (Figure 3.5A). Furthermore, mass spectral analysis of the product showed two major peaks at m/z 370 and 386 which corresponded to sodium and potassium conjugated AEA, respectively (Figure 3.5B). To confirm the biological activity of synthesized AEA, murine tumorigenic JWF2 keratinocytes were treated with 5, 10, 15, 20 or 30 µM AEA and cell viability was measured by MTS assay (Figure 3.5C). Synthesized AEA decreased the cell viability by 43% at 20 µM and 92% at 30 µM. These values were found to be comparable with commercially available AEA, validating the cytotoxic activity of synthetic AEA in tumorigenic keratinocytes. These data demonstrate successful synthesis and biological activity of AEA.

3.2.4 Synthesis and verification of 15-deoxy-$\Delta^{12,14}$-prostamide J_2

To synthesize 15-deoxy-$\Delta^{12,14}$-prostamide J_2 (15d-PMJ_2), the commercially available non-ethanolamide J-series prostaglandin, 15 deoxy-$\Delta^{12,14}$-prostaglandin J_2 (15d-PGJ_2), was used as the synthetic substrate (Figure 3.6A). Prior to conducting the synthesis, the precursor molecule, 15d-PGJ_2, was characterized by ^{1}H-NMR (Figure 3.6C). To a solution containing 10 mg 15d-PGJ_2, 1.1 molar equivalents TBTU, 2 molar equivalents of N,N-diisoproylethylamine (DIEA) followed by 2 molar equivalents ethanolamine were added. The work-up of 15d-PMJ_2 was carried out using the same method found to successfully produce AEA. Unfortunately, product recovery using this method was severely diminished to 15%. Extractions of the discarded aqueous phase with ethyl acetate recovered much of the lost product, however, oxidation of the double bonds was apparent from analysis. Moving forward, diethyl ether was replaced with ethyl acetate as the primary extraction solvent during work-up. This change increased recovery, but the higher boiling temperature of ethyl acetate required greater heating during rotary evaporation which decreased double bond retention. In light of these findings, the use of high performance liquid chromatography (HPLC) was employed to purify 15d-PMJ_2. The crude product was dissolved in 1:1 H_2O:ACN and run through a BioRad HPLC C18 prep column with a H_2O/ACN solvent gradient. The retention time for 15d-PMJ_2 was found to be 13.80 minutes at 71% ACN (Figure 3.6B). The collected peak was then freeze dried over night to yield a clear oil.

Verification of 15d-PMJ_2 was carried out by performing ^{1}H-NMR and mass spectrometry. ^{1}H-NMR spectra of 15d-PMJ_2 was almost identical to the synthetic substrate (15d-PGJ_2), but also reported proton peaks associated with the addition of the ethanolamide group (Figure 3.6C, D denoted with red letters). Analysis of ^{1}H-NMR confirmed the retention of all double bonds and integration of peaks demonstrated a ~98% reaction yield. Mass spectral analysis of the product

showed one major peak corresponding to the m/z of 382.2 which was determined to be sodium conjugated 15d-PMJ_2 (data not shown). These data definitive demonstrate the first reported synthesis of 15d-PMJ_2.

Figure 3.3 Analytical verification of heptadecanoyl-ethanolamide by ^{1}H-NMR.

Spectra was acquired from a 400 MHz Bruker instrument with molecules dissolved in $CDCl_3$. Peak integration was performed using Bruker Top-spin software.

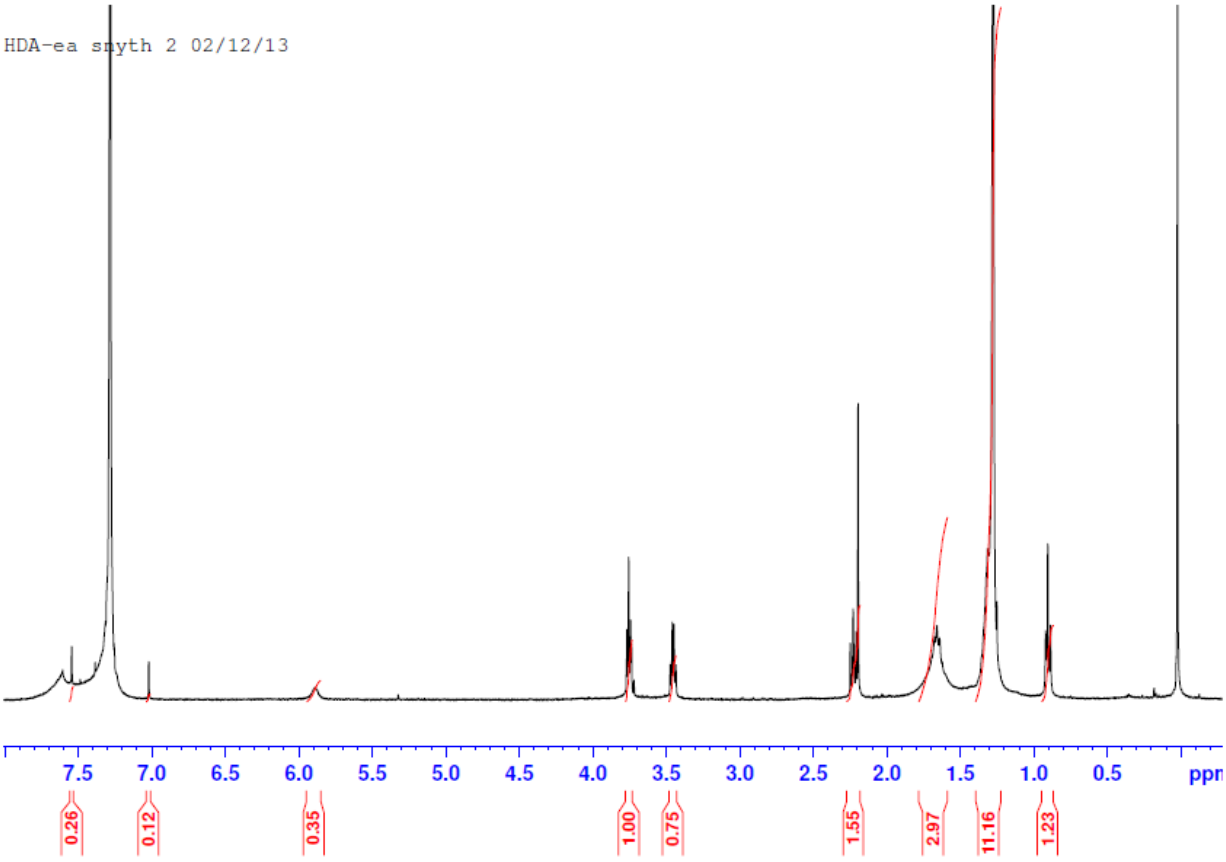
HDA-ea snyth 2 02/12/13
7.5
7.0
6.5
6.0
5.5
5.0
4.5
4.0
3.5
3.0
2.5
2.0
1.5
1.0
0.5
ppm
0.26
0.12
0.35
1.00
0.75
1.55
2.97
11.16
1.23

Figure 3.4 Analytical verification of linoleoyl-ethanolamide.

Linoleoyl-ethanolamide was synthesized according to the procedure described above. ^{1}H-NMR spectra was acquired from a 400 MHz Bruker instrument with molecules dissolved in $CDCL_3$. Numbers on molecular structure indicate proton shifts in spectra. Peak integration was performed using Bruker Top-spin software.

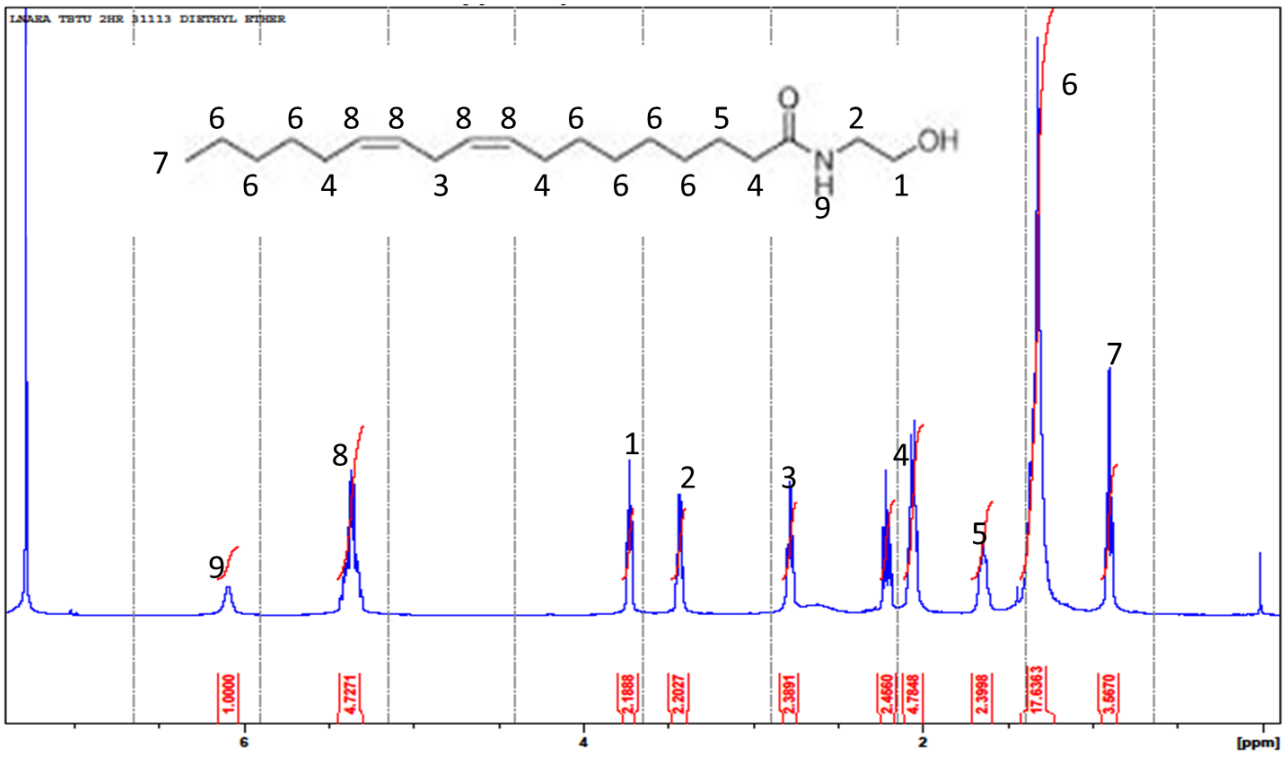
LMARA TBTU 2HR 31113 DIETHYL ETHER
6 6 8 8 8 8 6 6 5 O 2 OH
7 6 4 3 4 6 6 4 NH 9 1
6
7
8
9
1
2
3
4
5
1.0000
4.7271
2.1888
2.2027
2.3891
2.4660
4.7848
2.3998
17.6383
3.6670
6
4
2
[ppm]

Figure 3.5 Analytical and biological validation of arachidonoyl-ethanolamide

Arachidonoyl-ethanolamide was synthesized according to the procedure described above. (A) ^{1}H-NMR Spectra was acquired from a 400 mHz Bruker instrument with molecules dissolved in d-$CDCL_3$. (B) Mass spectral verification of arachidonoyl-ethanolamide was performed on a MircoMass time-of-flight mass spectrometer by direct injection with molecules dissolved in MS-grade ACN. (C) JWF2 tumorigenic keratinocytes were treated with 5 µM, 10 µM, 15 µM, 20 µM and 30 µM concentrations of synthesized AEA for 24 hours. Cell viability was evaluated by conducting MTS experiments. Data represent mean ± SEM of three independent experiments and are expressed as percent of untreated group. * $P < 0.05$, as compared to vehicle.

A.

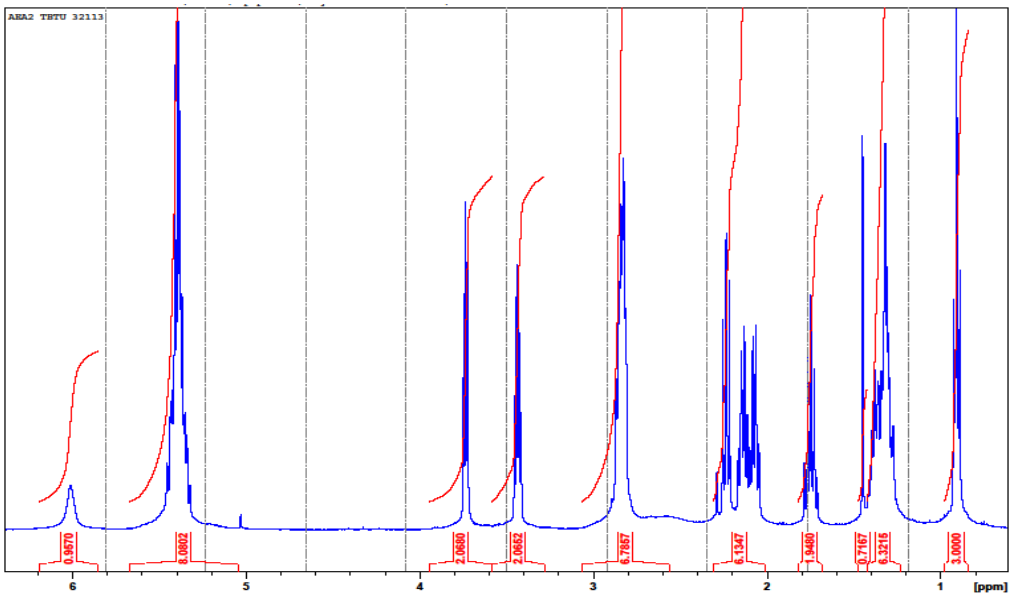
AHA2 TBTU 32113
0.9870
8.0802
2.0680
2.0652
6.7857
6.1347
1.9480
0.7167
6.3215
3.0000
6
5
4
3
2
1
[ppm]

B.

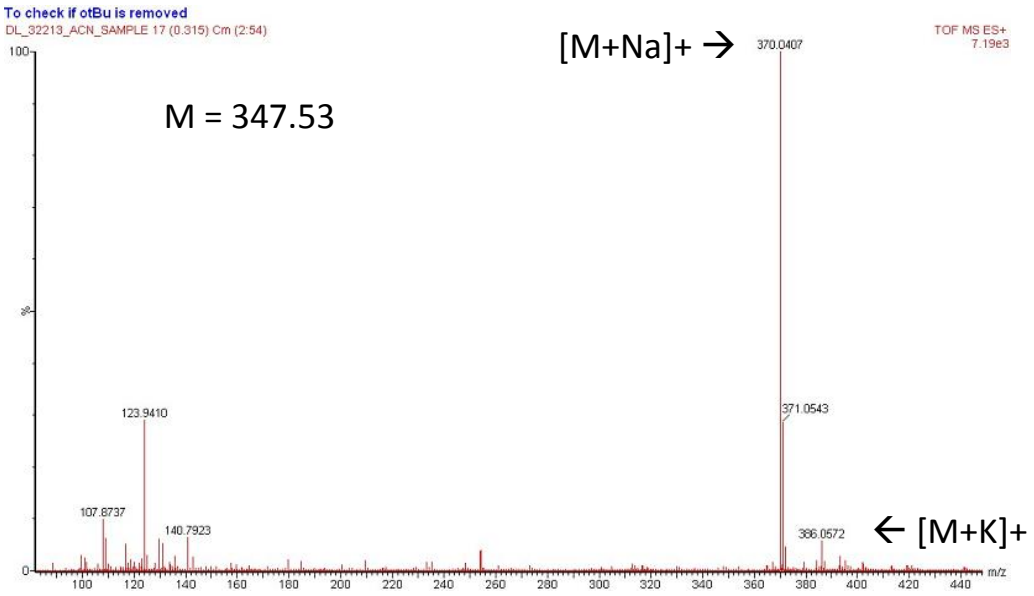
To check if otBu is removed
DL_32213_ACN_SAMPLE 17 (0.315) Cm (2:54)
TOF MS ES+
7.19e3
100
%
0
M = 347.53
[M+Na]+ →
370.0407
371.0543
123.9410
107.8737
140.7923
386.0572
← [M+K]+
100
120
140
160
180
200
220
240
260
280
300
320
340
360
380
400
420
440
m/z

C.

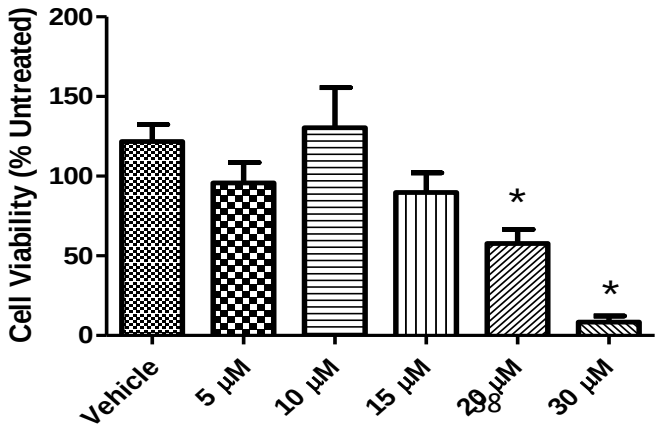
Cell Viability (% Untreated)
200
150
100
50
0
*
*
Vehicle
5 μM
10 μM
15 μM
20 μM
30 μM

Figure 3.6 Synthesis and verification of 15 deoxy-$\Delta^{12,14}$-prostamide J_2.

(A) 15 deoxy-$\Delta^{12,14}$ prostaglandin J_2 was reacted with ethanolamine in the presence of diisopropylethylamine and the uronium coupling reagent TBTU. Reaction was conducted in 100% acetonitrile under nitrogen atmosphere. (B) HPLC chromatograph for 15d-PMJ_2 . (C) H^1-NMR and structure of synthetic substrate 15 deoxy-$\Delta^{12,14}$ prostaglandin J_2 (15d-PGJ_2). (D) H^1-NMR and structure of 15 deoxy-$\Delta^{12,14}$ prostamide J_2. Spectra was acquired from 400 MHz Bruker instrument with molecules dissolved in $CDCL_3$.

A

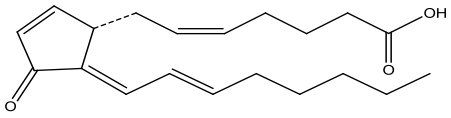

15-Deoxy-$\Delta^{12,14}$ Prostaglandin J_2

1. TBTU
2. Diisopropylethylamine
3. Ethanolamine

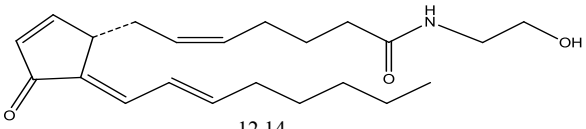

15-Deoxy-$\Delta^{12,14}$ Prostamide J_2 †

B

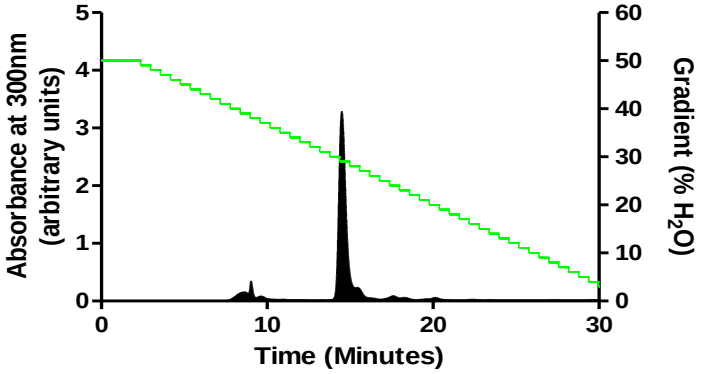

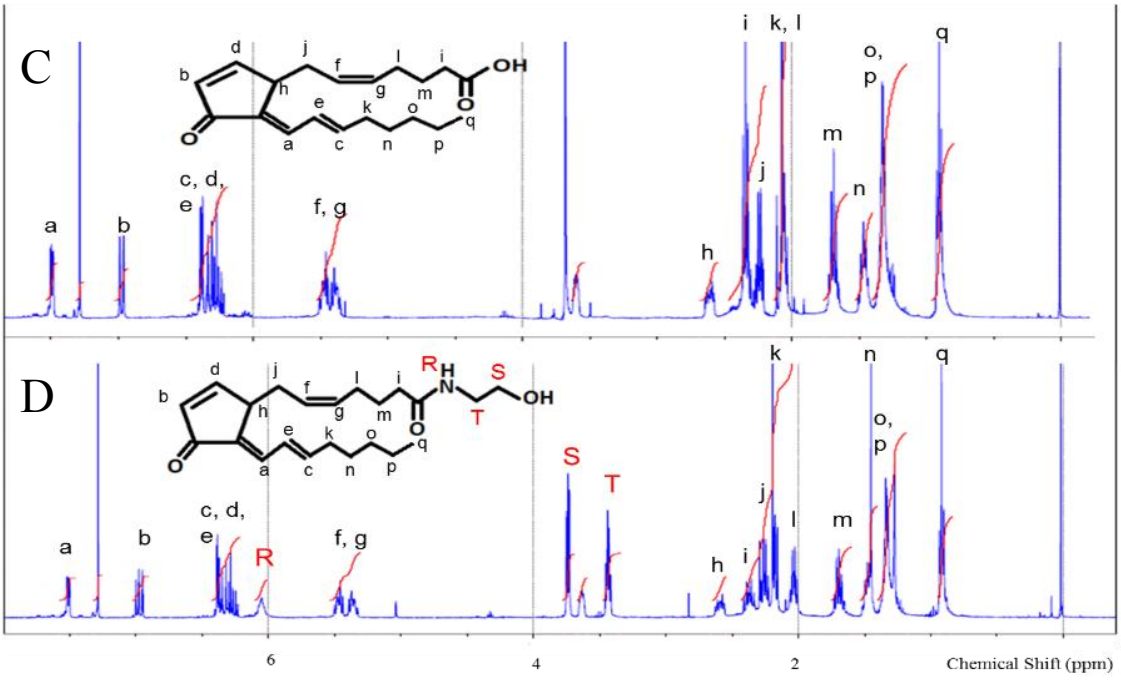

3.4 DISCUSSION

Gaining insight into the mechanisms associated with COX-2 mediated AEA cytotoxicity is an important topic of interest. Hence, the goal of this study was to perform the first synthesis of the terminal COX-2 AEA metabolite, 15d-PMJ_2. In order to accomplish this task, our approach employed the use of model compounds to develop the ideal synthetic conditions for the attachment of an ethanolamine group to a J-series prostaglandin, yielding the first J-series prostamide. To proceed with this approach, we explored chemical and solubility properties of various coupling reagents for amide bond formation. The use of diisopropylcarbodiimide (DIC) was explored as a potential coupling reagent in early synthetic schemes of linoleoyl-ethanolamide, but was quickly eliminated due to difficulty in work-up and low recovery. Uronium coupling reagents were found to be the best fit for our scenario due to their high yield and ease of removal. The solubility of HBTU was limited to DMF, which proved nearly impossible to remove, hence, TBTU was chosen due to its versatile solubility, particularly in acetonitrile.

Model compounds such as linoleic acid and arachidonic acid provided valuable synthetic insight regarding acceptable work-up conditions for unstable molecules possessing double bonds. These compounds demonstrated physical changes upon oxidation which was useful in developing the best practices for handling unsaturated lipids during processes of transferring, pipetting, storage etc. These physical changes were noted as yellowing or browning of the solution color, increased viscosity of the product oil, or irreversible adhesion to glass surfaces. We found that the model compounds, linoleic and arachidonic acid do not possess quite the same partition coefficient, thus initial recovery of 15d-PMJ_2 was low. Preliminary synthesis using diethyl ether were found to be successful in working up linoleoyl-ethanolamide and AEA, but not 15d-PMJ_2. As such, the best purification method for recovery was found to be high performance liquid

chromatography (HPLC). Interestingly, 15d-PMJ_2 was also found to considerably less stable than that of arachidonic acid or AEA. Indeed, our observations indicate that 15d-PMJ_2 is significantly more susceptible to degradation by oxidation, which is most likely due to highly electrophilic nature of the cyclopentenone ring. Exceptional care should be used whenever handling or transferring 15d-PMJ_2 in the presence of atmospheric oxygen.

The biological activity of AEA was confirmed in tumorigenic keratinocytes by means of cytotoxicity assay. Furthermore, cell death measured in keratinocytes treated with synthesized AEA was greater than that of commercially available AEA (data not shown). This may be attributed to the fact that synthetic AEA is recently produced whereas commercial AEA may be been stored for long periods of time, leading to slow degradation. To more extensively characterize the biological activity of synthesized AEA, future studies may include detecting its binding to cannabinoid receptors, to confirm its physiological role as an endogenous cannabinoid.

CHAPTER FOUR: EVALUATION OF THE ANTI-TUMOR ACTIVITY OF 15D-PMJ$_2$ IN VITRO AND IN VIVO

4.1 ABSTRACT

Skin cancer including melanoma and non-melanoma skin cancer (NMSC) is the most prevalent form cancer in the US. Many malignancies including skin cancer overexpress the enzyme cyclooxygenase-2 (COX-2). The major role of COX-2 is to convert arachidonic acid to prostaglandins (PGs) including prostaglandin E_2 (PGE_2). PGE_2 is known to promote cancer by activating anti-apoptotic signals and angiogenesis. In contrast, the COX-2 metabolite, 15-deoxy, $\Delta^{12,14}$prostaglandin J_2 (15d-PGJ_2) inhibits cancer cell survival by promoting apoptosis via mechanisms including oxidative- and endoplasmic reticulum (ER)-stress. We previously reported that the endocannabinoid, AEA, selectively induced apoptosis in tumorigenic NMSC cells and that this activity was dependent on the metabolic formation of J-series prostamides. As such, we set out to evaluate the anti-tumor activity of 15-deoxy-$\Delta^{12,14}$-prostamide J_2 (15d-PMJ_2) *in vitro* and *in vivo*. We began by evaluating the antineoplastic activity of PMD_2, the upstream metabolite of 15d-PMJ_2 and found that the D-series prostamide derivative exhibited greater cytotoxic and apoptotic properties in NMSC and melanoma cells compared to PGD_2. Like PMD_2, 15d-PMJ_2 was found to induce cell death and apoptosis in both non-melanoma skin cancer and melanoma cell lines at considerably lower concentrations than 15d-PGJ_2. To evaluate whether 15d-PMJ_2 exhibits preferential toxicity and induction of apoptosis, tumorigenic and non-tumorigenic keratinocytes and melanocytes were assayed for viability and the cleavage of pro-apoptotic proteins caspase-3 and PARP following 15d-PMJ_2 treatment. We report a significant difference in cell death between tumorigenic and non-tumorigenic cell lines. Furthermore, 15d-PMJ_2 was found to induce cleavage of caspase-3 and PARP in tumorigenic but not non-tumorigenic cells. To determine the activity of

15d-PMJ_2 against melanoma *in vivo*, B16F10 allograft tumors grown in C57/BL6 mice were dosed subcutaneously with 0.5 mg/kg 15d-PMJ_2 for 5 days. Tumors treated with 15d-PMJ_2 exhibited significantly reduced growth and mean weights compared to vehicle and untreated animals. TUNEL analysis of tumor tissues demonstrated significant levels of cell death in 15d-PMJ_2-treated tumors compared to vehicle and untreated tumors. Taken together, these findings show that the endocannabinoid metabolite, 15d-PMJ_2, possesses potent and selective activity against cancer cells *in vitro* and *in vivo*.

4.2 INTRODUCTION

Skin cancer is the most common human neoplasm in America with one in every five individuals developing this malignancy in their lifetimes [3]. Skin cancer is comprised of two major subtypes including non-melanoma skin cancer (NMSC) and melanoma. NMSC consists of basal and squamous cell carcinoma and is less aggressive and metastatic compared to melanoma. The annual cost of treating all types of skin cancer is estimated to be a staggering $8.1 billion dollars annually [65]. Furthermore, studies indicate that the incidence of these cancers is on the rise primarily due to increased exposure to ultraviolet radiation.

Currently, treatment for NMSC involves surgical excision, low-dose radiation, or application of chemotherapeutic agents including 5-fluorouracil and imiquimod. NMSCs most often occur on highly sun-exposed areas such as the face and ears. In some instances, surgical procedures may be disfiguring, leaving large scars or blemishes. The most common anti-neoplastic agent for the treatment of NMSC, 5-fluorouracil, acts principally by interrupting the synthesis of the nucleoside thymidine through inhibition of the enzyme thymidylate synthase. Adverse effects associated with this agent include skin inflammation when administered topically and myelosuppression when administered systemically. Imiquimod, a more recently developed immunomodulating agent, activates toll-like receptors (TLR7) within the immune system, resulting in the release of cytokines and the activation of the adaptive immune system. The culminating effect is the recruitment of natural killer (NK) cells, macrophages and lymphocytes which target the tumor for destruction. Side effects from imiquimod include skin damage, severe inflammation, and flu-like syndrome. While these agents provide effective treatment for the management of NMSC, the adverse effects generated from these agents arises from the lack NMSC cell selectivity.

Treatment of melanoma skin cancer is very distinct from NMSC. The inherent danger associated with melanoma is its highly aggressive and metastatic nature, making management clinically challenging. Primary melanoma tumors are surgically removed and if metastasis to other organs has occurred, immunotherapy and radiation therapy is initiated. Biological checkpoint inhibitors such as ipilimumab are a newer class of immunotherapeutic agents which block cytotoxic T-lymphocyte-associated protein 4 (CTLA4) thereby initiating T-lymphocyte-mediated tumor recognition and destruction of metastatic melanoma cells. These agents have increased survival rates of patients with unresectable melanoma, however the potentially fatal immunological adverse effects of check-point inhibitors coupled with the difficulty of predicting patient response limits their clinical use. As such, the need for novel chemotherapeutic agents to improve patient survival while causing fewer side effects is greater than ever.

Apoptosis is a tightly regulated form of immune-tolerant programmed cell death which is characterized by the activation of distinct energy-dependent cellular pathways. Morphologically, hallmarks of apoptotic cells include the condensation of chromatin and the formation of distinct plasma membrane blebs known as apoptotic bodies. The initiation of apoptosis can by stimulated through three separate pathways including the intrinsic pathway, the extrinsic pathway, and the T-cell-mediated granzyme pathway all of which converge onto activation of the major executioner protein, caspase-3. The intrinsic pathway involves permeabilization of the mitochondrial membrane, causing release of cytochrome c into the cytosol which then forms the apoptosome and subsequently activates caspase-3. In cancer, achieving apoptosis as a therapeutic outcome provides numerous advantages over necrotic-type cell death including decreased inflammatory response and reduced collateral non-tumor cell killing. Indeed, it is reported that in chemotherapy-treated cancers such as leukemia, remission is almost exclusively associated with induction of apoptotic

mechanisms. As such, chemotherapeutic agents which demonstrate proficiency at selectively targeting tumor-cells for apoptotic cell death can ultimately provide therapeutic success with less incidence of adverse effects.

Endocannabinoids are endogenously synthesized lipids that bind to and signal through cannabinoid receptors. These lipid messengers modulate neuronal signaling, inflammation, cardiovascular function and other physiological processes. In addition, endocannabinoids and their receptors are reported to be involved in both the development and elimination of cancer, indicating that the pathophysiological interaction between cancer and endocannabinoids requires further study [66-68]. Several reports suggest that the antitumor activity of AEA occurred through cannabinoid receptor-dependent and -independent mechanisms including the induction of endoplasmic reticulum (ER) stress [69-73].

Our group previously reported that the endocannabinoid, AEA, caused selective induction of apoptosis and cell death in NMSC cells. Furthermore, recent data from our group identified a newly discovered J-series prostaglandin-ethanolamide (prostamide), 15-deoxy, $\Delta^{12,14}$-prostamide J_2 (15d-PMJ_2) [43;74]. Specifically, we found that AEA was metabolized by cyclooxygenase-2 (COX-2) to prostaglandin-ethanolamide D_2 [prostamide D2 (PMD_2)] which was converted to the terminal product, 15d-PMJ_2. Previous studies by our group demonstrated that metabolism by COX-2 was needed for AEA cytotoxicity but that the cannabinoid receptors had little impact on its activity. The prevention of AEA-mediated cell death by blocking 15d-PMJ_2 production suggested that the anti-proliferative action of AEA was caused by 15d-PMJ_2. Therefore, in the current study, we evaluated whether the novel prostamide, 15d-PMJ_2, was an inducer of tumor cell death *in vitro* and *in vivo*. We also examined whether apoptotic effects of 15d-PMJ_2 were preferentially observed in tumorigenic vs. non-tumorigenic cells. These studies were designed to

assess the feasibility of utilizing 15d-PMJ_2 as a potential selective anti-tumor agent against skin cancer.

4.3 RESULTS

4.3.1 Upstream metabolic precursor of 15d-PMJ_2, PMD_2 induces apoptotic cell death in melanoma and non-melanoma skin cancer cells.

The endocannabinoid, AEA, undergoes COX-2 mediated conversion to prostamides followed by metabolism to D-series prostamides by prostaglandin D synthase. Our group demonstrated that D-series prostamides are subsequently dehydrated to the terminal end-product, 15d-PMJ_2 [43]. To determine the anti-proliferative activity of the D-series prostanoids against skin cancer cells, JWF2 (non-melanoma skin cancer) and B16F10 (melanoma) cells were treated with increasing concentrations of PMD_2 and PGD_2 for 24 hours and cell viability was measured by MTS assay. JWF2 and B16F10 cells treated with 10 and 20 μM PMD_2 displayed a significant reduction in cell survival (Figure 4.1A and B). Alternatively, PGD_2 only decreased viability at the 20 μM concentration, suggesting that PMD_2 possesses greater cytotoxicity. To determine whether D-series prostanoids induce apoptotic cell death, JWF2 and B16F10 cells were treated with 10 or 20 μM PMD_2 or PGD_2 for 24 hours and the cleavage of PARP was measured by Western blot analysis. At 20 μM, the presence of both PMD_2 and PGD_2 led to increased expression of cleaved PARP in both melanoma and non-melanoma skin cancer cells when compared to vehicle treated cells (Figure 1C and D). These results suggested that D-series prostanoids induce apoptotic cell death in skin cancer lines.

4.3.2 15d-PMJ_2 is a potent inducer of cell death in skin cancer cells.

To evaluate the cytotoxic activity of 15d-PMJ_2 in skin cancer cells, B16F10 melanoma cells, along with A431 and JWF2 squamous cell carcinoma cell lines were treated with increasing concentrations of 15d-PMJ_2 and 15d-PGJ_2 and cell viability measurements performed by MTS

assay. 15d-PMJ_2 caused a concentration dependent decrease in cell viability. The LC_{50} (concentration of agent which causes death in 50% of the cells) value of 15d-PMJ_2 was calculated and is determined to be 4.7 µM for A431 and 3.3 µM JWF2 cells (Figure 4A, C). In B16F10 melanoma and patient derived primary melanoma cells, the LC_{50} values were calculated to be 3.3 µM and 3.0 µM respectively (Figure 4B, D). 15-deoxy, $\Delta^{12,14}$ prostaglandin J_2 (15d-PGJ_2) is a molecule that is distinct, yet structurally related to 15d-PMJ_2. 15d-PGJ_2 is synthesized by COX-2 from the substrate arachidonic acid rather than AEA. Because arachidonic acid-derived 15d-PGJ_2 induces tumor cell death [75], the cytotoxic activity of this molecule was compared to novel, 15d-PMJ_2. In non-melanoma skin cancer cells the LC_{50} values for 15d-PGJ_2 were found to be greater than 20 µM for A431 and 11.4 µM for JWF2 (Figure 4A, C). In melanoma skin cancer cells, the LC_{50} values for this agent were calculated to be 15.5 µM and 10.5 µM in B16F10 and patient derived primary melanoma respectively (Figure 4B, D). Overall, 15d-PMJ_2 and 15d-PGJ_2 exhibited cytotoxic properties in all skin cancer cell lines tested, however, 15d-PMJ_2 was found to be 3- to 4-times more potent than 15d-PGJ_2 (Figure 4E).

4.3.3 15d-PMJ_2 treatment elicits apoptotic cell death in skin cancer cells.

J-series prostaglandins induce apoptosis in tumorigenic cell lines [76]. As such, we sought to test the mechanism of cell death associated with 15d-PMJ_2 adminstration by measuring caspase-3/7 activity. In JWF2 and A431 NMSC cells, exposure to 5 µM 15d-PMJ_2 led to an approximate 600 and 1000 fold increase in caspase-3/7 activity respectively, when compared to vehicle (Figure 5). Furthermore, melanoma cell lines treated with 15d-PMJ_2 exhibited 400- and 900- fold increase in caspase-3/7 activity respectively, when compared to vehicle (Figure 5). These data demonstrated that 15d-PMJ_2 is a potent inducer of apoptotic cell death in skin cancer cell lines.

4.3.4 15d-PMJ_2 demonstrates preferential cytotoxicity toward tumorigenic skin cells.

To examine whether 15d-PMJ_2 preferentially targets tumor cells, tumorigenic (A431, JWF2 and B16F10) and non-tumorigenic (HaCaT, C-50 and Melan-A) skin cells were treated with increasing concentrations of 15d-PMJ_2 and viability was assessed by conducting MTS assays. Tumorigenic A431 keratinocytes were more susceptible to 15d-PMJ_2 cytotoxicity as reflected by a 53% and 83% reduction in viability at 5 µM and 10 µM respectively, whereas a minimal reduction in viability (5% at 5 µM and 8% at 10 µM) was observed at the same concentration in HaCaT cells (Figure 4.4A). In tumorigenic JWF2 cells, 5 µM and 10 µM exposure to 15d-PMJ_2 led to a 77% and 99% reduction in viability, while in non-tumorigenic C-50 cells, a 21% and 64% reduction in cell viability respectively, was observed (Figure 4.4B). Similarly, B16F10 melanoma cells were preferentially targeted by 15d-PMJ_2 with a 64% and 90% decrease in viability at 5 µM and 10 µM respectively, compared to Melan-A cells whose survival increased at 5µM and decreased by 24% at the 10 µM concentration (Figure 4.4C). At the 5 µM concentration, the fold difference in cytotoxicity between tumorigenic and non-tumorigenic cell lines was found to be 2 (A431), 39 (JWF2) and 3.6 (B16F10), providing strong evidence for induction of selective toxicity by 15d-PMJ_2 (Figure 4.4).

4.3.5 15d-PMJ_2 selectively induces apoptosis in tumorigenic skin cells.

To investigate whether 15d-PMJ_2 (5 µM) selectively induces apoptosis, caspase-3 and PARP cleavage was examined by Western blot in tumorigenic and non-tumorigenic cell lines. Our results showed that 15d-PMJ_2 markedly increased caspase-3 and PARP cleavage in A431 cells while caspase-3 and PARP cleavage was not detected in HaCaT cells (Figure 4.5A). A prominent increase in the cleavage of caspase-3 and PARP was also observed in B16F10 melanoma cells

while Melan-A cells treated under identical conditions showed no significant caspase or PARP cleavage (Figure 4.5B). Furthermore, arachidonic acid derived 15d-PGJ_2, exhibited significantly less PARP and caspase-3 cleavage in tumorigenic A431 and B16F10 compared to its ethanolamide conjugated counterpart thereby supporting our previous observation that 15d-PMJ_2 exhibits greater potency than 15d-PGJ_2. Collectively, these data indicate that 15d-PMJ_2 preferentially causes apoptotic cell death in tumorigenic compared to non-tumorigenic skin cells.

4.3.6 Solid tumors treated with 15d-PMJ_2 exhibit retarded growth, decreased mass, and increased tumor cell death.

To evaluate the anti-tumor effect of 15d-PMJ_2 *in vivo*, C57BL/6 mice allografted with B16F10 tumors were dosed with 0.5 mg/kg of 15d-PMJ_2, PBS or tumors were left untreated for 5 consecutive days. Animals dosed with 0.5 mg/kg displayed significantly reduced tumor size compared to vehicle and untreated. Tumor volumes measured on day 3 were found to be 14.4 mm^3, 57.0 mm^3 and 46.9 mm^3 for 0.5 mg/kg, vehicle and untreated respectively. Differences in tumor volumes reached significance by day 5, with the 0.5 mg/kg dosed group possessing a mean tumor volume of 20.0 mm^3 compared to 115.6 and 85.3 mm^3 in vehicle and untreated tumors (Figure 4.6A). In addition, the mass of resected tumors was found to be dramatically decreased in the 0.5 mg/kg group compared to the control groups (figure 4.6B).

To address the question of whether the anti-tumor effect of 15d-PMJ_2 was caused by inducing tumor cell death, terminal deoxynucleotidyl transferase dUTP nick-end labeling (TUNEL) positive cells were measured in resected tumors. The TUNEL assay employs a fluorescent tagged nucleotide to detect double stranded DNA breaks which are indicative of late stage apoptosis and other forms of cell death. Tumors dosed with 0.5 mg/kg 15d-PMJ_2 displayed a marked elevation of nuclear localized TUNEL fluorescence compared to vehicle and untreated

groups (Figure 4.7). These data coupled with our previous findings demonstrate the anti-tumor activity of 15d-PMJ_2 *in vivo*.

4.4 FIGURES

Figure 4.1: PMD_2 and PGD_2 induce potent apoptotic cell death in melanoma and non-melanoma skin cancer cells.

(A) JWF2 keratinocytes and (B) B16F10 melanoma cells were treated with 2.5 µM, 5.0 µM, 10 µM and 20 µM concentrations of PMD_2 or PGD2 for 24 hours. Cell viability was evaluated by MTS assay according to the manufacturer's instructions. (C) JWF2 and (D) B16F10 cells were treated with 10 µM and 20 µM PMD_2 or PGD2 for 24 hours. The cleavage of PARP was assayed by Western blot analysis. Data and images represent mean ± SEM of three independent experiments and are expressed as percent of untreated group. Data were analyzed using one way ANOVA followed by Tukey's multiple comparison test (* $P < 0.05$, as compared to vehicle treated).

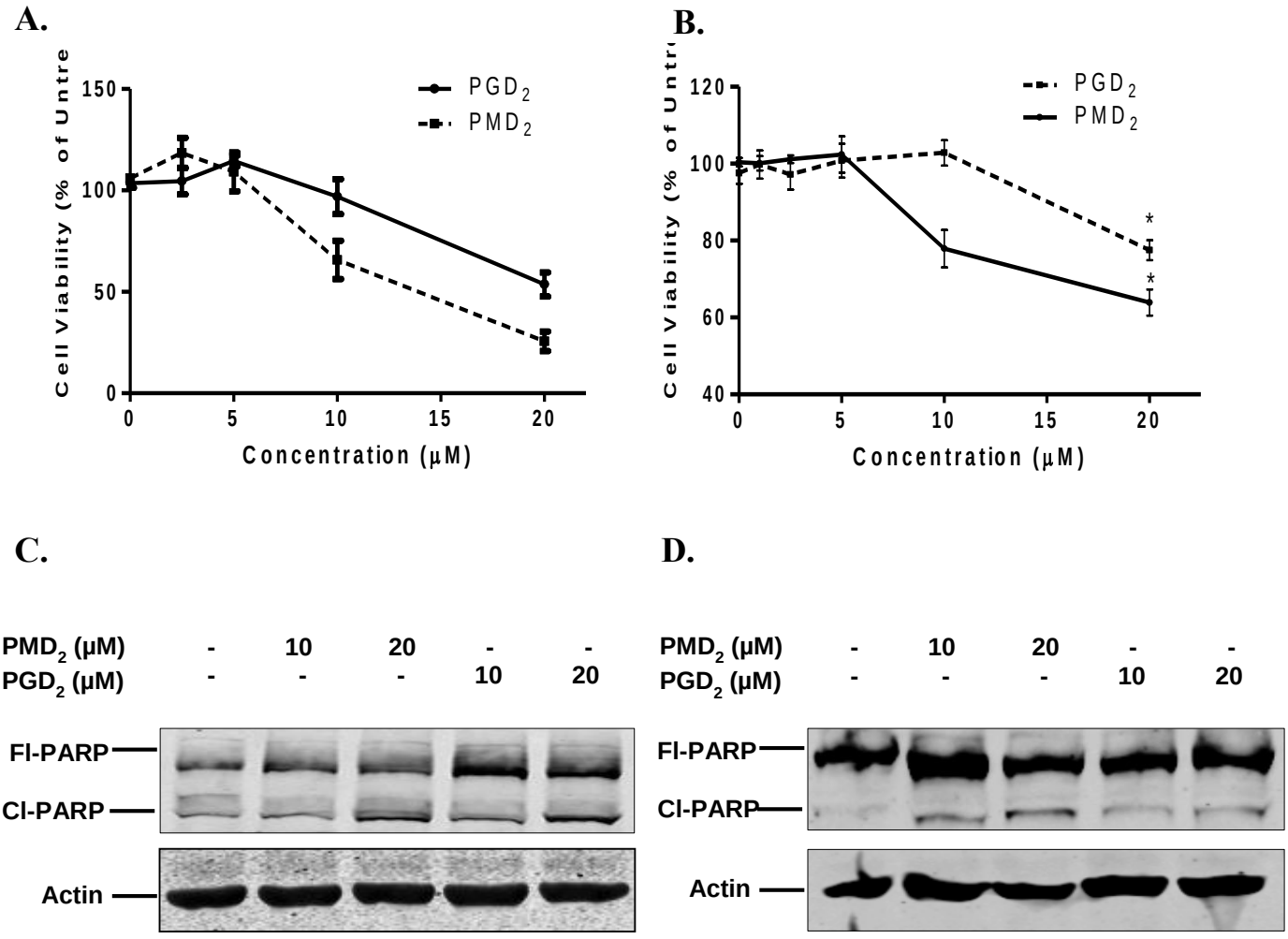
A.
B.
C.
D.
PGD2
PMD2
Cell Viability (% of Untre
Concentration (μM)
PMD2 (μM)
PGD2 (μM)
Fl-PARP
Cl-PARP
Actin

Figure 4.2: 15d-PMJ_2 displays potent cytotoxicity in skin cancer cells.

(A) JWF2 non-melanoma skin cancer cells, (B) B16F10 melanoma cells, (C) A431 non-melanoma skin cancer cells and (D) patient derived primary melanoma cells were treated with 1 µM – 20 µM concentrations of 15d-PMJ_2 of 15d-PGJ_2 for 24 hours. Cell viability was measured by MTS assay and is expressed as percentage of untreated control cells. (E) Tabulated LC_{50} values calculated for 15d-PMJ_2 and 15d-PGJ_2. Data represent mean ± SEM of three independent experiments. *P < 0.05, as compared to 15d-PGJ_2.

A.

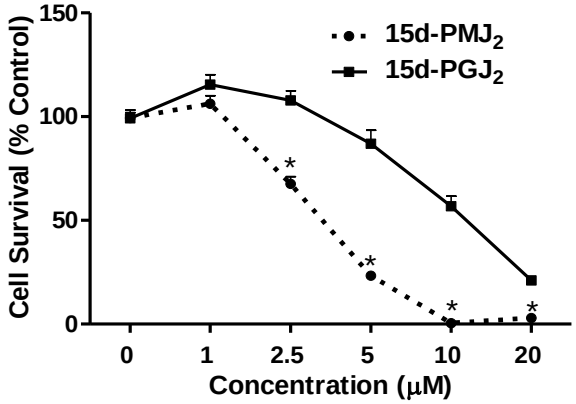

B.

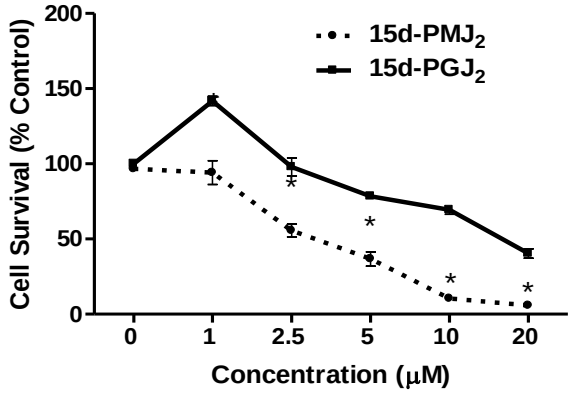

C.

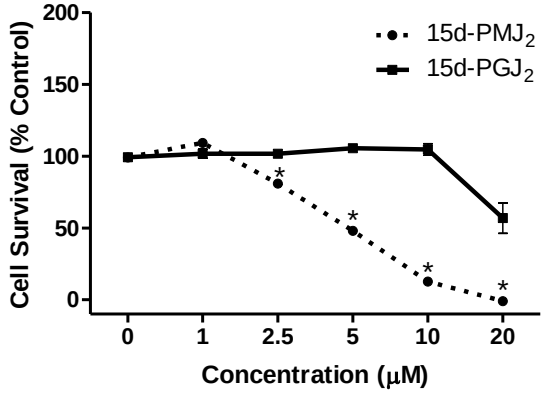

D.

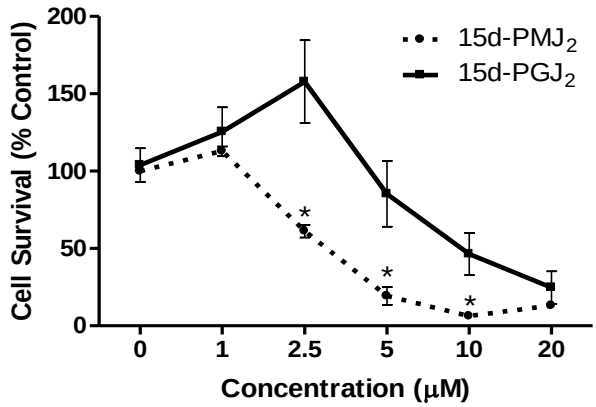

E.

	15d-PMJ$_2$	15d-PGJ$_2$
A431	4.7 μM	> 20 μM
JWF2	3.3 μM	11.4 μM
B16F10	3.3 μM	15.5 μM
Primary Melanoma	3.0 μM	10.5 μM

Figure 4.3: 15d-PMJ_2 induces apoptotic cell death in skin cancer cell lines.

JWF2, A431, B16F10, or patient primary melanoma cells were treated with 5 μM 15d-PMJ_2 or vehicle for 24 hours and caspase-3/7 activity was measured by Caspase-Glo. Values are represented as percent of untreated. *$P < 0.05$, as compared to vehicle.

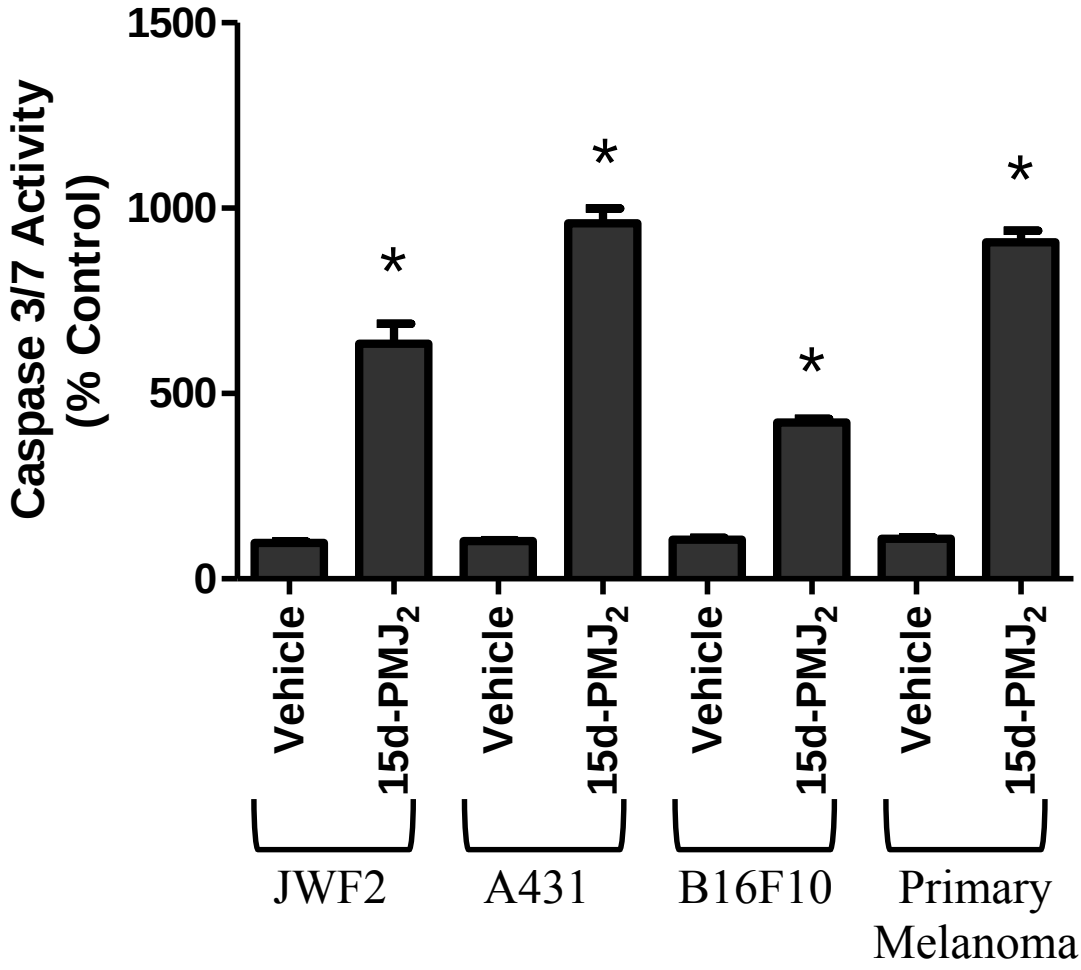
Caspase 3/7 Activity
(% Control)
1500
1000
500
0
*
*
*
*
Vehicle
15d-PMJ2
Vehicle
15d-PMJ2
Vehicle
15d-PMJ2
Vehicle
15d-PMJ2
JWF2
A431
B16F10
Primary
Melanoma

Figure 4.4: 15d-PMJ_2 demonstrates preferential cytotoxicity in tumorigenic skin cancer cells. (A) A431 and HaCaT keratinocytes treated with 1 µM - 20 µM 15d-PMJ_2 or vehicle for 12 hours. (B) JWF2 and C-50 cells were treated with 1 µM - 20 µM 15d-PMJ_2 or vehicle for 24 hours. (C) B16F10 melanoma and Melan-A melanocytes were treated with 1 µM -20 µM 15d-PMJ_2 or vehicle for 24 hours. Cell viability was evaluated by conducting MTS assay and is expressed as percentage of untreated cells. Data represent mean ± SEM of three independent experiments. * $P < 0.05$, when comparing tumor cells to non-tumor cells

A.

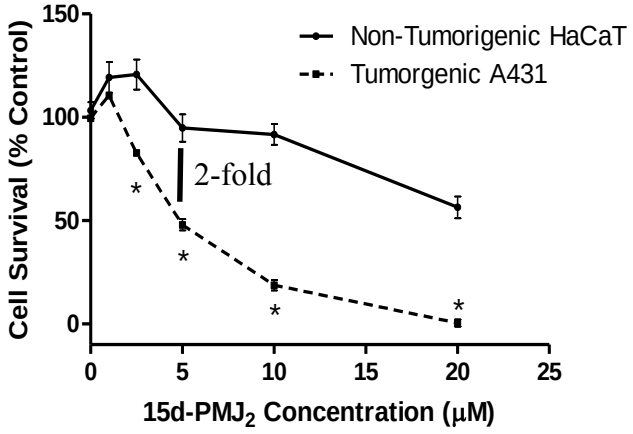
Non-Tumorigenic HaCaT
Tumorgenic A431
2-fold
Cell Survival (% Control)
15d-PMJ2 Concentration (μM)

B.

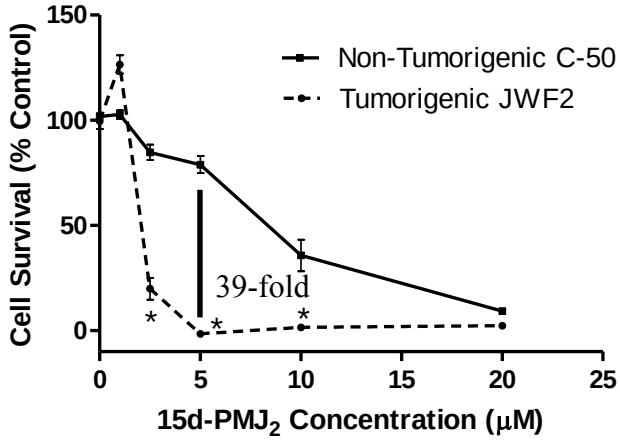
Non-Tumorigenic C-50
Tumorigenic JWF2
39-fold
Cell Survival (% Control)
15d-PMJ2 Concentration (μM)

C.

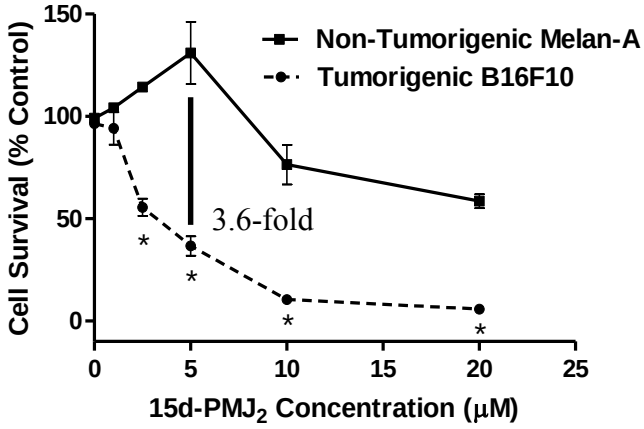
Non-Tumorigenic Melan-A
Tumorigenic B16F10
3.6-fold
Cell Survival (% Control)
15d-PMJ2 Concentration (μM)

Figure 4.5: 15d-PMJ_2 selectively induces apoptosis in tumorigenic skin cells.

(A) A431 and HaCaT cells were treated with vehicle, 5μM 15d-PGJ_2 or 15d-PMJ_2 for 6 and 8 hours. (B) B16F10 and Melan-A cells were treated with vehicle, 5μM 15d-PGJ_2 or 15d-PMJ_2 for 16 and 20 hours. The cleavage of PARP and caspase-3 was assayed by Western blot analysis. Fold increase was determined via densitometry with ImageJ software.

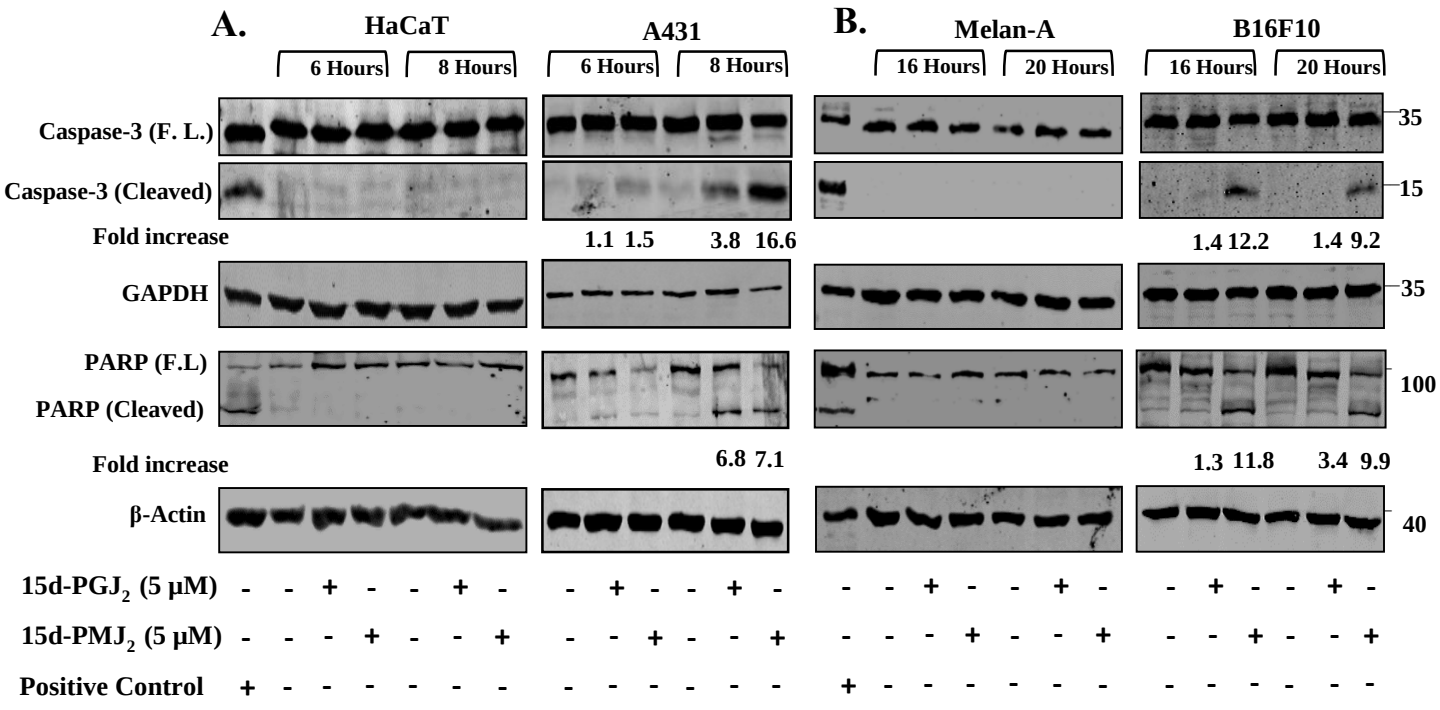
A.
HaCaT
A431
6 Hours
8 Hours
6 Hours
8 Hours
B.
Melan-A
B16F10
16 Hours
20 Hours
16 Hours
20 Hours
Caspase-3 (F. L.)
Caspase-3 (Cleaved)
35
15
Fold increase
1.1 1.5 3.8 16.6
1.4 12.2 1.4 9.2
GAPDH
35
PARP (F.L)
PARP (Cleaved)
100
Fold increase
6.8 7.1
1.3 11.8 3.4 9.9
β-Actin
40
15d-PGJ2 (5 µM)
15d-PMJ2 (5 µM)
Positive Control

Figure 4.6: Treatment with 15d-PMJ_2 inhibits solid melanoma tumor growth *in vivo*.

(A) B16F10 allografted tumors were subcutaneously treated with vehicle (0.1% DMSO in PBS) or 0.5 mg/kg 15d-PMJ_2 and the tumor volume was measured daily. (B) Tumors were resected 24 hours following the final treatment, blotted dry, and weighed. * $P < 0.05$, when comparing 15d-PMJ_2 treated to vehicle.

A.

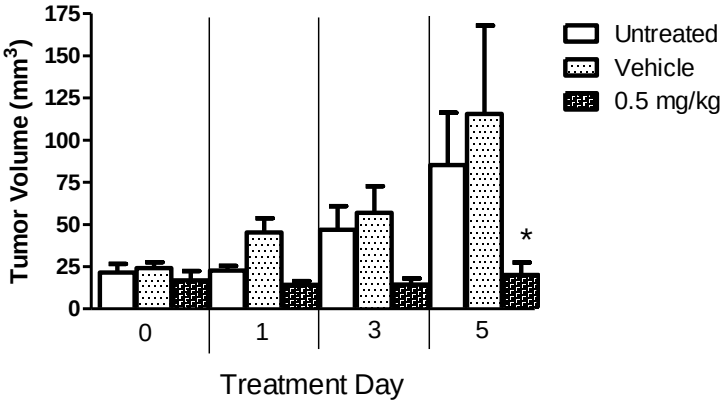
Tumor Volume (mm3)
175
150
125
100
75
50
25
0
0
1
3
5
Treatment Day
Untreated
Vehicle
0.5 mg/kg
*

B.

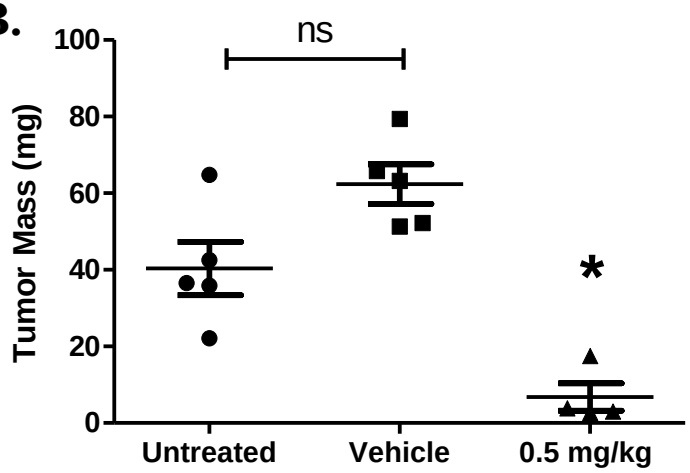
Tumor Mass (mg)
100
80
60
40
20
0
ns
*
Untreated
Vehicle
0.5 mg/kg

Figure 4.7: 15d-PMJ$_2$ induces tumor cell death *in vivo*.

Paraffin embedded tumor sections were analyzed by TUNEL assay for cell death. TUNEL positive cells (green fluorescence) and nuclear DAPI staining (blue fluorescence) were detected by confocal microscopy.

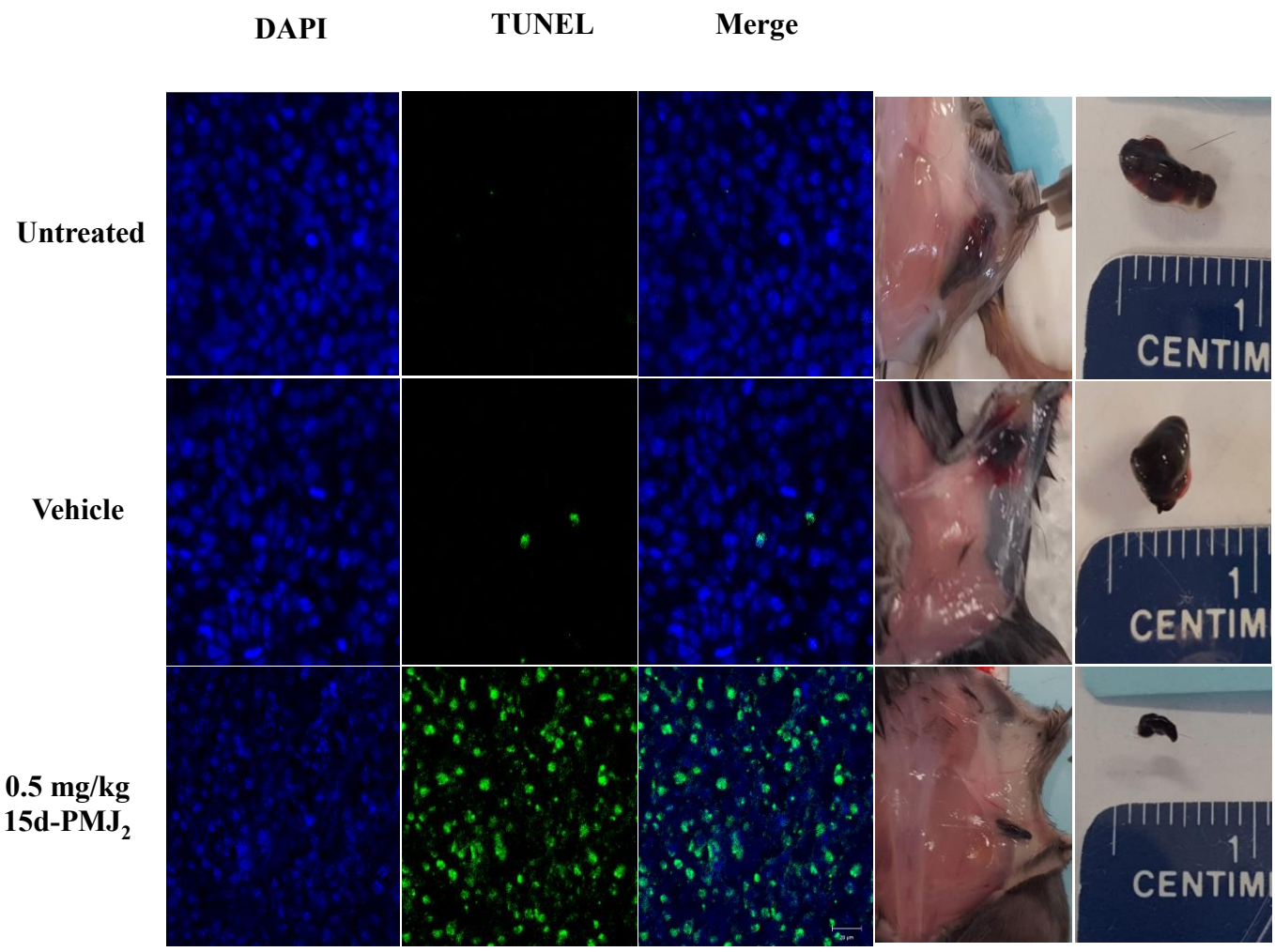
DAPI
TUNEL
Merge
Untreated
Vehicle
0.5 mg/kg
15d-PMJ2
1
CENTIM

4.5 DISCUSSION

With the prevalence of skin cancer on the rise due to increased sun and UV light exposure, the need for novel and effective anti-neoplastic agents is greater than ever. As such, this study was first to biologically characterize the novel AEA metabolite, 15-deoxy-prostamide J_2, and evaluate its anti-cancer activity *in vitro* and *in vivo*. In the present report, we determined that 15d-PMJ_2 induced apoptotic tumor cell death in both non-melanoma and melanoma skin cancer cells. Furthermore, our results showed that 15d-PMJ_2 demonstrated significantly higher potency compared to the non-ethanolamide J-series prostaglandin 15d-PGJ_2. Tumorigenic keratinocytes and melanocytes treated with exogenous PMD_2 (which is the upstream metabolic precursor of 15d-PMJ_2) produced similar levels of cell death and PARP cleavage as 15d-PMJ_2 suggesting that PMD_2 elicits its activity through metabolism to 15d-PMJ_2 (Figure 4.1). Of clinical importance, 15d-PMJ_2 exhibited preferential cytotoxicity and induction of apoptosis in tumorigenic vs non-tumorigenic cells suggesting this agent will produce fewer adverse effects. Lastly, we determined that 15d-PMJ_2 induces cell death in solid tumors using a B16F10 allograft model. Taken together, these results support our hypothesis that 15d-PMJ_2 is a potent and preferential inducer of cell death in skin cancer.

15d-PMJ_2 exhibited striking cytotoxicity against skin cancer cell lines, primary patient melanoma cells, as well as xenograft melanoma tumors suggesting a potential role for this agent in cancer chemotherapeutic regimens. The IC_{50} values of 15d-PMJ_2 treated tumorigenic cells were in the low micromolar range. Our results also demonstrated that 15d-PMJ_2 displayed anti-tumor activity *in vivo*, with a 0.5 mg/kg dose producing a substantial reduction in tumor growth and weight by promoting tumor cell death (Figures 4.6-7). In support of our findings, other research groups reported that arachidonic acid derived 15d-PGJ_2, reduced tumor growth and increased cell

death in leukemia, melanoma and colorectal carcinoma xenografts [77;78]. Another group showed that cholangiocarcinoma xenograft tumor growth was also decreased with AEA treatment, a precursor of 15d-PMJ_2 [79;80]. Furthermore, a non-degradable analog of AEA, methanandamide (met-F-AEA) prevented lung xenograft tumor development [81]. In light of the fact that our group has shown that the cytotoxic effect of AEA is primarily mediated by 15d-PMJ_2 [43], these findings support the assertion that 15d-PMJ_2 most likely prevents tumor growth in various animal models and may potentially curb tumor growth in humans.

Prostaglandins are formed as a result of the metabolism of AA by COX-2 whereas prostaglandin-ethanolamides (prostamides) are produced from the metabolism of AEA by COX-2. However, little is known about the biological differences between these structurally-related molecules. Kozak et. al. found that prostamides possessed significantly longer plasma half-lives and were less subject to metabolic degradation than prostaglandins [82]. Matias et al, established that prostamides of the E, F, and D-series possessed unique pharmacological and biological activity compared to their prostaglandin counterparts as they did not bind to traditional prostaglandin receptors [45]. As a result of these findings, considerable effort is now focused on identifying cellular receptors of prostamide ligands [83;84]. We determined that the activity of 15d-PMJ_2, was similar to 15d-PGJ_2, but that 15d-PMJ_2 was a considerably more potent inducer of cell death and apoptosis. We report that IC_{50} the values calculated for 15d-PGJ_2 were consistently 3-5 times higher than that of 15d-PMJ_2, indicating the superior potency of 15d-PMJ_2. Furthermore, 15d-PGJ_2 only demonstrated the capability to induce apoptotic cleavage of caspase-3 and PARP in NMSC but not melanoma cells, suggesting 15d-PGJ_2 may not be suitable for as an anti-melanoma agent. In agreement with these findings, structure-activity relationship studies carried out by Nicolaou et al. found that ester, amide and alcohol substitutions on the terminal carboxylic

acid of Δ^{12}-PGJ_3 significantly increased J-series prostaglandin potency against leukemia [85]. Like J-series prostaglandins, upstream metabolites PMD_2 and PGD_2, showed differences in killing capacity of tumor cells with potency found to be higher in the prostamide variation. This evidence strongly suggests that 15d-PMJ_2 may interact with distinct cellular targets or possess robust stability compared to 15d-PGJ_2 providing a potential explanation for the differences in activity shown here.

Targeting cancers using agents which display selective tumor cell cytotoxicity results in fewer dose-limiting adverse effects and better overall patient quality of life. This study reports that 15d-PMJ_2 possesses preferential toxicity toward both tumorigenic melanocytes and keratinocytes. We demonstrated previously that the endocannabinoid AEA selectively induced apoptosis in tumorigenic keratinocytes through the formation of J-series prostamides [43]. Furthermore, prostaglandins of the D- and J-series induced apoptosis in tumorigenic but not non-tumorigenic cell lines [86]. Indeed, 15d-PGJ_2 caused cell death in tumorigenic T-cells while possessing limited toxicity in non-tumor T-cells and other normal cell types suggesting differential effects based on drug concentrations and cell type characteristics (16) [87]. At 5 µM, 15d-PMJ_2 was found to induce greater than 50% cell death in tumorigenic keratinocytes and melanocytes whereas no or only partial cell death was reported in non-tumorigenic cells (Figure 4.4). Of perhaps greater importance, 15d-PMJ_2 promoted significant cleavage of pro-apoptotic caspase-3 and PARP in tumorigenic but not non-tumorigenic skin cells (Figure 4.5). Selective tumor cell death through induction of apoptosis provides numerous clinical advantages such as decreased immunogenic response and reduced inflammation. Overall, these findings agree with our earlier reports that AEA preferentially eliminates tumorigenic keratinocytes [88]. Since overt toxicity was not observed in

this or other studies utilizing J-series prostaglandins or cannabinoids [78;79], 15d-PMJ_2 may be a safe and effective agent for cancer treatment.

CHAPTER FIVE: THE ANTI-TUMOR ACTIVITY OF 15D-PMJ_2 IS CONFERED THROUGH ER-STRESS MEDIATED CALCIUM CHANNEL ACTIVATION.

5.1 ABSTRACT

Our lab previously demonstrated that the endocannabinoid, AEA, induces apoptotic cell death in an ER- and oxidative stress-dependent manner without engagement of the cannabinoid receptors. We also determined that the cytotoxic activity of AEA was primarily mediated by its metabolic product, 15d-PMJ_2. Therefore, we sought to elucidate the mechanism of 15d-PMJ_2 mediated apoptotic cell death. The data show that ER-stress markers, phospho-PERK and CHOP10 were required for 15d-PMJ_2 mediated apoptosis and were also selectively upregulated in tumor but not non-tumor skin cancer cells. We also observed increased phosphor-PERK and CHOP10 in allografted melanoma tumors *in vivo*. In cultured skin cancer cells, 15d-PMJ_2 also increased intracellular Ca^{2+} whose elevated levels were important for initiation of ER-stress mediated cell death. Although 15d-PMJ_2 significantly increase oxidative stress, this process was not required for tumor cell death. 15d-PMJ_2 contains and electrophilic α,β-unsaturated carbonyl group on its cyclopentenone ring that readily adducts to free sulfhydryls of cellular proteins. As such, we examined the role of this moiety in cell death by synthesizing a neutral analog of 15d-PMJ_2 that lacked the double bond. Our results showed that neutral-15d-PMJ_2 did not cause cell death at doses at which 15d-PMJ_2 was lethal. We also report that 15d-PMJ_2 induced oxidative stress, ER stress and Ca^{2+} mobilization was also regulated by the electrophilic double bond. Based on these findings, the ability of 15d-PMJ_2 to selectively induce ER stress mediated tumor cell apoptosis indicates that this agent may be a valuable addition to current chemotherapeutic regimes for skin cancer.

5.2 INTRODUCTION

The ER is a major site for folding of secreted, transmembrane and organelle localized proteins. The ER provides an ideal environment for protein due to the presence of chaperones that catalyze oxidative-, calcium-, disulfide-mediated bond formation. Under some circumstances, the number of proteins which require folding assistance will inundate the protein folding machinery of the ER and elicit what is known as the unfolded protein response (UPR) [46;47]. In attempt to restore homeostasis, HSP70/GRP78 (BiP), a multifunctional ER-chaperone, localizes to the unfolded proteins within the ER lumen and releases three distinct UPR sensors, to which BiP was previously attached. When BiP dissociates from the ER-membrane localized sensors, PERK, ATF6, and IRE1α, the ER-stress signaling cascade is activated [48]. In tumor cells, the decision to resolve the unfolded insult or undergo apoptosis is dependent on the intensity and duration of the ER stress signal. During short bouts of ER-stress, IRE1, PERK and ATF6 activate signal transduction pathways that culminate in increased peptide folding and protein degradation responses with the goal of restoring ER homeostasis and promoting survival [49]. However, during times of prolonged ER-stress signaling, the UPR sensors upregulate the expression of pro-apoptotic transcriptional factor C/EBP homologous protein (CHOP10)/growth arrest and DNA damage inducible 153 (GADD153), leading to cell death [89].

Recently, cellular death inducer protein-1 (CDIP1) was found to be a key regulator of ER-stress mediated apoptosis *in vitro* and *in vivo* [50]. Indeed, CDIP1 was found to act as signal transducer during the ER stress response through its complexation with the integral ER membrane protein, B-cell receptor-associated protein 31 (BAP31). BAP31 is an important participant in ER-mitochondria induced death as it has been reported that the cleavage of BAP31 into p20-BAP31 initiates apoptotic signals from the ER by increasing IP_3 receptor mediated Ca^{2+} release, leading

to mitochondrial Ca^{2+} uptake and subsequent apoptosis [90]. Furthermore, complex formation between CDIP1 and p20-BAP31 has been demonstrated to induce caspase-8 activation and sequestration of pro-survival B-cell lymphoma-2 (Bcl-2) proteins [50]. As such, BAP31 leads to transduction of signals between the ER and mitochondria in ER-stress mediated cell death.

The ER and mitochondria serve as the major Ca^{2+} reservoirs within the cell due to the essential role Ca^{2+} plays in maintaining a favorable environment for protein folding and cellular metabolism. In the ER, Ca^{2+} gradients needed for oxidative protein folding are established by the sarco/endoplasmic reticulum Ca^{2+}-ATPase (SERCA) while excess calcium is pumped out of the ER by the ryanodine (RyR) and inositol 1,4,5-triphosphate receptors (IP_3R). Similarly, Ca^{2+} that is required for cellular metabolism and ATP production is pumped into the outer mitochondrial membrane through the voltage-dependent anion-selective channel (VDAC) and into the mitochondrial lumen through the mitochondrial calcium uniporter (MCU). Slow discharge of Ca^{2+} from the mitochondria occurs through the VDAC, while large bursts of Ca^{2+} can exit during apoptosis through the mitochondrial permeability transition pore (mPTP). In addition, Ca^{2+} flux between these two organelles occurs at specialized ER-mitochondrial interfaces known as mitochondrial-associated ER membranes (MAMs) [91]. Indeed, the ER-IP_3R and mitochondrial-VDACs located within the MAM are anchored to one another through a tethering protein known as cytosolic chaperone glucose-regulated protein 75 (GRP75) [92]. Under normal circumstances, IP_3R-mediated Ca^{2+} transmission from the ER to the mitochondria supports ATP production and is under control of the ER chaperone Sigma-1 receptor (Sig-1R) [93]. During prolonged ER stress, sustained Ca^{2+} release may occur through interactions of IP_3R with numerous ER stress protein effectors including ER-membrane associated oxidoreductase-α (ERO1α), p20-BAP31, and Sig1R [55;94]. Within the mitochondria, elevated levels of Ca^{2+} promote several different processes

including generation of ROS and sensitization of cyclophilin D, which contributes to the opening of the mPTP [58]. Stimulation of the mPTP results in the bolus release of cytochrome c, a crucial event in formation of the apoptosome, that causes irreversible induction of the intrinsic apoptotic pathway. Thus, Ca^{2+} transfer between the ER and mitochondria plays a vital role in regulating ER-stress mediated apoptotic cell death.

Numerous lines of evidence demonstrate that ER stress facilitates ROS production and reciprocally, ROS activates ER stress induction [95;96]. Under normal conditions, oxidative protein folding occurring within the ER carried out by protein disulfide isomerase (PDI) and ERO1α, is believed to contribute approximately 25% of ROS generated by the cell [97]. In fact, the misfolding of proteins under stress conditions is reported to perturb ER redox status and generate ROS by influencing ERO1α and PDI activity leading to decreased levels of reduced glutathione [98]. In addition, the depletion of Ca^{2+} from the ER has also been reported to induce ROS by causing mitochondrial dysfunction, decreased neutralization of ROS and stimulating NO synthesis [99;100]. Hence an intimate relationship between protein folding, ROS, and Ca^{2+} flux exists.

Our group previously demonstrated that the upstream metabolite of 15d-PMJ_2, AEA, induced ER- and oxidative-stress which was required for apoptosis [88]. As such, we hypothesize that the anti-tumor activity of 15d-PMJ_2 is reliant on these mechanisms, however, the role of these pathways on cell death is unclear. Preliminary data from our group also suggested that treatment with AEA increased intracellular Ca^{2+} levels and based on this finding, we investigated the importance of Ca^{2+} signaling on cell death induced by 15d-PMJ_2. Furthermore, it was reported that J-series prostaglandins confer induction of ROS and cell death through an electrophilic cyclopentenone ring, known to react with cysteine containing residues of proteins [101]. To

evaluate the significance of this moiety in 15d-PMJ_2, a neutral analog (neutral-5d-PMJ_2) was synthesized and compared to the fully active form.

5.3 RESULTS

5.3.1 15d-PMJ_2 induces ER-stress *in vitro* and *in vivo.*

The ER stress pathway has been identified as a chemotherapeutic target that can confer selective toxicity [102]. Previous work conducted by our group demonstrated that AEA induced ER-stress in tumorigenic keratinocytes and that the cytotoxicity of AEA was mediated by its metabolic product 15d-PMJ_2. To determine the effect of 15d-PMJ_2 on ER-stress production in tumorigenic skin cells, we measured the expression of the early-phase ER-stress marker, PERK, and the late ER-stress/apoptotic marker, CHOP10 by Western blot analysis. During ER stress, PERK becomes activated by undergoing homodimerization and autophosphorylation. Furthermore, insurmountable or prolonged ER stress increases the expression of pro-apoptotic CHOP10. As such, PERK phosphorylation and CHOP10 expression were examined as indicators of ER stress. ER stress was selectively activated by 15d-PMJ_2 in tumorigenic but not non-tumorigenic skin cells as demonstrated by the notable increase in phospho-PERK levels in tumorigenic A431 and B16F10 cells (Figure 5.1A, B). Moreover, expression of the cytotoxic ER stress protein, CHOP10, was also significantly increased in tumorigenic but not non-tumorigenic cells (Figure 5.1A, B). Arachidonic acid derived 15d-PGJ_2 was also found to upregulate both ER stress proteins selectively in the tumorigenic cell lines although 15d-PMJ_2 elicited greater induction of cytotoxic CHOP10 (Figure 5.1A, B). To investigate the whether 15d-PMJ_2 generates ER-stress *in vivo*, phospho-PERK and CHOP10 levels were examined in solid tumors treated with 0.5 mg/kg 15d-PMJ_2. 15d-PMJ_2 promoted ER stress as demonstrated by significant increases both phospho-PERK and CHOP10 content in the tumors (Figure 5.1C, D). As anticipated, none of the treatments altered the levels of total PERK expression in the tumors.

5.3.2 Oxidative stress is generated by 15d-PMJ_2 in skin cancer cells.

In addition to the ability of J-series prostanoids to promote tumor cell death through propagation of ER-stress, many groups have proposed that redox alterations caused by these biomolecules are a possible mechanism of apoptosis [76]. Furthermore, 15d-PGJ_2 has been shown to induce intracellular ROS and oxidative stress by decreasing glutathione levels, inhibiting mitochondrial complex 1 and generating reactive aldehydes. To evaluate if 15d-PMJ_2 induces oxidative stress, tumorigenic JWF2 and B16F10 cells were treated with 5 μM 15d-PMJ_2 and oxidative stress was examined by measuring fluorescence of the redox sensitive probe, DCFDA. 15d-PMJ_2 increased DCFDA fluorescence by roughly 380% in JWF and 450% in B16F10 compared to vehicle treated cells (Figure 5.2A, B). In accordance with our previous results, oxidative stress from 15d-PMJ_2 was also found to be significantly higher than that of 15d-PGJ_2.

5.3.3 ER-but not oxidative-stress is required for 15d-PMJ_2-mediated apoptotic cell death.

Some groups have reported that oxidative stress generated by the arachidonic acid derived 15d-PGJ_2 is required for cell death, while our group has reported that both ER- and oxidative stress were required for AEA-mediated cell death [43;76]. To test if the generation of ER- and/or oxidative-stress, is required for 15d-PMJ_2-mediated apoptosis the use of an antioxidant and two ER-stress inhibitors were employed. ER-stress was blocked by using the pharmacological ER-stress inhibitors, salubrinal and 4-phenylbutrate (4-PBA), while oxidative stress was inhibited by using trolox. Salubrinal elicits its activity by selectively inhibiting PP1/GADD34 thereby preventing the dephosphorylation of phospho-eIF2α. Dephosphorylation of eIF2α is required to allow protein translation to resume. In constast, PBA inhibits ER-stress by acting as a chemical chaperone that enhances resolution of unfolded proteins [103;104]. Consistent with previous

findings that ER-stress is a key regulator of AEA mediated apoptosis, both salubrinal and to a greater extent, 4-PBA significantly prevented caspase-3/7 activity in A431, B16F10 and JWF2 skin cancer cells treated with 15d-PMJ_2 (Figure 5.3A-C). Next we examined the role of oxidative stress in 15d-PMJ_2 induced death using trolox a water-soluble vitamin E analog that exhibits anti-oxidant activity by neutralizing free radicals. In JWF2 and B16F10 cells pretreated with trolox, a significant reduction in DCFDA fluorescence occured. However, trolox did not prevent caspase-3/7 activity or tumor cell death (Figure 5.4A-F). These results indicate that ER stress but not oxidative stress is required for 15d-PMJ_2 cytotoxicity.

5.3.4 Induction of cell death by PMD_2 and PGD_2 is mediated by ER-stress but not DP or PPAR gamma receptors.

D-series prostaglandins spontaneously undergo non-enzymatic conversion to J-series prostaglandins by dehydration. Moreover, this non-enzymatic reaction form an equilibrium in which J-series prostaglandins can also rehydrate to produce D-series prostaglandins [19]. As such, we investigated the antineoplastic mechanism of upstream metabolite, PMD_2. To test whether ER-stress was required for PMD_2-mediated cell death in JWF2 and B16F10 tumor cells, ER-stress was blocked by 30-minute pretreatment with salubrinal and GSK2606414 (a small molecule inhibitor) followed by treatment with 20 µM PMD_2 or PGD_2 (the arachidonic acid counterpart). GSK2606414 prevents the propagation of ER-stress by inhibiting the phosphorylation of eIF2α by PERK [105]. In JWF2 and B16F10 cells, both salubrinal and GSK2606414 significantly reduced cell death induced by both PMD_2 and PGD_2 confirming the role of ER-stress in D-series prostanoid activity (Figure 5.5A, B).

PGD_2 is a well-known agonist of D type prostanoid receptors [subtype 1 (DP1) and 2 (DP2)], whereas the metabolic product of PGD_2, 15d-PGJ_2, is widely established to be an

endogenous ligand of peroxisome proliferator activated receptor gamma (PPARγ). The DP1 and DP2 receptors are G-protein coupled receptors while PPARγ is a nuclear receptor. DP1, a Gαs coupled receptor, and DP2 a Gi coupled receptor, are known to regulate the anti-inflammatory effect of PGD_2, however the effect of these receptors on cancer cell progression remains widely unknown [106-108]. 15d-PGJ_2 is thought to covalently bind to a free cysteine residue within the binding pocket of PPARγ, causing nuclear localization, heterodimerization with the retinoic acid receptor (RXR) and expression of target genes [36]. In the context of cancer, there is increasing evidence that PPARγ signaling may be important in regulating processes including inflammation, proliferation, differentiation, and apoptosis [109-111]. As such, we examined the requirement for DP1, DP2 and PPARγ receptors in PGD_2 and PMD_2-mediated cell death. To investigate the role of DP1 and DP2 receptors on the anti-tumorigenic properties of PMD_2 and PGD_2, the use of selective receptor antagonists BWA868C (BW, DP1), BAYU3405 (BAY, DP2) were employed [26;76]. JWF2 cells were pretreated with BW (1μM) and BAY (10μM) followed by treatment with PMD_2 or PGD_2. Pretreatment with DP receptor antagonists did not reverse the cytotoxic effects of either PMD_2 or PGD_2 suggesting that DP receptors are not required for the anti-cancer activity (Figure 5.5C). Likewise, to determine the role of PPARγ on the cytotoxic properties of PGD_2 and PMD_2, JWF2 cells were pretreated with 5 or 20 μM of the irreversible receptor antagonist, GW9662 [112]. Similarly, pretreatment with GW9662 caused no change in the cytotoxic behavior of PMD_2 or PGD_2 suggesting that the anti-cancer activity of these molecules is not mediated by PPARγ (Figure 5.5D).

5.3.5 ER-stress mediated calcium channel activation is essential for 15d-PMJ_2 activity.

It has been established that ER Ca^{2+} concentration modulates cellular sensitivity to apoptosis [113]. Furthermore, Ca^{2+} efflux during stress from the ER lumen into cytosol or mitochondria has been demonstrated to facilitate the apoptosis [57]. As such, we sought to determine if ER-stress mediated Ca^{2+} flux is involved in 15d-PMJ_2 cytotoxicity. To characterize the influence of 15d-PMJ_2 on intracellular Ca^{2+} flux, JWF2 and B16F10 cells were treated with 15d-PMJ_2 and intracellular Ca^{2+} was measured. 15d-PMJ_2 caused a significant increase in intracellular Ca^{2+} compared to control (Figure 5.6A, B). To evaluate whether the 15d-PMJ_2-mediated increase in intracellular Ca^{2+} was due to the activation of IP_3, a selective IP_3 receptor inhibitor, 2-aminoethoxydiphenyl borate (2-APB), and a non-selective calcium channel inhibitor, ruthenium red (RR), were employed. Pretreatment with both 2-APB and RR caused a nearly complete reversal of the 15d-PMJ_2-mediated increase in intracellular Ca^{2+} suggesting that the intracellular calcium is originated from IP_3 ER stores (Figure 5.6C, D). It has been reported that ER-stress associated pathway proteins such as the PERK and BAP31 mediate pro-apoptotic ER Ca^{2+} efflux [114;115]. To determine if induction of ER-stress by 15d-PMJ_2 was responsible for the increase in intracellular Ca^{2+}, ER-stress was blocked with salubrinal or GSK2606414 followed by treatment with 15d-PMJ_2. NMSC and melanoma skin cancer cells pretreated with salubrinal and GSK2606414 displayed significantly lower intracellular Ca^{2+} levels compared to cells treated with 15d-PMJ_2 (Figure 5.6E, F). This data provides evidence that ER stress activation is necessary for increasing intracellular Ca^{2+} content. To determine whether increased intracellular Ca^{2+} was needed for cell death, the viability of NMSC and melanoma skin cancer cells was measured following pretreatment with calcium channel blockers 2-APB and RR. RR and 2-APB abrogated

15d-PMJ_2-mediated cytotoxicity in JWF2 cells (Figure 5.6G). In addition, 2-APB and RR reversed 15d-PMJ_2 cytotoxicity by 60-to-70% in B16F10 cells (Figure 5.6H).

5.3.6 Initiation of apoptotic cell death by 15d-PMJ_2 is mediated by the cyclopentenone double bond.

Thus far, we have demonstrated that 15d-PMJ_2 treated tumor cells undergo apoptosis involving an ER-stress-calcium channel-dependent mechanism. However, we have yet to examine the molecular mechanisms responsible for this activity. Indeed, this information would provide valuable insight toward synthesizing more potent derivatives. As such, our group undertook the task of identify the specific molecular pharmacophore associated with 15d-PMJ_2 mediated activity.

J-series prostaglandins, are known to covalently modify cysteine residue present on proteins through interaction with the cyclopentenone moiety [101]. We hypothesized that through this mechanism, 15d-PMJ_2 may confer its anti-tumor activity by activating the ER stress pathway. Hence, the molecular mechanism by which 15d-PMJ_2 elicits anti-tumor activity was examined by investigating the role of the double bond contained within the cyclopentenone ring of the molecule. To address this question, a neutral analog of 15d-PMJ_2 (neutral-15d-PMJ_2; Figure 5.7A) lacking the reactive double bond was synthesized (Materials and Methods section). To determine the role of this reactive double bond on cytotoxicity, A431, JWF2, B16F10 and patient-derived melanoma cells were treated with increasing concentrations of neutral-15d-PMJ_2 and compared to 15d-PMJ_2. Neutral-15d-PMJ_2 did not decrease cell viability in A431, B16F10 or patient-derived melanoma cells, but decreased survival in JWF2 cells at 20 μM. In contrast, concentrations of 15d-PMJ_2 greater than 1 μM significantly decreased viability in each cell line (Figure 5.7B-E). Next, we sought to determine whether neutral-15d-PMJ_2 induces apoptosis in skin cancer cells by measuring caspase-3/7 activity. In A431, JWF2, and B16F10 cells, 5 μM neutral-15d-PMJ_2 caused no

significant increase in caspase-3/7 activity compared to vehicle treated cells. This was in stark comparison to 15d-PMJ_2 which increased caspase-3/7 activity by 501%, 372%, and 768% in A431, JWF2, and B16F10 cells, respectively.

5.3.7 ER stress, oxidative stress and calcium mobilization are mediated by the cyclopentenone double bond of 15d-PMJ_2.

It has been demonstrated that the double bond structure in arachidonic acid derived 15d-PGJ_2 promotes oxidative stress through covalent interactions with cysteine-containing proteins in an ordered fashion [116]. The role of the cyclopentenone double bond in ER stress however, has not been investigated. To determine the role of the reactive double bond in the generation of ER- and oxidative-stress, JWF2 and B16F10 skin cancer cells were probed for ER-and oxidative-stress markers following treatment with 5 μM neutral-15d-PMJ_2 or 15d-PMJ_2. 15d-PMJ_2 and neutral 15d-PMJ_2 caused a significant increase in DCFDA fluorescence compared to vehicle cells, however 15d-PMJ_2 was more potent than the neutral derivative (Figure 5.8A, B). In addition, the phosphorylation of PERK and the expression of CHOP10 were significantly blunted in neutral-15d-PMJ_2 compared to 15d-PMJ_2 cells, demonstrating the requirement for the reactive double bond in the generation of ER-stress (Figure 5.8C, D). Lastly, we assessed calcium flux in the presence of neutral-15d-PMJ_2 and found that accumulation of intracellular Ca^{2+} was also dependent on the double bond (Figure 5.8E, F).

5.3.8 15d-PMJ_2 induces ER-stress associated CDIP1-BAP31 signaling.

To further characterize the mechanism of 15d-PMJ_2-mediated ER stress-apoptosis, additional modulators of this cytotoxic pathway were examined. CDIP1 has been identified as a p53 transcriptional target that is a key transducer of ER stress apoptosis signals [117]. In the

presence of ER stress, CDIP1 expression is upregulated and the protein dimerizes with constitutively expressed BAP31. BAP31-CDIP complexes are necessary for BAX oligomerization and apoptosis via caspase-8 [50]. In addition, caspase-4 is known to be selectively cleaved as a consequence of ER stress initiated apoptosis [118]. 15d-PMJ_2, but not neutral 15d-PMJ_2 significantly upregulated the expression of CDIP1 and cleavage of caspase-4 (Figure 5.9A). Furthermore, CDIP1 was observed to co-localize with Bap31 whereas the neutral molecule failed to promote co-localization (Figure 5.9B). Moreover, the cleaved form of caspase 8 was selectively induced by 15d-PMJ_2 rather than its neutral analog. These results provide the first evidence that the cyclopentenone double bond is required for expression of CDIP1 and subsequent propagation of ER-stress apoptotic signals.

5.4 FIGURES

Figure 5.1: 15d-PMJ_2 induces ER-stress *in vitro* and *in vivo*.

(A) A431 and HaCaT cells were treated with vehicle, 5μM 15d-PGJ_2 or 5 μM15d-PMJ_2 for 2 (upper panel) and 4 hours (lower panel). (B) B16F10 and Melan-A cells were treated with vehicle, 5μM 15d-PGJ_2 or 15d-PMJ_2 for 6 (upper panel) and 8 (lower panel) hours. The phosphorylation of PERK and expression of CHOP10 was assayed by Western blot analysis. Fold increase was determined via densitometry with ImageJ software. (C) CHOP10, total-PERK, and phospho-PERK expression was evaluated in B16F10 allografted tumors by conducting immunohistochemical analysis. (D) Histograms show the mean optical density of CHOP10, phospho-PERK, and total PERK analyzed using ImageJ software. Data are presented as mean ± SEM and represent three independent experiments. * $P < 0.05$, when comparing to vehicle.

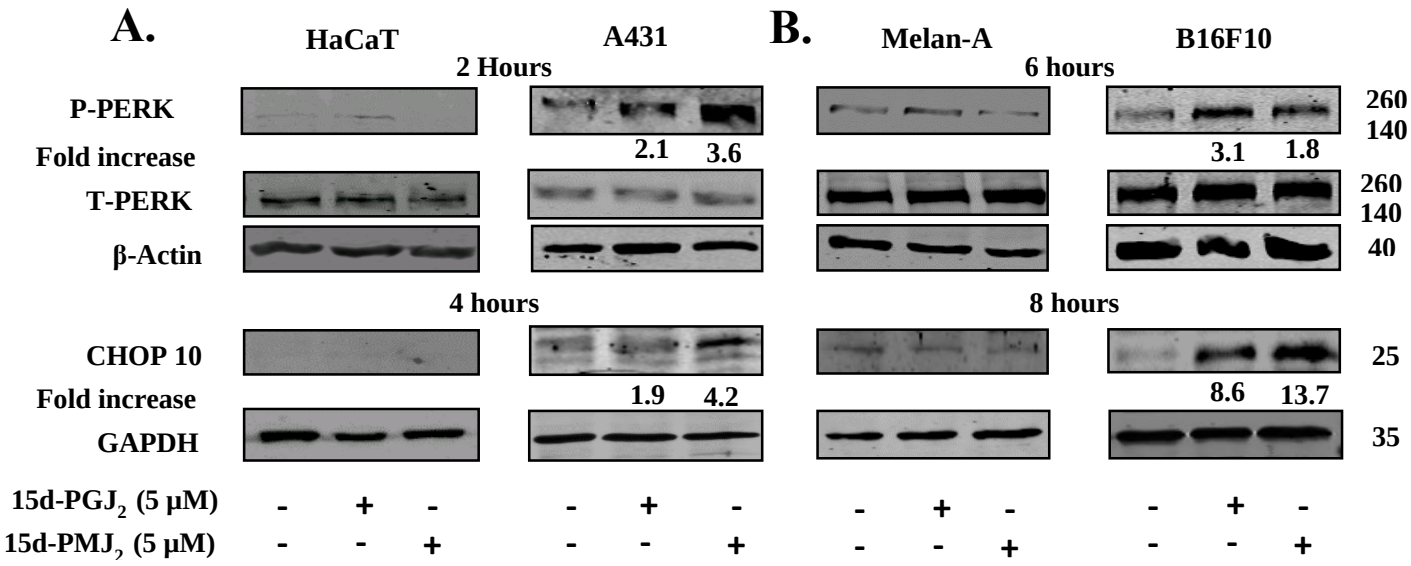
A.
HaCaT
A431
2 Hours
P-PERK
Fold increase
2.1
3.6
T-PERK
β-Actin
4 hours
CHOP 10
Fold increase
1.9
4.2
GAPDH
B.
Melan-A
B16F10
6 hours
3.1
1.8
8 hours
8.6
13.7
260
140
260
140
40
25
35
15d-PGJ2 (5 μM)
15d-PMJ2 (5 μM)

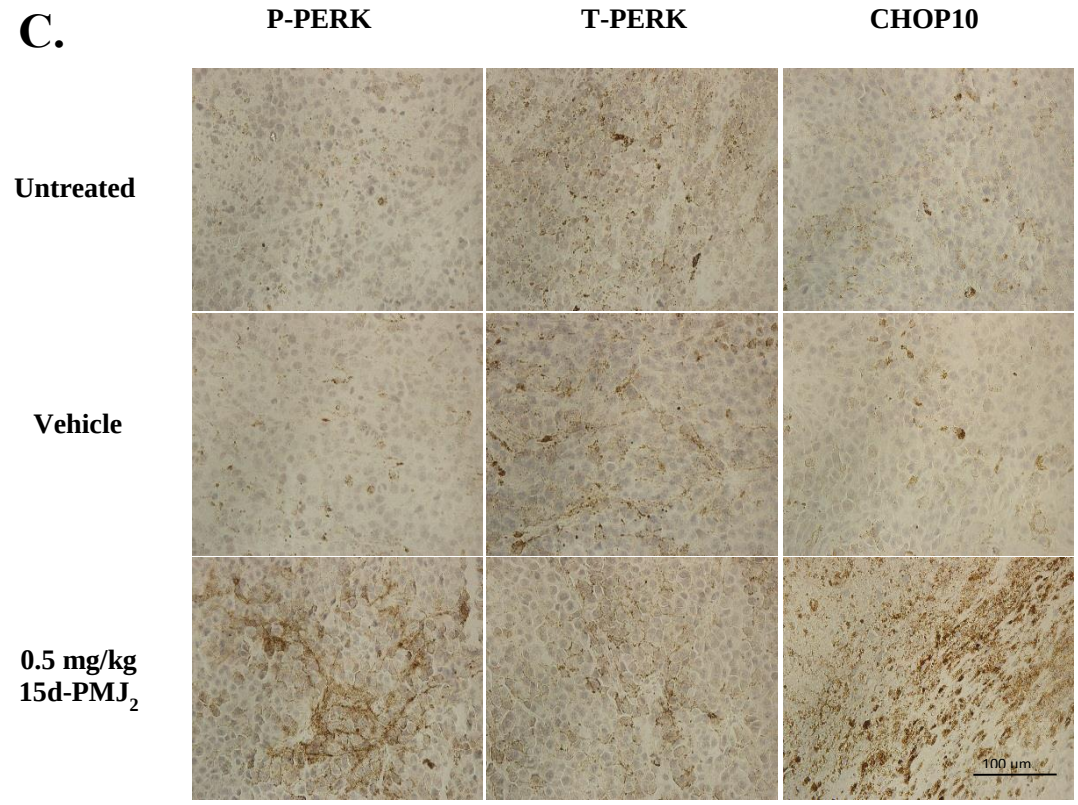
C.
P-PERK
T-PERK
CHOP10
Untreated
Vehicle
0.5 mg/kg
15d-PMJ2
100 μm

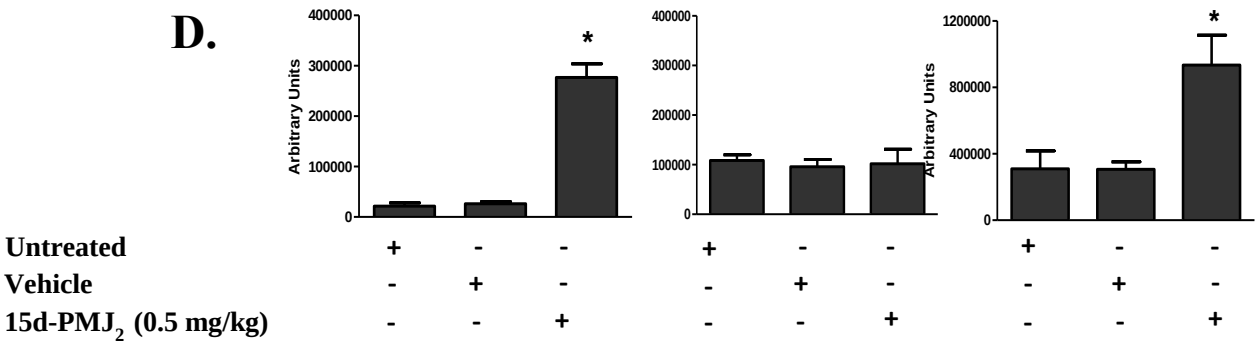
D.
Arbitrary Units
400000
300000
200000
100000
0
1200000
800000
400000
*
Untreated
Vehicle
15d-PMJ2 (0.5 mg/kg)

Figure 5.2: 15d-PMJ_2 induces oxidative stress.

(A) JWF2 and (B) B16F10 cells were treated with 5 μM 15d-PMJ_2, 15d-PGJ_2 or vehicle for 2 hours. Oxidative stress was measured using flow cytometry with CM-H_2DCFDA reagent. Fluorescence was measured as a percent increase from untreated control. Data are presented as mean ± SEM and represent three independent experiments. * $P < 0.05$, when comparing 15d-PMJ_2 or 15d-PGJ_2 treated to vehicle.

A.

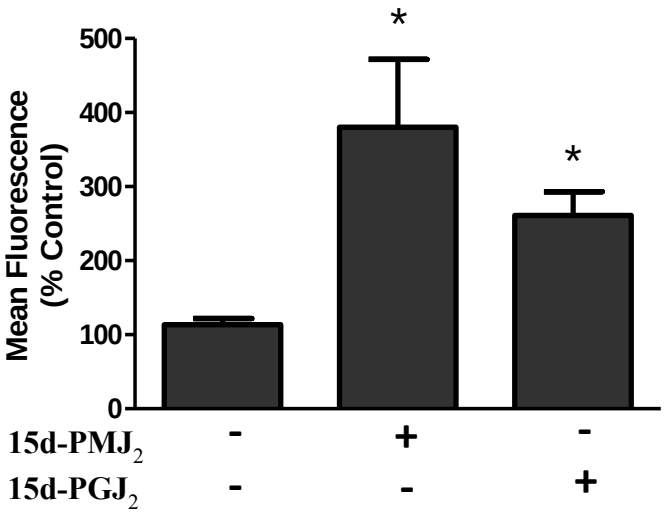
Mean Fluorescence (% Control)
500
400
300
200
100
0
*
*
15d-PMJ2 - + -
15d-PGJ2 - - +

B.

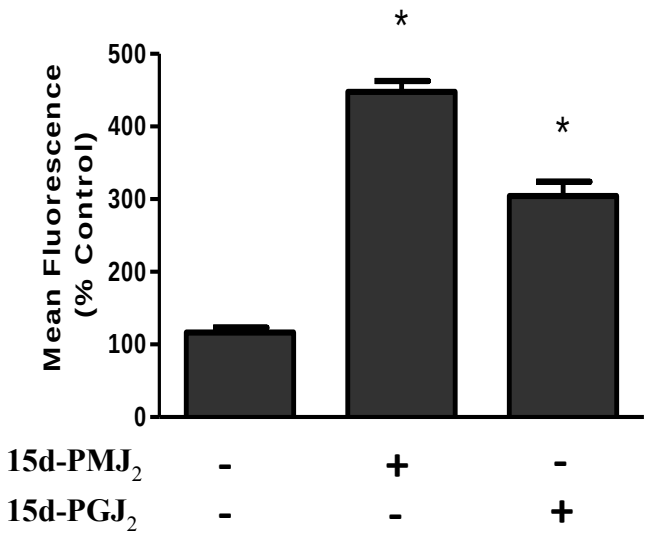
Mean Fluorescence (% Control)
500
400
300
200
100
0
*
*
15d-PMJ2 - + -
15d-PGJ2 - - +

Figure 5.3: ER-stress is required for 15d-PMJ$_2$–mediated apoptosis.

(A) A431, (B) B16F10 and (C) JWF2 cells were pretreated with salubrinal or 4-PBA for 30 minutes followed by treatment with vehicle or 5 μM 15d-PMJ$_2$ for 6 (A, C) or 16 (B) hours. Caspase-3/7 activity was measured and is represented as percent of untreated. Data are presented as mean ± SEM and represent three independent experiments. * $P < 0.05$, when comparing samples and 15d-PMJ$_2$-treated cells.

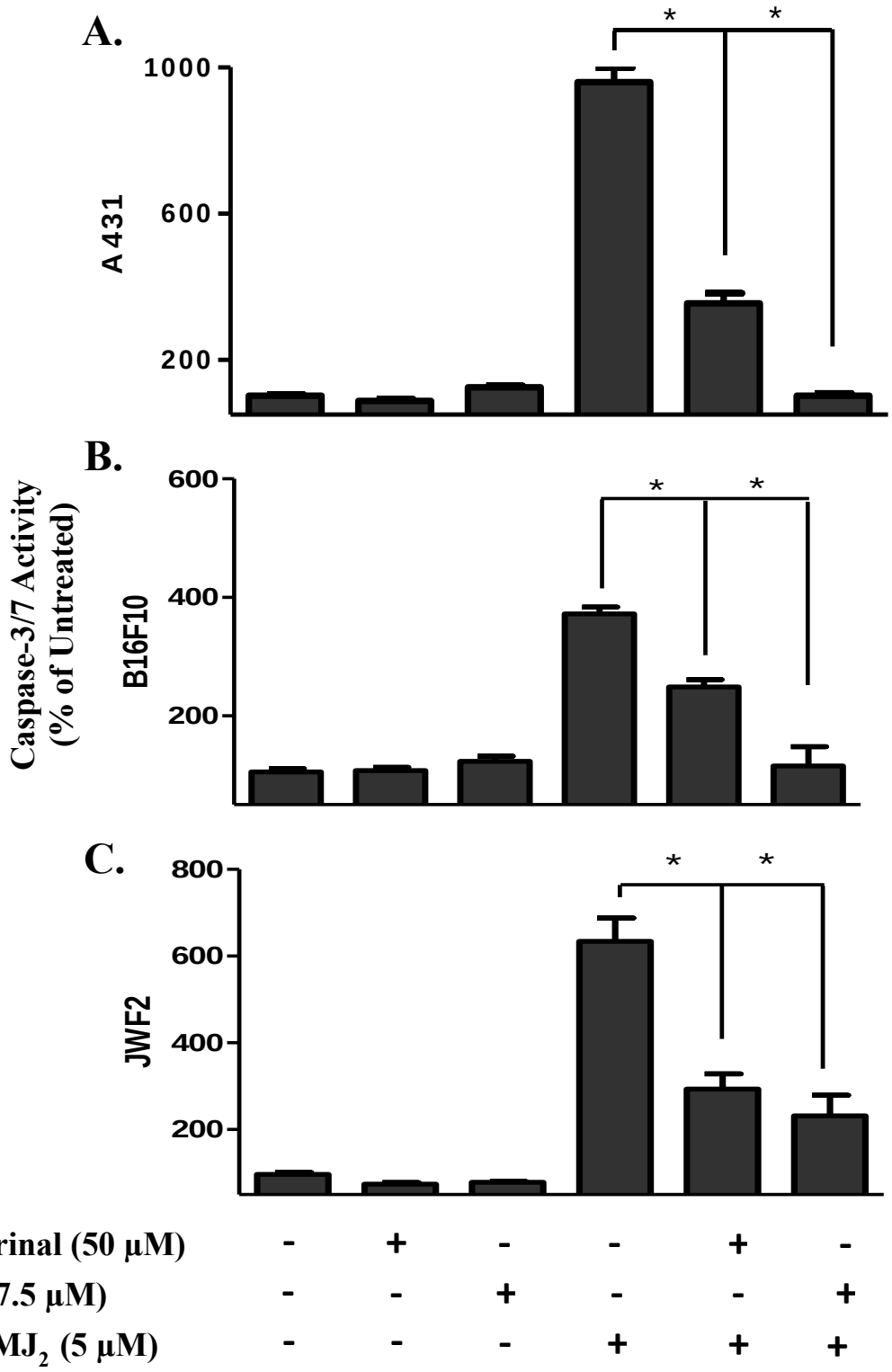
A.
1000
600
200
A431
*
*
B.
600
400
200
B16F10
Caspase-3/7 Activity
(% of Untreated)
*
*
C.
800
600
400
200
JWF2
*
*
Salubrinal (50 µM) - + - - + -
PBA (7.5 µM) - - + - - +
15d-PMJ2 (5 µM) - - - + + +

Figure 5.4: Oxidative stress is not required for 15d-PMJ_2–mediated activity.

(A) JWF2 and (B) B16F10 cells were pretreated with 0.5 mM trolox for 30 minutes followed by treatment with vehicle or 5 μM 15d-PMJ_2 for 2 hours. Oxidative stress was measured by CM-H_2DCFDA fluorescence by flow cytometry. DCF fluorescence is reported as percent of untreated. (C) JWF2 and (D) B16F10 cells were pretreated with 0.5 mM trolox for 30 minutes followed by treatment with vehicle or 5 μM 15d-PMJ_2 for 2 hours. Caspase-3/7 activity was measure used Caspase-Glo according to the manufacturer's protocol. Trolox pretreated (E) JWF2 and (F) B16F10 was treated with 15d-PMJ_2 and cell viability was measured by MTS assay. Data are presented as mean ± SEM and represent three independent experiments.* $P < 0.05$, when comparing samples to 15d-PMJ_2-treated cells, # $P < 0.05$, when comparing samples to vehicle-treated cells

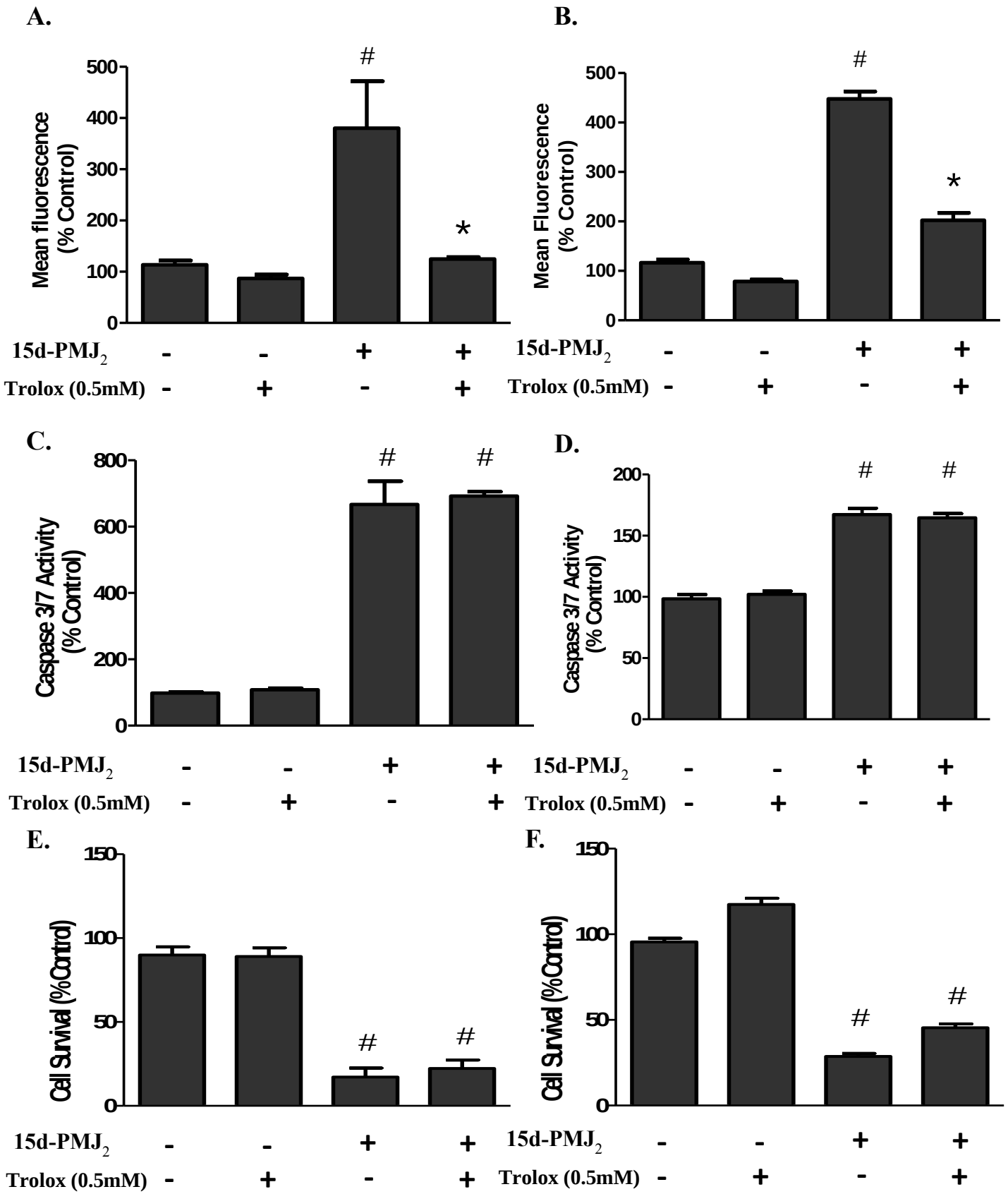
A.
Mean fluorescence (% Control)
500
400
300
200
100
0
#
*
15d-PMJ2 - - + +
Trolox (0.5mM) - + - +
B.
Mean Fluorescence (% Control)
500
400
300
200
100
0
#
*
15d-PMJ2 - - + +
Trolox (0.5mM) - + - +
C.
Caspase 3/7 Activity (% Control)
800
600
400
200
0
# #
15d-PMJ2 - - + +
Trolox (0.5mM) - + - +
D.
Caspase 3/7 Activity (% Control)
200
150
100
50
0
# #
15d-PMJ2 - - + +
Trolox (0.5mM) - + - +
E.
Cell Survival (%Control)
150
100
50
0
# #
15d-PMJ2 - - + +
Trolox (0.5mM) - + - +
F.
Cell Survival (%Control)
150
100
50
0
# #
15d-PMJ2 - - + +
Trolox (0.5mM) - + - +

Figure 5.5: Cytotoxic activity conferred by PMD_2 is ER-stress dependent, but DP-and PPARγ receptor independent.

JWF2 cells were pretreated with (A) selective DP1 and DP2 receptor antagonists, BW and BAY for 1 hour or (B) the irreversible PPARγ antagonist GW9662 for 2 hours followed by treatment with PMD_2 and PGD_2 for 24 hours. (C) JWF2 or (D) B16F10 cells were pretreated with ER-stress inhibitors salubrinal and GSK2606414 for 30 minutes followed by treatment with PMD_2 and PGD_2 for 24 hours. Cell viability was determined by MTS assay. Data are presented as mean ± SEM and represent three independent experiments.* $P < 0.05$, when comparing samples to vehicle-treated cells and # $P < 0.05$, when comparing samples to 15d-PMJ_2-treated cells

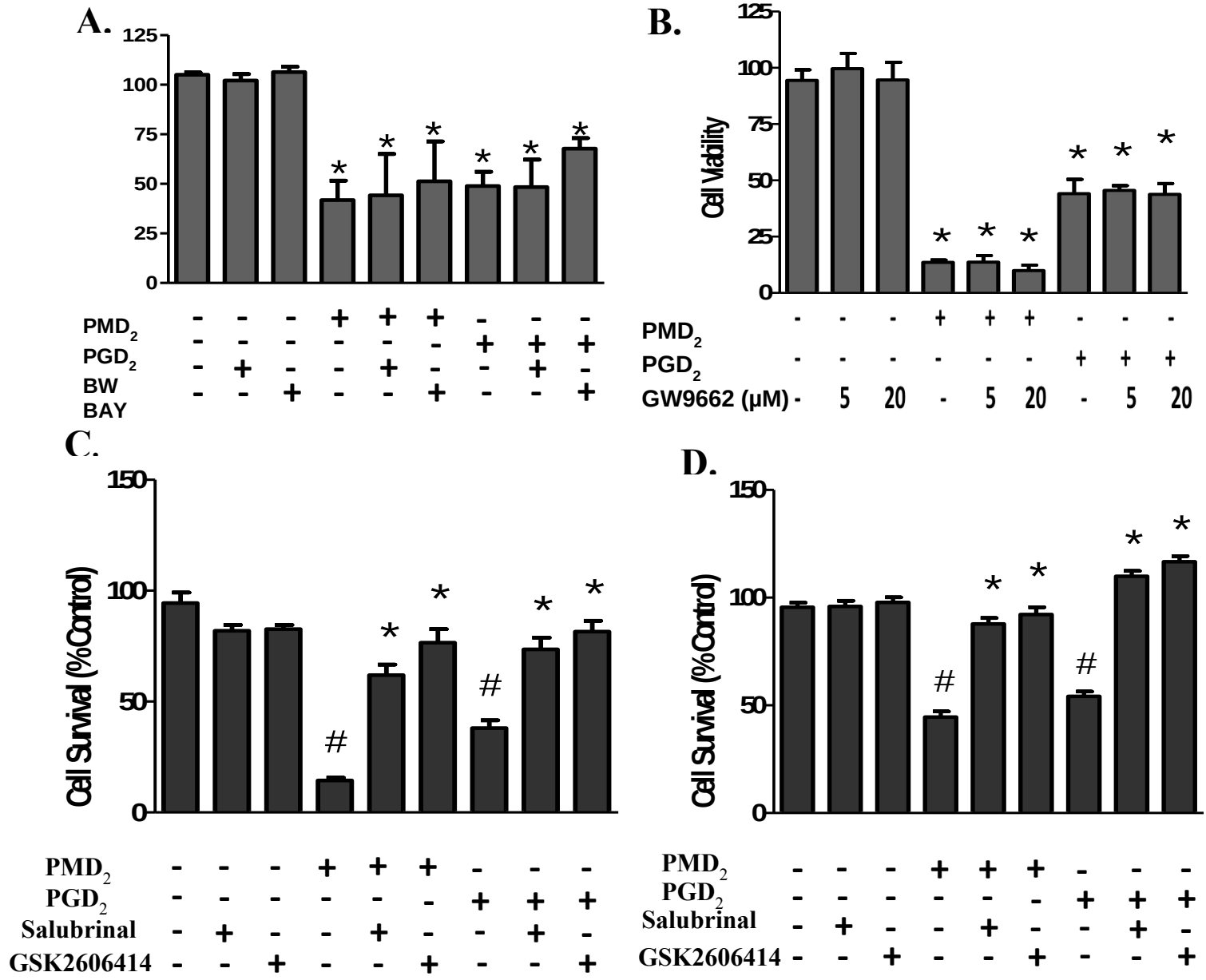
A.
125
100
75
50
25
0
PMD2
PGD2
BW
BAY
B.
Cell Viability
125
100
75
50
25
0
PMD2
PGD2
GW9662 (μM) - 5 20 - 5 20 - 5 20
C.
Cell Survival (%Control)
150
100
50
0
PMD2
PGD2
Salubrinal
GSK2606414
D.
Cell Survival (%Control)
150
100
50
0
PMD2
PGD2
Salubrinal
GSK2606414

Figure 5.6: Activation of Ca^{2+} channels by 15d-PMJ_2 is ER-stress mediated and required for cell death.

(Left side) JWF2 and (Right side) B16F10 cells were pretreated with calcium channel blockers ruthenium red, 2-APB (C, D) for 1 hour or ER-stress inhibitors salibrunal, GSK2606414 (E, F) for 30 minutes followed by treatment with 5 µM 15d-PMJ_2 or 10 µM thapsigargin for 1 hour. Intracellular Ca^{2+} levels were measured Fluor-4 NW assay. (G) JWF2 and (H) B16F10 cells were pretreated with ruthenium red (0.25 or 2.5 µM) or 2-APB (10 or 20 µM) for 1 hour followed by treatment with 15d-PMJ_2. Cell viability was determined by MTS assay. Data are presented as mean ± SEM and represent three independent experiments.* $P < 0.05$, when comparing samples to vehicle-treated cells and # $P < 0.05$, when comparing samples to 15d-PMJ_2-treated cells

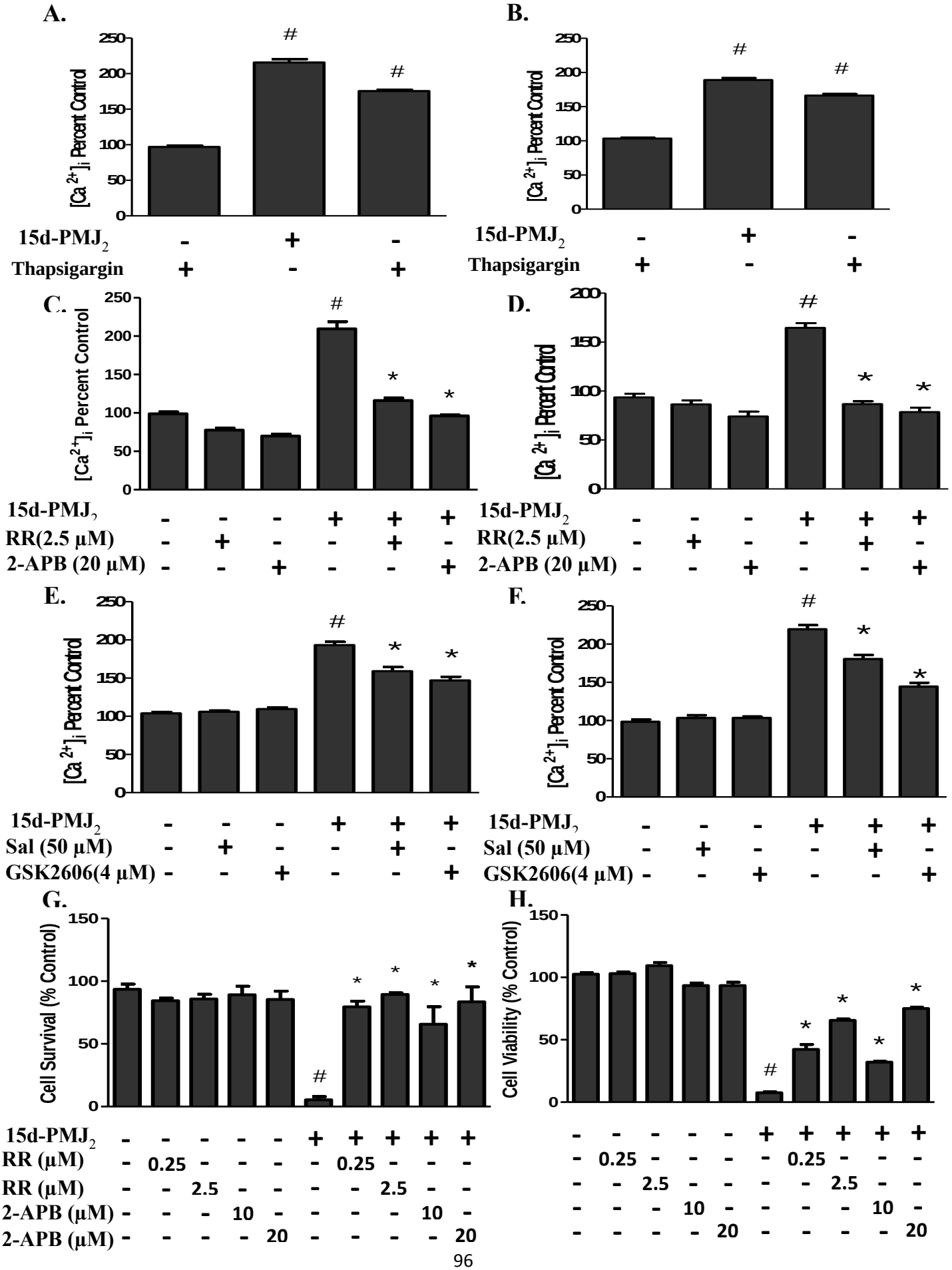
A.
B.
C.
D.
E.
F.
G.
H.
[Ca2+]i Percent Control
Cell Survival (% Control)
Cell Viability (% Control)
15d-PMJ2
Thapsigargin
RR(2.5 μM)
2-APB (20 μM)
Sal (50 μM)
GSK2606(4 μM)
RR (μM)
2-APB (μM)

Figure 5.7: The cytotoxic and apoptotic effects of 15d-PMJ_2 are mediated by the α,β-unsaturated electrophilic double bond.

(A) To determine the role of the cyclopentenone moiety in 15d-PMJ_2-mediated anti-tumor activity, neutral-15d-PMJ_2 was synthesized using the same synthetic approach described in chapter 3. (B) A431, (C) patient-derived melanoma, (D) JWF2, and (E) B16F10 cells were treated with 1, 2.5, 5, 10, or 20 μM concentrations of 15d-PMJ_2 or neutral-15d-PMJ_2 for 24 hours and cell viability was measured by MTS assay. (F) JWF2, (G) B16F10, and (H) patient-derived melanoma cells were treated with 15d-PMJ_2 for 6 hours. Caspase-3/7 activity was measured and is represented as percent of untreated. Data are presented as mean ± SEM and represent three independent experiments. * $P < 0.05$, when comparing samples to vehicle-treated cells

A.

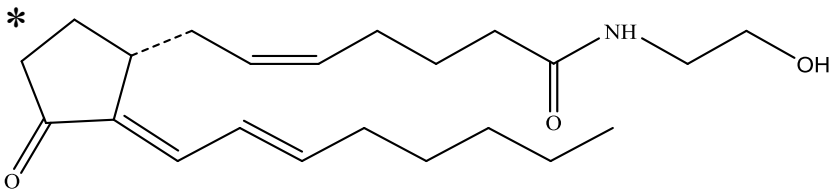

9,10-Dihydro-Prostamide J_2 (Neutral-15d-PMJ_2)

B.

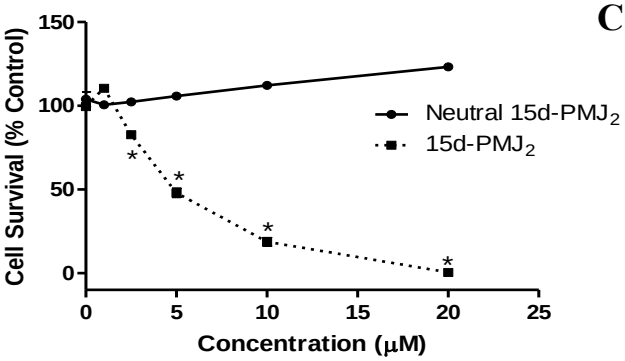

C.

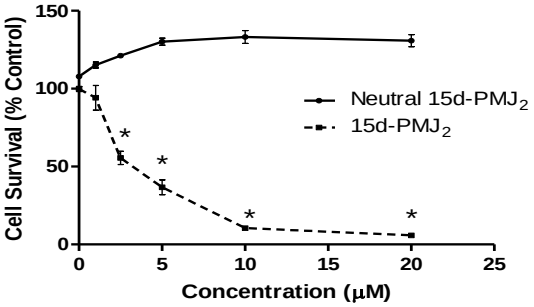

D.

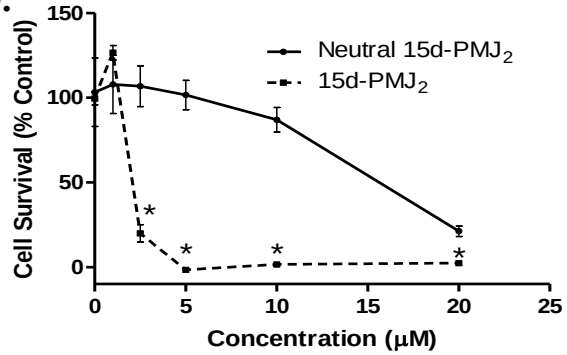

E.

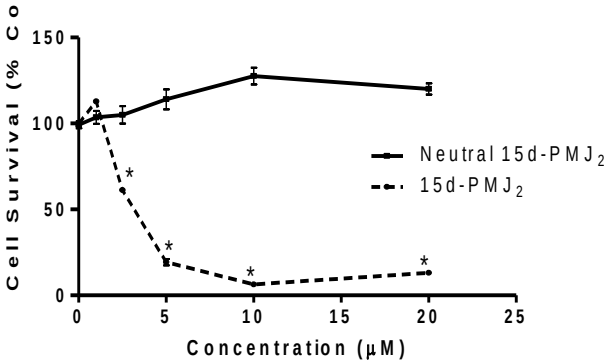

F. **G.** **H.**

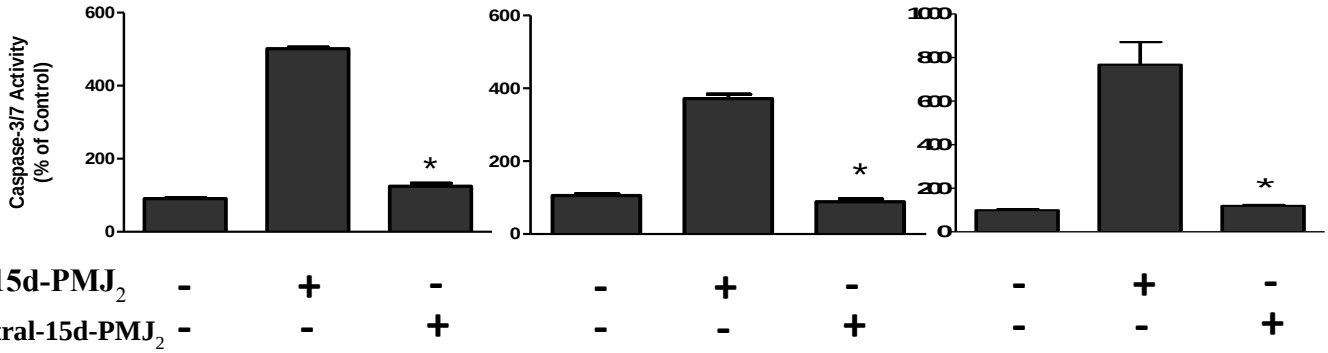

Figure 5.8: The induction of oxidative and ER-stress as well as calcium channel activation by 15d-PMJ$_2$ are mediated by the electrophilic double bond.

(A) JWF2 and (B) B16F10 cells were treated with 5 μM 15d-PMJ$_2$, neutral-15d-PMJ$_2$ or vehicle for 2 hours. Oxidative stress was measured using flow cytometry with CM-H$_2$DCFDA reagent. Fluorescence was measured as a percent increase from untreated control. (C) A431 cells were treated with vehicle, 5μM 15d-PMJ$_2$ or neutral-15d-PMJ$_2$ for 6 (upper panel) and 8 (lower panel) hours. The phosphorylation of PERK and expression of CHOP10 was assayed by Western blot analysis. Fold increase was determined via densitometry with ImageJ software. (D) JWF2 and (E) B16F10 cells treated with vehicle, 5 μM 15d-PMJ$_2$ or neutral-15d-PMJ$_2$ for 1 hour. Intracellular Ca^{2+} levels were measured Fluor-4 NW assay. Data are presented as mean ± SEM and represent three independent experiments. * $P < 0.05$, when comparing to 15d-PMJ$_2$-treated cells and # $P < 0.05$, when comparing samples to vehicle-treated cells.

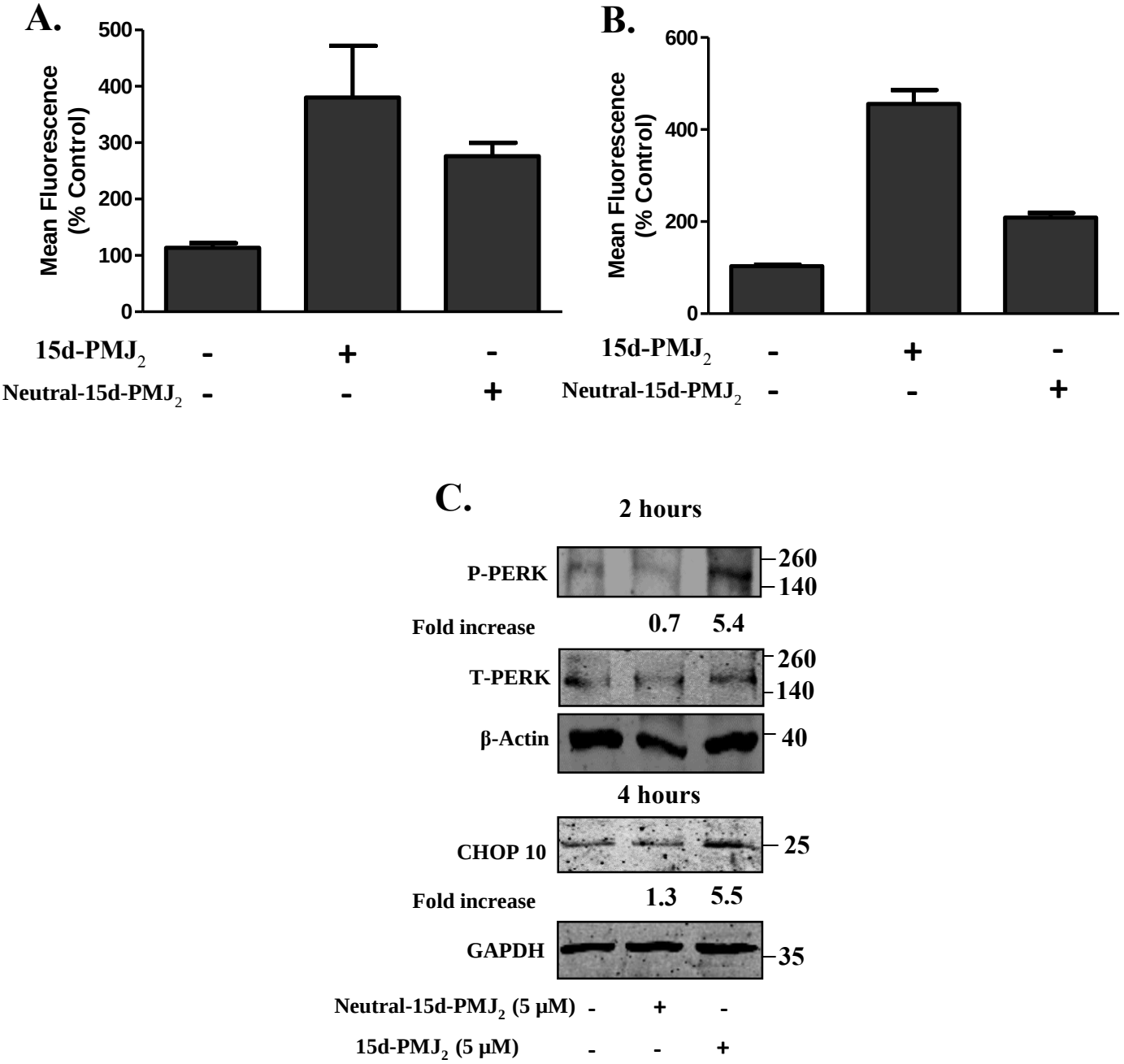
A.
Mean Fluorescence (% Control)
500
400
300
200
100
0
15d-PMJ2 - + -
Neutral-15d-PMJ2 - - +
B.
Mean Fluorescence (% Control)
600
400
200
0
15d-PMJ2 - + -
Neutral-15d-PMJ2 - - +
C.
2 hours
P-PERK
260
140
Fold increase
0.7 5.4
T-PERK
260
140
β-Actin
40
4 hours
CHOP 10
25
Fold increase
1.3 5.5
GAPDH
35
Neutral-15d-PMJ2 (5 μM) - + -
15d-PMJ2 (5 μM) - - +
D.
[Ca2+]i Percent Control
250
200
150
100
50
0
#
*
15d-PMJ2 - + -
Neutral-15d-PMJ2 - - +
E.
[Ca2+]i Percent Control
250
200
150
100
50
0
#
*
15d-PMJ2 - + -
Neutral-15d-PMJ2 - - +

Figure 5.10: 15d-PMJ_2 induces CDIP1-BAP31 signaling.

(A) A431 cells were treated with vehicle, 5 μM 15d-PMJ_2 or neutral-15d-PMJ_2 for 6 hour. Expression levels of CDIP1 and cleavage of caspase-4 and caspase-8 was assayed by Western blot analysis. Fold increase was determined via densitometry with ImageJ software. (B) A431 cells were treated with vehicle, 5 μM 15d-PMJ_2 or neutral-15d-PMJ_2 for 6 hour. Colocalization of CDIP1 (red fluorescence) and BAP31 (green fluorescence) was detected by confocal microscopy. Histogram shows quantification of intensity of CDIP1 and BAP31 fluorescence. Data were analyzed using ANOVA followed by Tukey multiple comparison test. Data are represented as mean ± SEM of three independent experiments. * $P < 0.05$, when comparing samples to vehicle-treated cells.

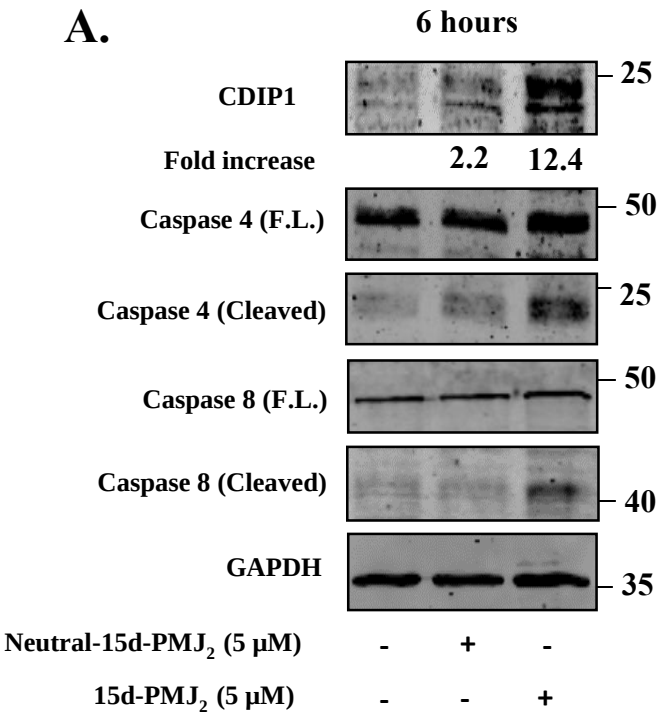
A.
6 hours
CDIP1
25
Fold increase
2.2
12.4
Caspase 4 (F.L.)
50
Caspase 4 (Cleaved)
25
Caspase 8 (F.L.)
50
Caspase 8 (Cleaved)
40
GAPDH
35
Neutral-15d-PMJ2 (5 µM)
- + -
15d-PMJ2 (5 µM)
- - +

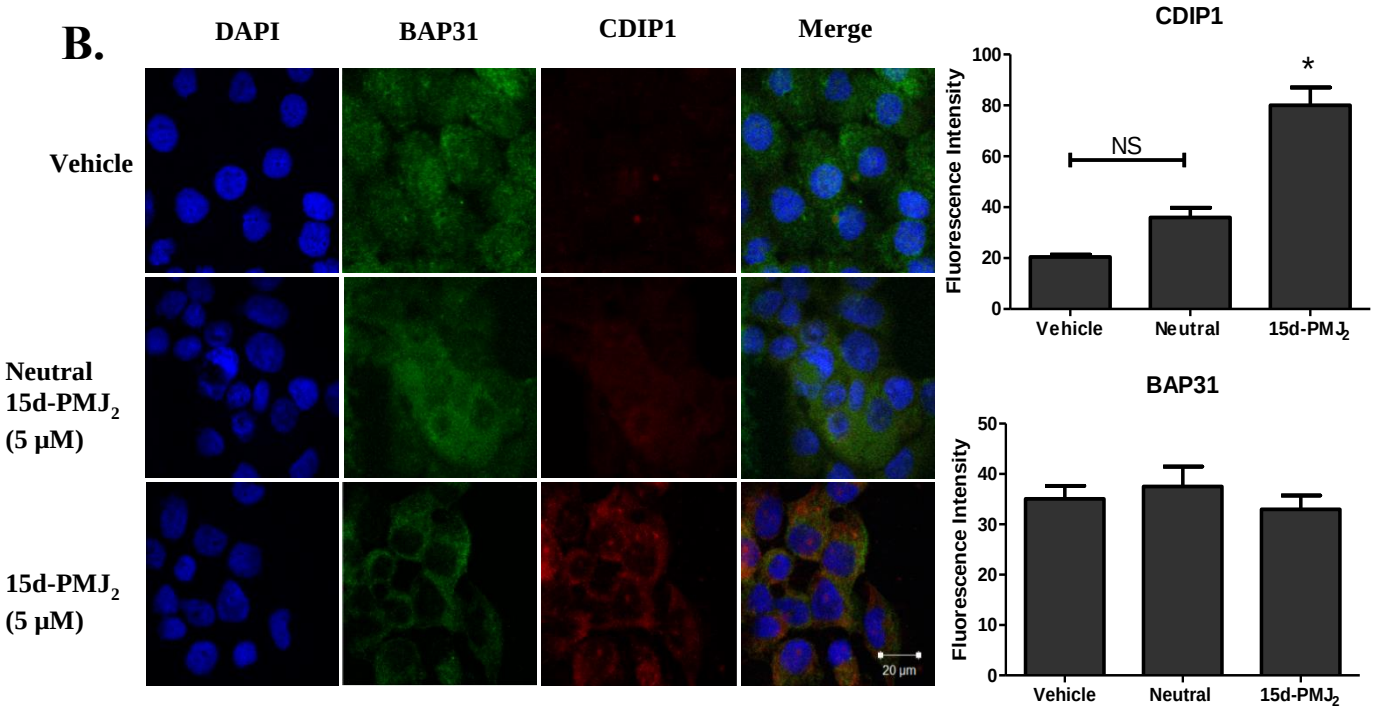
B.
DAPI
BAP31
CDIP1
Merge
Vehicle
Neutral 15d-PMJ2 (5 µM)
15d-PMJ2 (5 µM)
20 µm
CDIP1
Fluorescence Intensity
NS
*
Vehicle
Neutral
15d-PMJ2
BAP31
Fluorescence Intensity
Vehicle
Neutral
15d-PMJ2

5.5 DISCUSSION

The goal of the present report was to gain insight into the molecular mechanisms underlying the apoptotic activity of the novel prostamide 15d-PMJ_2. In the previous chapter, we found that 15d-PMJ_2 selectively induced cell death in tumorigenic but not non-tumorigenic skin cancer lines. Consistent with these findings, 15d-PMJ_2 was also found to be a selective inducer of ER-stress in malignant skin cancer cells and this pathway was determined to be necessary for 15d-PMJ_2-mediated tumor cell death. Immunohistochemical analysis of tumor sample treated with 15d-PMJ_2 confirmed that ER-stress was also upregulated *in vivo.* Conversely, oxidative stress was heightened in 15d-PMJ_2 treated cells, but this pathway was not required for cell death. 15d-PMJ_2 treatment in melanoma and NMSC cells significantly increased intracellular Ca^{2+} levels and these increased Ca^{2+} were necessary for cell death. In addition, activation of the ER-stress pathway was required to activate increased intracellular Ca^{2+} levels. Moreover, the cyclopentenone double bond in 15d-PMJ_2 was critical for anti-tumor activity and the generation of ER-and oxidative stress. These results uncover mechanisms by which 15d-PMJ_2 selectively induces tumor cell death and may possibly help determine phenotypes associated with tumor susceptibility for targeted therapy with agents such as 15d- PMJ_2 and those possessing a similar mechanisms of action.

ER stress plays a key role in initiating apoptosis and agents that target this pathway can inhibit proliferation and induce death selectively in cancer cells. ER stress is heightened in cancer cells as a result of the increased protein folding demand that is needed to drive uncontrolled cell proliferation [49]. In addition, hypoxic conditions within most tumors impairs ATP production leading to an accumulation of unfolded proteins [49]. As such, agents that increase ER stress cause the cytotoxic threshold to be reached more readily in tumor cells than in non-tumor cells whose endogenous stress levels are lower. The data shown here indicate that ER-stress was preferentially

activated in tumor cells and that this pathway was required for 15d-PMJ_2 and PMD_2 mediated cell death. ER-stress was also found to be upregulated in tumors of animals treated with 15d-PMJ_2. In alignment with these results, others reported that arachidonic acid derived J-series prostaglandins induced cytotoxic ER stress in tumor cell lines although the selectivity of ER-stress induction in tumor cells was not examined [119]. Indeed, antineoplastic agents including bortezomib are being utilized clinically to modulate the ER-stress pathway as a therapeutic strategy suggesting that 15d-PMJ_2 may be a useful therapeutic through this mechanism [60].

More recently, induction of ER-stress has been linked to increased expression of damage associated molecular patterns (DAMPs) and has also been demonstrated to play a role in the induction of immunogenic cell death (ICD). ICD is associated with an anti-tumor immune response mediated through dendritic cell activation and subsequent cytotoxic T-cell recruitment. Clinical used agents such as bortezomib, doxorubicin and oxaliplatin are known ICD inducers and are thought to exert additional anti-tumor activity through this mechanism [120]. Hence, agents such as 15d-PMJ_2 which promote cytotoxic ER stress may also induce ICD and provide an added benefit for treating cancers in which ER stress levels can be exploited.

Oxidative stress can be defined as the imbalance between production of ROS and redox buffering anti-oxidants. Altered redox status and increased oxidative stress is a hallmark of cancer cells due to increased cellular metabolism and proliferation. Similar to ER-stress, promotion of oxidative stress can overload cellular redox capacity causing damage to DNA, proteins and lipids, thereby inducing apoptosis. In this dissertation, we report that 15d-PMJ_2 potently induced the generation of oxidative stress in tumorigenic skin cancer cells, but that this phenomenon was not required for 15d-PMJ_2-mediated apoptosis. Other cyclopentenone prostaglandins including 15d-PGJ_2 have also been reported to induce oxidative stress but in some cases, generation of ROS was

found to be required for 15d-PGJ_2 activity [76;121]. In virtually all of these reports, the primary anti-oxidant used to prevent 15d-PGJ_2-mediated activity was the thiol-containing compound, N-acetylcysteine (NAC). Since cyclopentenone prostaglandins are hypothesized to exert activity by electrophilic Michael addition to thiol containing residues, an interaction between cyclopentenone prostaglandins and NAC would result in neutralization of the prostaglandin, instead of NAC-mediated increases in GSH generation. Indeed, induction of cell death, ER-stress, autophagy, and heme oxygenase-1 (HO-1) by 15d-PGJ_2 were found to be ameliorated with NAC but not other non-thiol anti-oxidants such as trolox and TEMPOL [119]. As such, we utilized the non-thiol, vitamin E analog trolox which we found to significantly decrease 15d-PMJ_2-mediated oxidative stress, but not apoptosis or cell death. Moreover, oxidative stress has been shown to originate from mechanisms associated with ER-stress including elevated ERO1α activity and increased ER to mitochondrial Ca^{2+} flux [98;122]. This evidence suggests that the role of oxidative stress may be peripheral in nature or perhaps occurring through ER-stress related mechanisms, but nonetheless, are most likely not responsible for the cytotoxic activity of 15d-PMJ_2.

Our group and others have proposed that D-series prostanoids can exert cytotoxic behavior through dehydration to J-series prostanoids [123]. We report that antagonism of DP-and PPARγ receptors had no effect on D-series prostanoid-mediated cell death. While PPARγ receptors are known to play a regulatory role cancer cell proliferation, other groups have shown that 15d-PGJ_2 exhibits activity independent of PPARγ [87;124;125]. Likewise, DP1- and DP2-receptor signaling has been reported in numerous cancer types including colon, gastic and ovarian [126-128]. Activation of these receptors produced a variety of receptor-dependent effects on tumor cells including decreased growth and angiogenesis [126;129]. As mentioned previously however, prostamides including PMD_2, do not bind to traditional prostanoid receptors including DP1 and

DP2 receptors [45]. Our data demonstrated that employing selective DP1 and DP2 receptor antagonists did not alter the cytotoxic capacity of either PGD_2 or PMD_2, supporting our hypothesis that conversion to cyclopentenone J-series prostanoids is a metabolic requirement for activity.

It is well established that fluctuations in intracellular Ca^{2+} can regulate important cellular processes including hormone secretion, cellular metabolism, and induction of signal transduction cascades. Moreover, Ca^{2+} also plays a pivotal role in cell division and conversely, cell death [53]. During the process of cell death, elevations in cytosolic Ca^{2+} levels participate in apoptosis through three distinct mechanisms, the activation of pro-apoptotic Ca^{2+}- dependent proteases known as calpains, alteration in membrane structure by Ca^{2+}-dependent phospholipid scramblases and opening of the mPTP due to mitochondrial Ca^{2+} overload [113]. In the current study, we report that 15d-PMJ_2 treatments increased intracellular Ca^{2+} levels and that these changes were required for cell death. Moreover, we report that 15d-PMJ_2 also increased mitochondrial Ca^{2+} (in future directions) perhaps implicated the mitochondria as the Ca^{2+}-mediated apoptotic initiator of 15d-PMJ_2. Similar to our results, the Lin group reported that the arachidonic acid derived J-series prostaglandin, 15d-PGJ_2, also dramatically increased Ca^{2+} levels and that treatment with the Ca^{2+} sequestering agent, BAPTA, significantly reduced induction of pro-apoptotic proteins, death receptor-5 (DR-5) and CHOP10 [130]. Our results implicate IP_3R as the most probable source of ER Ca^{2+} since 2-APB, an IP_3R-specific inhibitor exhibited greater efficacy in decreasing Ca^{2+} transit and cell death compared to the non-selective Ca^{2+} channel blocker, ruthenium red (RR). Curiously, differential rescue using Ca^{2+} channel blockers was observed in NMSC compared to melanoma cell suggesting that basal tumor cell levels of ER Ca^{2+} may dictate sensitivity to 15d-PMJ_2-mediated death. Indeed, the notion that ER Ca^{2+} concentration modulates apoptotic sensitivity was confirmed through the observation that anti-apoptotic proteins such as Bcl-2 are

involved in decreasing basal ER Ca^{2+} levels [113]. Additionally, we found that PERK-specific ER-stress inhibitors significantly reversed Ca^{2+} changes suggesting that the effect of 15d-PMJ_2 on Ca^{2+} channel activation is PERK mediated. These results are consistent with our previous data that inhibition of the PERK pathway with salibrunal and GSK2606414 reversed 15d-PMJ_2, PMD_2 and AEA-mediated cell death [43]. As such, we hypothesize that 15d-PMJ_2-mediated Ca^{2+} channel activation is through the PERK pathway. Although the specific ER-stress effector regulating homeostatic Ca^{2+} changes is not known, we report that 15d-PMJ_2 increased BAP31 activation which is a PERK regulated protein and a known inducer of IP_3R activity. Therefore we postulate that BAP31 may be the key transducer in PERK-mediated Ca^{2+} outflow.

15d-PMJ_2 contains and electrophilic α,β-unsaturated carbonyl group on its cyclopentenone ring that readily reacts with thiol of cellular proteins [27]. The same electrophilic double bond is present in all cyclopentenone prostaglandins including the J- and A-series prostaglandins and prostamides. Generation of oxidative stress by arachidonic acid-derived 15d-PGJ_2 has been attributed to interactions with anti-oxidants including glutathione and thioredoxin reductase [27;101]. These covalent interactions neutralize the anti-oxidants thereby allowing unchecked oxidant activity. However, it was unclear whether the cyclopentenone double bond also regulated ER-stress as disulfide bond formation plays a critical role in oxidative protein folding. To address this question our group synthesized a neutral-PMJ_2 analog using the same approach described in chapter 3. Elimination of the reactive group in 15d-PMJ_2 prevented apoptotic cell death in NMSC, melanoma and patient derived melanoma. Moreover, induction of oxidative/ ER-stress and increased intracellular Ca^{2+} was also prevented, thereby identifying the double bond as a critical moiety for activity of 15d-PMJ_2. Studies are currently underway by our group to identify ER-stress modulating proteins that form covalent interactions with 15d-PMJ_2.

In the present study, we investigated the molecular mechanism of 15d-PMJ_2, finding that this novel prostamide exerts its anti-tumor activity through the generation of ER, but not oxidative stress. Activation of ER-stress was also found to mediate increases in intracellular Ca^{2+} levels, which were also required to induce apoptosis. In agreement with previous work conducted with 15d-PGJ_2, elimination of the electrophilic double bond abolished the activity of 15d-PMJ_2 implicating the cyclopentenone moiety as the pharmacological "warhead" within this prostamide.

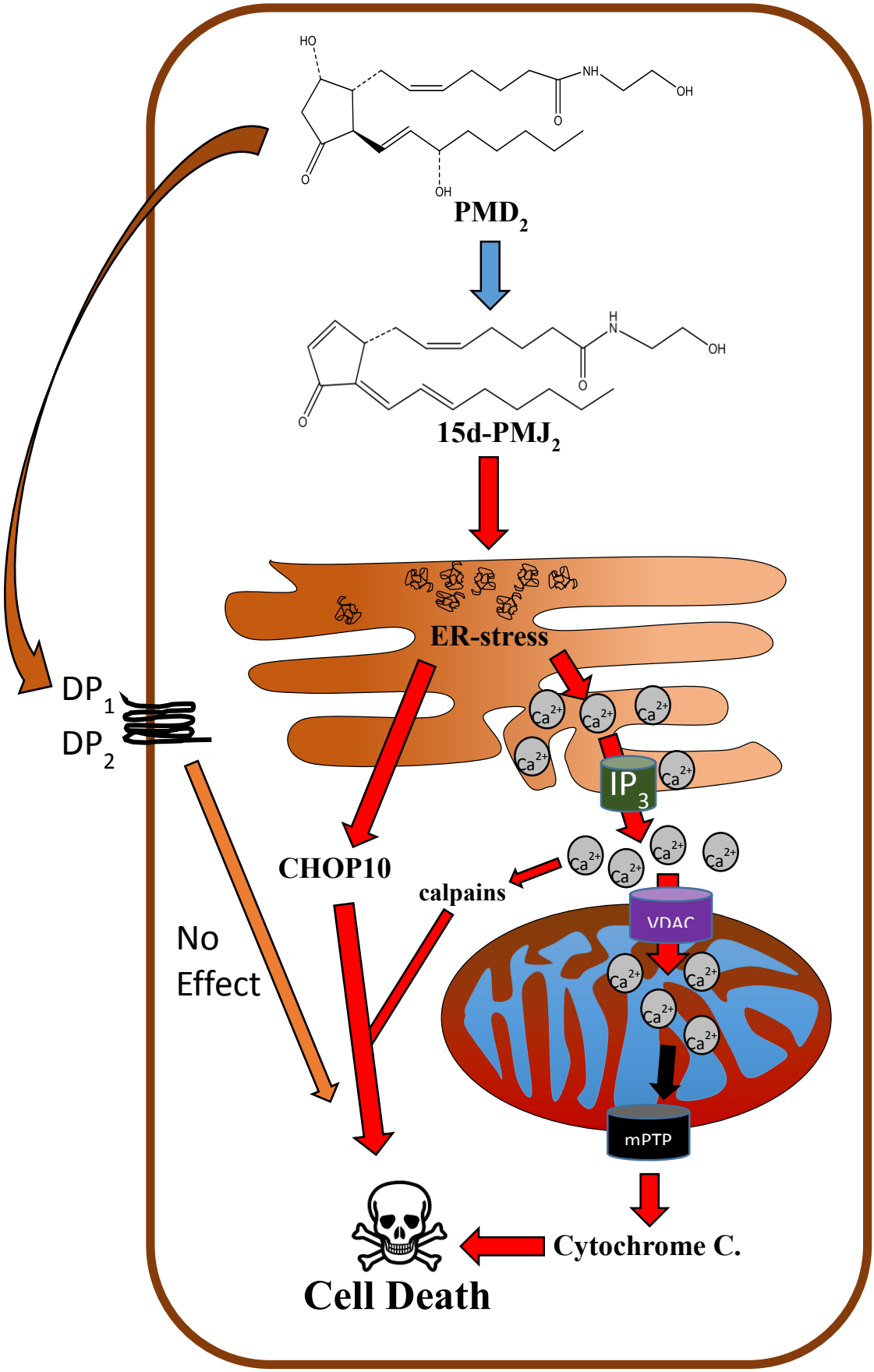
HO
NH
OH
O
O
OH
PMD2
H
N
OH
O
O
15d-PMJ2
ER-stress
DP1
DP2
Ca2+
IP3
CHOP10
calpains
No
Effect
VDAC
mPTP
Cytochrome C.
Cell Death

CHAPTER SIX: GENERAL DISCUSSION AND SUMMARY

Non-melanoma and melanoma skin cancers represent a substantial cost to the United States health care system as the combined cost of treatment for these conditions is estimated to be 8.1 billion dollars annually [3]. Chemotherapeutic treatments for NMSC involve the administration of 5-fluorouricil and imquimod, which are effective but cause serious side effects. Melanoma, on the other hand is associated with significant mortality compared to NMSC and is treated with radiation and immunotherapy. The main objective of this dissertation project was to investigate the potential of 15d-PMJ_2 as a novel therapeutic for the treatment of skin cancers, to provide a clinical alternative with less dose-limiting side-effects. This project was also focused on elucidating the mechanisms responsible for 15d-PMJ_2-mediated apoptosis, thereby shedding light on tumor phenotypes associated with drug susceptibility.

The first step in achieving our objective was to perform the first chemical synthesis and purification of 15d-PMJ_2. Our general synthetic approach was to react a carboxyl-possessing J-series prostaglandin with ethanolamine and an amide coupling reagent in the presence of N'N-diisopropylethylamine to yield the J-series prostaglandin-ethanolamine. In order to determine the most appropriate solvents and optimize ideal synthetic conditions, we employed the use of fatty acid model compounds. Heptadecanoyl-ethanolamide was the first compound successfully synthesized using this method with the coupling reagent, HBTU. During the synthesis of the second model compound, linoleoyl-ethanolamide, HBTU was found to be an inappropriate coupling reagent due to its limited solubility. As such, we substituted HBTU with TBTU, which was found to be readily soluble in acetonitrile. The synthesis of arachidonoyl-ethanolamide offered unique challenges due to the four unsaturated double bonds but was structurally similar to the J-series prostaglandin. To prevent degradation, reactions were carried out under nitrogen gas and

under low light conditions. The synthesis of 15d-PMJ_2 was performed by reacting 15d-PGJ_2 with TBTU in the presence of ethanolamine and N'N-diisopropylethylamine, with purification being conducted on HPLC. Verification of molecule structures were performed by proton nuclear magnetic spectroscopy (^{1}H-NMR) and electro-spray ionization mass spectrometry (ESI-MS).

Our data provided the first pre-clinical characterization of 15d-PMJ_2 which had superior cytotoxic activity compared to the synthetic substrate 15d-PGJ_2. Unlike the endocannabinoid AEA, which required COX-2 to elicit its anti-tumor activity, we found that the cytotoxicity of 15d-PMJ_2, a downstream metabolite of AEA, was independent of this enzyme, demonstrating induction of apoptosis in NMSC and melanoma regardless of COX-2 expression. Moreover, selective toxicity of 15d-PMJ_2 was found when comparing tumor vs. non-tumor cells from both murine and human origin, demonstrating pre-clinical consistency. *In vivo* peritumoral treatment of melanoma tumors with 15d-PMJ_2 significantly retarded tumor growth and induced tumor cell death. Moreover, overt systemic toxicity was not observed during this study suggesting that the selective properties of 15d-PMJ_2 may also apply to *in vivo* systems.

Our group previously reported that AEA induced tumor cell apoptosis through mechanisms involving the induction of ER- and oxidative-stress [88]. Our similar yet distinct findings report that 15d-PMJ_2-mediated toxicity was ER- but not oxidative stress dependent. We also report that the generation of ER-stress was also observed *in vivo*. The requirement for oxidative stress to induce AEA-mediated death may be a result of other cyclooxygenase or lipoxagenase associated metabolites, a peroxidated variation of one of these bioactive lipids, or activation of their respective receptors. Treatment of cancer cells with AEA and 15d-PGJ_2 produced a notable decrease in the redox buffering protein glutathione [88]. In addition to buffering free radicals, glutathione is also a substrate for various oxidative protein folding enzymes, which upon depletion is reported to

induce ER-stress [131]. The fact that J-series prostaglandins have been shown to localize to the ER may indicate that the effect of glutathione depletion on the generation of ROS and ER-stress is dependent on the sub-cellular locality [132]. Nevertheless, our data demonstrated that the non-thiol containing anti-oxidant trolox reduced oxidative stress but not cell death, suggesting that oxidative-stress is dependent on the generation of ER-stress or is a parallel phenomenon.

In our system, Ca^{2+} homeostasis was found to be a key regulator of 15d-PMJ_2-mediated cell death. Previous reports indicate that related molecules, AEA and 15d-PGJ_2, had the propensity to increase intracellular Ca^{2+} and some studies reported that this mechanism regulated apoptosis [130;133]. We found that increased cytosolic Ca^{2+} was required for cell death and was dependent on PERK-mediated ER-stress. We hypothesize that this effect is IP_3-receptor mediated as selective antagonism of this channel provided greatest reversal of both Ca^{2+} flux and cell death. As such, further studies are required to determine whether cytosolic players such as calpain or the mitochondria are the major contributors during initiation of apoptosis.

Lastly, this project sought to investigate the structural pharmacophore responsible for J-series prostamide activity. Building on previous reports that J-series prostanoids confer activity through a reactive double bond within the cyclopentenone ring, we used the synthetic approach described in chapter 3 to produce the first J-series prostamide lacking this double bond. Our data definitively showed that this moiety was required for virtually all aspects of 15d-PMJ_2-mediated activity. These data provide a valuable structure-activity relationship between the novel molecule, 15d-PMJ_2, and its mechanism, the selective generation ER-stress. These insights may ultimately help in developing novel and potent cyclopentenone/prostaglandin derivatives to combat cancers other than non-melanoma and melanoma skin cancers in a safe and effective manner.

FUTURE DIRECTIONS

This dissertation provided strong evidence that generation of ER-stress was the most likely mechanism tumor-cell selective toxicity exhibited by 15d-PMJ_2. In order to answer this question more definitively, protein folding abnormalities occurring within the ER of tumor cells should be mimicked to non-tumor cells, demonstrating the specific ER conditions required for 15d-PMJ_2 activity. This would provide valuable insights regarding potential off-target toxicities observed during administration. Our results demonstrated that 15d-PMJ_2 dramatically increased intracellular Ca^{2+} levels, however the ultimate fate and consequence of this phenomena is still unknown. Increases in mitochondrial calcium are known to contribute to apoptotic cascade induction by resulting in cytochrome c release [57]. To investigate this role we examined whether 15d-PMJ_2-mediated increased intracellular Ca^{2+} was coinciding with increased mitochondrial Ca^{2+} levels. B16F10 and JWF2 cells treated for 4 hours with 15d-PMJ_2 and 15d-PGJ_2 displayed significant elevations in Rhod-2 fluorescence, a charged calcium probe which accumulates in the mitochondria (Figure 6.1). These data suggest that ER-mediated increased intracellular Ca^{2+} is most likely transiting to the mitochondria and contributing to initiation of apoptosis. To examine whether the cyclopentenone double bond was required for increased mitochondrial Ca^{2+}, B16F10 and JWF2 cells treated with neutral-15d-PMJ_2 and 15d-PMJ_2 for 4 hours were assayed for mitochondrial calcium using a Rhod-2 mitochondrial Ca^{2+} probe. Similarly to results regarding intracellular Ca^{2+}, loss of the reactive double bond significantly decreased the level of mitochondria Ca^{2+} further demonstrating the importance of this moiety in 15d-PMJ_2 efficacy (Figure 6.1).

We demonstrated that 15d-PMJ_2 decreased *in vivo* tumors using an immune-competent allograft melanoma model. Future studies should include *in vivo* studies using immune-

compromised models (such as patient-derived xenograft), which would shed light on both, the agents' effect on patient derived tumors and the anti-tumor immunogenicity of 15d-PMJ_2. Finally, formulating 15d-PMJ_2 into a topical solution would enable the execution of a UV-induced skin cancer study, providing evidence that 15d-PMJ_2 is effective against naturally occurring skin cancers.

Figure 6.1: Mitochondrial Ca^{2+} levels are induced by 15d-PMJ_2 and is mediated by the electrophilic double bond. (A) JWF2 and (B) B16F10 cells treated with vehicle, 15d-PMJ_2, or 15d-PGJ_2 for 4 hours. (C) JWF2 and (D) B16F10 cells treated with vehicle, 15d-PMJ_2, or Neutral-15d-PMJ_2 for 4 hours. Mitochondrial Ca^{2+} levels were measured using Rhod-2. Data are presented as mean ± SEM and represent three independent experiments.* $P < 0.05$, when comparing samples to vehicle-treated cells and # $P < 0.05$, when comparing samples to 15d-PMJ_2 -treated cells

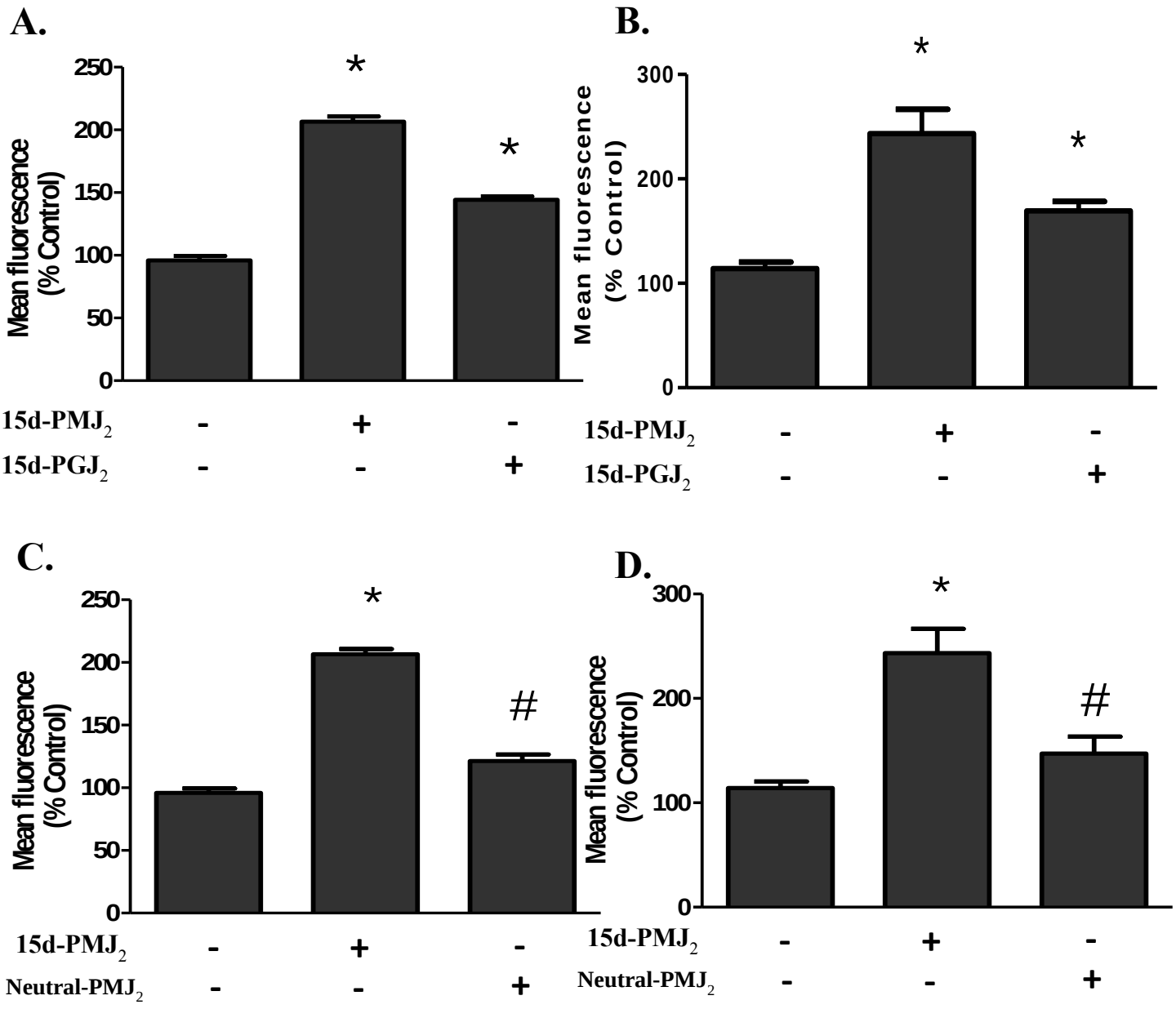
A.
Mean fluorescence (% Control)
250
200
150
100
50
0
*
*
15d-PMJ2 - + -
15d-PGJ2 - - +
B.
Mean fluorescence (% Control)
300
200
100
0
*
*
15d-PMJ2 - + -
15d-PGJ2 - - +
C.
Mean fluorescence (% Control)
250
200
150
100
50
0
*
#
15d-PMJ2 - + -
Neutral-PMJ2 - - +
D.
Mean fluorescence (% Control)
300
200
100
0
*
#
15d-PMJ2 - + -
Neutral-PMJ2 - - +

Reference List

1 Miller KD, Siegel RL, Lin CC, Mariotto AB, Kramer JL, Rowland JH, Stein KD, Alteri R, Jemal A: Cancer treatment and survivorship statistics, 2016. CA Cancer J Clin 2016;66:271-289.

2 Rogers HW, Weinstock MA, Feldman SR, Coldiron BM: Incidence Estimate of Nonmelanoma Skin Cancer (Keratinocyte Carcinomas) in the U.S. Population, 2012. JAMA Dermatol 2015;151:1081-1086.

3 Robinson JK: Sun exposure, sun protection, and vitamin D. JAMA 2005;294:1541-1543.

4 Miller SJ, Alam M, Andersen J, Berg D, Bichakjian CK, Bowen G, Cheney RT, Glass LF, Grekin RC, Kessinger A, Lee NY, Liegeois N, Lydiatt DD, Michalski J, Morrison WH, Nehal KS, Nelson KC, Nghiem P, Olencki T, Perlis CS, Rosenberg EW, Shaha AR, Urist MM, Wang LC, Zic JA: Basal cell and squamous cell skin cancers. J Natl Compr Canc Netw 2010;8:836-864.

5 Glud M, Omland SH, Gniadecki R: [Basal cell carcinoma surgery]. Ugeskr Laeger 2016;178.

6 Siegel RL, Miller KD, Jemal A: Cancer statistics, 2016. CA Cancer J Clin 2016;66:7-30.

7 Stamataki Z, Brunton L, Lorigan P, Green AC, Newton-Bishop J, Molassiotis A: Assessing the impact of diagnosis and the related supportive care needs in patients with cutaneous melanoma. Support Care Cancer 2015;23:779-789.

8 Eggermont AM, Chiarion-Sileni V, Grob JJ, Dummer R, Wolchok JD, Schmidt H, Hamid O, Robert C, Ascierto PA, Richards JM, Lebbe C, Ferraresi V, Smylie M, Weber JS, Maio M, Bastholt L, Mortier L, Thomas L, Tahir S, Hauschild A, Hassel JC, Hodi FS, Taitt C, de P, V, de SG, Suciu S, Testori A: Prolonged Survival in Stage III Melanoma with Ipilimumab Adjuvant Therapy. N Engl J Med 2016;375:1845-1855.

9 Cohen C, Zavala-Pompa A, Sequeira JH, Shoji M, Sexton DG, Cotsonis G, Cerimele F, Govindarajan B, Macaron N, Arbiser JL: Mitogen-actived protein kinase activation is an early event in melanoma progression. Clin Cancer Res 2002;8:3728-3733.

10 Corazzari M, Rapino F, Ciccosanti F, Giglio P, Antonioli M, Conti B, Fimia GM, Lovat PE, Piacentini M: Oncogenic BRAF induces chronic ER stress condition resulting in increased basal autophagy and apoptotic resistance of cutaneous melanoma. Cell Death Differ 2015;22:946-958.

11 Cerezo M, Lehraiki A, Millet A, Rouaud F, Plaisant M, Jaune E, Botton T, Ronco C, Abbe P, Amdouni H, Passeron T, Hofman V, Mograbi B, Dabert-Gay AS, Debayle D, Alcor D, Rabhi N, Annicotte JS, Heliot L, Gonzalez-Pisfil M, Robert C, Morera S, Vigouroux A, Gual P, Ali MM, Bertolotto C, Hofman P, Ballotti R, Benhida R, Rocchi S: Compounds Triggering ER Stress Exert Anti-Melanoma Effects and Overcome BRAF Inhibitor Resistance. Cancer Cell 2016;29:805-819.

12 Teicher BA: Tumor models for efficacy determination. Mol Cancer Ther 2006;5:2435-2443.

13 Rundhaug JE, Simper MS, Surh I, Fischer SM: The role of the EP receptors for prostaglandin E2 in skin and skin cancer. Cancer Metastasis Rev 2011;30:465-480.

14 Greene ER, Huang S, Serhan CN, Panigrahy D: Regulation of inflammation in cancer by eicosanoids. Prostaglandins Other Lipid Mediat 2011;96:27-36.

15 Zha S, Yegnasubramanian V, Nelson WG, Isaacs WB, De Marzo AM: Cyclooxygenases in cancer: progress and perspective. Cancer Lett 2004;215:1-20.

16 Needleman P, Isakson PC: The discovery and function of COX-2. J Rheumatol Suppl 1997;49:6-8.

17 Vane JR, Bakhle YS, Botting RM: Cyclooxygenases 1 and 2. Annu Rev Pharmacol Toxicol 1998;38:97-120.

18 Garavito RM, DeWitt DL: The cyclooxygenase isoforms: structural insights into the conversion of arachidonic acid to prostaglandins. Biochim Biophys Acta 1999;1441:278-287.

19 Shibata T, Kondo M, Osawa T, Shibata N, Kobayashi M, Uchida K: 15-deoxy-delta 12,14-prostaglandin J2. A prostaglandin D2 metabolite generated during inflammatory processes. J Biol Chem 2002;277:10459-10466.

20 Nakanishi M, Rosenberg DW: Multifaceted roles of PGE2 in inflammation and cancer. Semin Immunopathol 2013;35:123-137.

21 Sugimoto Y, Narumiya S: Prostaglandin E receptors. J Biol Chem 2007;282:11613-11617.

22 Sharif NA, Williams GW, Davis TL: Pharmacology and autoradiography of human DP prostanoid receptors using [(3)H]-BWA868C, a DP receptor-selective antagonist radioligand. Br J Pharmacol 2000;131:1025-1038.

23 Abe H, Takeshita T, Nagata K, Arita T, Endo Y, Fujita T, Takayama H, Kubo M, Sugamura K: Molecular cloning, chromosome mapping and characterization of the mouse CRTH2 gene, a putative member of the leukocyte chemoattractant receptor family. Gene 1999;227:71-77.

24 Arima M, Fukuda T: Prostaglandin D(2) and T(H)2 inflammation in the pathogenesis of bronchial asthma. Korean J Intern Med 2011;26:8-18.

25 Arimura A, Yasui K, Kishino J, Asanuma F, Hasegawa H, Kakudo S, Ohtani M, Arita H: Prevention of allergic inflammation by a novel prostaglandin receptor antagonist, S-5751. J Pharmacol Exp Ther 2001;298:411-419.

26 Zhang A, Dong Z, Yang T: Prostaglandin D2 inhibits TGF-beta1-induced epithelial-to-mesenchymal transition in MDCK cells. Am J Physiol Renal Physiol 2006;291:F1332-F1342.

27 Uchida K, Shibata T: 15-Deoxy-Delta(12,14)-prostaglandin J2: an electrophilic trigger of cellular responses. Chem Res Toxicol 2008;21:138-144.

28 Fukuoka T, Yashiro M, Morisaki T, Kinoshita H, Hasegawa T, Kasashima H, Masuda G, Sakurai K, Toyokawa T, Tanaka H, Kubo N, Muguruma K, Ohira M, Hirakawa K: The role of type D prostanoid receptors and PPARgamma in gastric cancer progression. Anticancer Res 2014;34:2771-2778.

29 Brunjes PC, Collins LN, Osterberg SK, Phillips AM: The mouse olfactory peduncle. 3. Development of neurons, glia, and centrifugal afferents. Front Neuroanat 2014;8:44.

30 Van Dross RT: Metabolism of anandamide by COX-2 is necessary for endocannabinoid-induced cell death in tumorigenic keratinocytes. Mol Carcinog 2009;48:724-732.

31 Kuc C, Jenkins A, Van Dross RT: Arachidonoyl ethanolamide (AEA)-induced apoptosis is mediated by J-series prostaglandins and is enhanced by fatty acid amide hydrolase (FAAH) blockade. Mol Carcinog 2012;51:139-149.

32 Eucker J, Sterz J, Krebbel H, Zavrski I, Kaiser M, Zang C, Heider U, Jakob C, Elstner E, Sezer O: Peroxisome proliferator-activated receptor-gamma ligands inhibit proliferation and induce apoptosis in mantle cell lymphoma. Anticancer Drugs 2006;17:763-769.

33 Shin SW, Seo CY, Han H, Han JY, Jeong JS, Kwak JY, Park JI: 15d-PGJ2 induces apoptosis by reactive oxygen species-mediated inactivation of Akt in leukemia and colorectal cancer cells and shows in vivo antitumor activity. Clin Cancer Res 2009;15:5414-5425.

34 Clay CE, Namen AM, Atsumi G, Willingham MC, High KP, Kute TE, Trimboli AJ, Fonteh AN, Dawson PA, Chilton FH: Influence of J series prostaglandins on apoptosis and tumorigenesis of breast cancer cells. Carcinogenesis 1999;20:1905-1911.

35 Brunoldi EM, Zanoni G, Vidari G, Sasi S, Freeman ML, Milne GL, Morrow JD: Cyclopentenone prostaglandin, 15-deoxy-Delta12,14-PGJ2, is metabolized by HepG2 cells via conjugation with glutathione. Chem Res Toxicol 2007;20:1528-1535.

36 Soares AF, Nosjean O, Cozzone D, D'Orazio D, Becchi M, Guichardant M, Ferry G, Boutin JA, Lagarde M, Geloen A: Covalent binding of 15-deoxy-delta12,14-prostaglandin J2 to PPARgamma. Biochem Biophys Res Commun 2005;337:521-525.

37 Chen Y, Zackert WE, Roberts LJ, Morrow JD: Evidence for the formation of a novel cyclopentenone isoprostane, 15-A2t-isoprostane (8-iso-prostaglandin A2) in vivo. Biochim Biophys Acta 1999;1436:550-556.

38 Parker J: Prostaglandin A2 protein interactions and inhibition of cellular proliferation. Prostaglandins 1995;50:359-375.

39 Kozak KR, Prusakiewicz JJ, Marnett LJ: Oxidative metabolism of endocannabinoids by COX-2. Curr Pharm Des 2004;10:659-667.

40 Rouzer CA, Marnett LJ: Endocannabinoid oxygenation by cyclooxygenases, lipoxygenases, and cytochromes P450: cross-talk between the eicosanoid and endocannabinoid signaling pathways. Chem Rev 2011;111:5899-5921.

41 Alhouayek M, Muccioli GG: COX-2-derived endocannabinoid metabolites as novel inflammatory mediators. Trends Pharmacol Sci 2014;35:284-292.

42 Yu M, Ives D, Ramesha CS: Synthesis of prostaglandin E2 ethanolamide from anandamide by cyclooxygenase-2. J Biol Chem 1997;272:21181-21186.

43 Soliman E, Henderson KL, Danell AS, Van DR: Arachidonoyl-ethanolamide activates endoplasmic reticulum stress-apoptosis in tumorigenic keratinocytes: Role of cyclooxygenase-2 and novel J-series prostamides. Mol Carcinog 2015.

44 Woodward DF, Liang Y, Krauss AH: Prostamides (prostaglandin-ethanolamides) and their pharmacology. Br J Pharmacol 2008;153:410-419.

45 Matias I, Chen J, De PL, Bisogno T, Ligresti A, Fezza F, Krauss AH, Shi L, Protzman CE, Li C, Liang Y, Nieves AL, Kedzie KM, Burk RM, Di M, V, Woodward DF: Prostaglandin ethanolamides (prostamides): in vitro pharmacology and metabolism. J Pharmacol Exp Ther 2004;309:745-757.

46 Malhotra JD, Kaufman RJ: Endoplasmic reticulum stress and oxidative stress: a vicious cycle or a double-edged sword? Antioxid Redox Signal 2007;9:2277-2293.

47 Verfaillie T, Rubio N, Garg AD, Bultynck G, Rizzuto R, Decuypere JP, Piette J, Linehan C, Gupta S, Samali A, Agostinis P: PERK is required at the ER-mitochondrial contact sites to convey apoptosis after ROS-based ER stress. Cell Death Differ 2012;19:1880-1891.

48 Sano R, Reed JC: ER stress-induced cell death mechanisms. Biochim Biophys Acta 2013;1833:3460-3470.

49 Clarke HJ, Chambers JE, Liniker E, Marciniak SJ: Endoplasmic reticulum stress in malignancy. Cancer Cell 2014;25:563-573.

50 Namba T, Tian F, Chu K, Hwang SY, Yoon KW, Byun S, Hiraki M, Mandinova A, Lee SW: CDIP1-BAP31 complex transduces apoptotic signals from endoplasmic reticulum to mitochondria under endoplasmic reticulum stress. Cell Rep 2013;5:331-339.

51 Czabotar PE, Westphal D, Dewson G, Ma S, Hockings C, Fairlie WD, Lee EF, Yao S, Robin AY, Smith BJ, Huang DC, Kluck RM, Adams JM, Colman PM: Bax crystal structures reveal how BH3 domains activate Bax and nucleate its oligomerization to induce apoptosis. Cell 2013;152:519-531.

52 Araki K, Nagata K: Protein folding and quality control in the ER. Cold Spring Harb Perspect Biol 2012;4:a015438.

53 Krebs J, Agellon LB, Michalak M: Ca(2+) homeostasis and endoplasmic reticulum (ER) stress: An integrated view of calcium signaling. Biochem Biophys Res Commun 2015;460:114-121.

54 Rogers TB, Inesi G, Wade R, Lederer WJ: Use of thapsigargin to study Ca2+ homeostasis in cardiac cells. Biosci Rep 1995;15:341-349.

55 Li G, Mongillo M, Chin KT, Harding H, Ron D, Marks AR, Tabas I: Role of ERO1-alpha-mediated stimulation of inositol 1,4,5-triphosphate receptor activity in endoplasmic reticulum stress-induced apoptosis. J Cell Biol 2009;186:783-792.

56 Kiviluoto S, Vervliet T, Ivanova H, Decuypere JP, De SH, Missiaen L, Bultynck G, Parys JB: Regulation of inositol 1,4,5-trisphosphate receptors during endoplasmic reticulum stress. Biochim Biophys Acta 2013;1833:1612-1624.

57 Marchi S, Patergnani S, Missiroli S, Morciano G, Rimessi A, Wieckowski MR, Giorgi C, Pinton P: Mitochondrial and endoplasmic reticulum calcium homeostasis and cell death. Cell Calcium 2017.

58 Roy SS, Hajnoczky G: Calcium, mitochondria and apoptosis studied by fluorescence measurements. Methods 2008;46:213-223.

59 Boelens J, Lust S, Offner F, Bracke ME, Vanhoecke BW: Review. The endoplasmic reticulum: a target for new anticancer drugs. In Vivo 2007;21:215-226.

60 Kim H, Bhattacharya A, Qi L: Endoplasmic reticulum quality control in cancer: Friend or foe. Semin Cancer Biol 2015;33:25-33.

61 Castellone RD, Leffler NR, Dong L, Yang LV: Inhibition of tumor cell migration and metastasis by the proton-sensing GPR4 receptor. Cancer Lett 2011;312:197-208.

62 Matsueda R, Higashida S, Albericio F, Andreu D: Compatibility of the S-(3-nitro-2-pyridinesulfenyl) protecting group with DCC/HOBt coupling chemistry. Pept Res 1992;5:262-264.

63 Balalaie S, Mahdidoust M, Eshaghi-Najafabadi R: 2-(1H-Benzotriazole-1-yl)-1,1,3,3-tetramethyluronium Tetrafluoroborate as an
Efficient Coupling Reagent for the Amidation and Phenylhydrazation of Carboxylic
Acids at Room Temperature; Journal of the Iranian Chemical Society, 7 A.D., pp 364-369.

64 Delhaye L, Ceccato A, jacobs P, Kottgen C, Michalik L: Removal of Reaction Solvent by Extractive Workup:? Survey of Water and Solvent Co-extraction in Various Systems; American Chemical Society, 2007, pp 160-164.

65 Guy GP, Jr., Machlin SR, Ekwueme DU, Yabroff KR: Prevalence and costs of skin cancer treatment in the U.S., 2002-2006 and 2007-2011. Am J Prev Med 2015;48:183-187.

66 Martinez-Martinez E, Gomez I, Martin P, Sanchez A, Roman L, Tejerina E, Bonilla F, Merino AG, de Herreros AG, Provencio M, Garcia JM: Cannabinoids receptor type 2, CB2,

expression correlates with human colon cancer progression and predicts patient survival. Oncoscience 2015;2:131-141.

67 Velasco G, Sanchez C, Guzman M: Endocannabinoids and Cancer. Handb Exp Pharmacol 2015;231:449-472.

68 Sailler S, Schmitz K, Jager E, Ferreiros N, Wicker S, Zschiebsch K, Pickert G, Geisslinger G, Walter C, Tegeder I, Lotsch J: Regulation of circulating endocannabinoids associated with cancer and metastases in mice and humans. Oncoscience 2014;1:272-282.

69 Orellana-Serradell O, Poblete CE, Sanchez C, Castellon EA, Gallegos I, Huidobro C, Llanos MN, Contreras HR: Proapoptotic effect of endocannabinoids in prostate cancer cells. Oncol Rep 2015;33:1599-1608.

70 Picardi P, Ciaglia E, Proto M, Pisanti S: Anandamide inhibits breast tumor-induced angiogenesis. Transl Med UniSa 2014;10:8-12.

71 Adinolfi B, Romanini A, Vanni A, Martinotti E, Chicca A, Fogli S, Nieri P: Anticancer activity of anandamide in human cutaneous melanoma cells. Eur J Pharmacol 2013;718:154-159.

72 Laezza C, d'Alessandro A, Malfitano AM, Bifulco M: Anandamide inhibits the Wnt/beta-catenin signalling pathway in human breast cancer MDA MB 231 cells. Eur J Cancer 2013;49:2066-2067.

73 Soliman E, Van DR: Anandamide-induced endoplasmic reticulum stress and apoptosis are mediated by oxidative stress in non-melanoma skin cancer: Receptor-independent endocannabinoid signaling. Mol Carcinog 2015.

74 Kingsley PJ, Marnett LJ: Analysis of endocannabinoids, their congeners and COX-2 metabolites. J Chromatogr B Analyt Technol Biomed Life Sci 2009;877:2746-2754.

75 Kuc C, Jenkins A, Van Dross RT: Arachidonoyl ethanolamide (AEA)-induced apoptosis is mediated by J-series prostaglandins and is enhanced by fatty acid amide hydrolase (FAAH) blockade. Mol Carcinog 2012;51:139-149.

76 Wang JJ, Mak OT: Induction of apoptosis by 15d-PGJ2 via ROS formation: an alternative pathway without PPARgamma activation in non-small cell lung carcinoma A549 cells. Prostaglandins Other Lipid Mediat 2011;94:104-111.

77 Shin SW, Seo CY, Han H, Han JY, Jeong JS, Kwak JY, Park JI: 15d-PGJ2 induces apoptosis by reactive oxygen species-mediated inactivation of Akt in leukemia and colorectal cancer cells and shows in vivo antitumor activity. Clin Cancer Res 2009;15:5414-5425.

78 Prakash J, Bansal R, Post E, de Jager-Krikken A, Lub-de Hooge MN, Poelstra K: Albumin-binding and tumor vasculature determine the antitumor effect of 15-deoxy-Delta-(12,14)-prostaglandin-J(2) in vivo. Neoplasia 2009;11:1348-1358.

79 Huang L, Ramirez JC, Frampton GA, Golden LE, Quinn MA, Pae HY, Horvat D, Liang LJ, DeMorrow S: Anandamide exerts its antiproliferative actions on cholangiocarcinoma by activation of the GPR55 receptor. Lab Invest 2011;91:1007-1017.

80 DeMorrow S, Francis H, Gaudio E, Venter J, Franchitto A, Kopriva S, Onori P, Mancinelli R, Frampton G, Coufal M, Mitchell B, Vaculin B, Alpini G: The endocannabinoid anandamide inhibits cholangiocarcinoma growth via activation of the noncanonical Wnt signaling pathway. Am J Physiol Gastrointest Liver Physiol 2008;295:G1150-G1158.

81 Bifulco M, Laezza C, Portella G, Vitale M, Orlando P, De PL, Di M, V: Control by the endogenous cannabinoid system of ras oncogene-dependent tumor growth. FASEB J 2001;15:2745-2747.

82 Kozak KR, Crews BC, Ray JL, Tai HH, Morrow JD, Marnett LJ: Metabolism of prostaglandin glycerol esters and prostaglandin ethanolamides in vitro and in vivo. J Biol Chem 2001;276:36993-36998.

83 Liang Y, Woodward DF, Guzman VM, Li C, Scott DF, Wang JW, Wheeler LA, Garst ME, Landsverk K, Sachs G, Krauss AH, Cornell C, Martos J, Pettit S, Fliri H: Identification and pharmacological characterization of the prostaglandin FP receptor and FP receptor variant complexes. Br J Pharmacol 2008;154:1079-1093.

84 Shelnut EL, Nikas SP, Finnegan DF, Chiang N, Serhan CN, Makriyannis A: Design and synthesis of novel prostaglandin E2 ethanolamide and glycerol ester probes for the putative prostamide receptor(s). Tetrahedron Lett 2015;56:1411-1415.

85 Nicolaou KC, Pulukuri KK, Rigol S, Heretsch P, Yu R, Grove CI, Hale CR, ElMarrouni A, Fetz V, Bronstrup M, Aujay M, Sandoval J, Gavrilyuk J: Synthesis and Biological Investigation of Delta(12)-Prostaglandin J3 (Delta(12)-PGJ3) Analogues and Related Compounds. J Am Chem Soc 2016;138:6550-6560.

86 Harris SG, Phipps RP: Prostaglandin D(2), its metabolite 15-d-PGJ(2), and peroxisome proliferator activated receptor-gamma agonists induce apoptosis in transformed, but not normal, human T lineage cells. Immunology 2002;105:23-34.

87 Haskew-Layton RE, Payappilly JB, Xu H, Bennett SA, Ratan RR: 15-Deoxy-Delta12,14-prostaglandin J2 (15d-PGJ2) protects neurons from oxidative death via an Nrf2 astrocyte-specific mechanism independent of PPARgamma. J Neurochem 2013;124:536-547.

88 Soliman E, Van DR: Anandamide-induced endoplasmic reticulum stress and apoptosis are mediated by oxidative stress in non-melanoma skin cancer: Receptor-independent endocannabinoid signaling. Mol Carcinog 2015.

89 Bommiasamy H, Popko B: Animal models in the study of the unfolded protein response. Methods Enzymol 2011;491:91-109.

90 Liu N, Scofield VL, Qiang W, Yan M, Kuang X, Wong PK: Interaction between endoplasmic reticulum stress and caspase 8 activation in retrovirus MoMuLV-ts1-infected astrocytes. Virology 2006;348:398-405.

91 Fujimoto M, Hayashi T: New insights into the role of mitochondria-associated endoplasmic reticulum membrane. Int Rev Cell Mol Biol 2011;292:73-117.

92 Betz C, Stracka D, Prescianotto-Baschong C, Frieden M, Demaurex N, Hall MN: Feature Article: mTOR complex 2-Akt signaling at mitochondria-associated endoplasmic reticulum membranes (MAM) regulates mitochondrial physiology. Proc Natl Acad Sci U S A 2013;110:12526-12534.

93 Hayashi T, Su TP: Sigma-1 receptor chaperones at the ER-mitochondrion interface regulate Ca(2+) signaling and cell survival. Cell 2007;131:596-610.

94 Breckenridge DG, Stojanovic M, Marcellus RC, Shore GC: Caspase cleavage product of BAP31 induces mitochondrial fission through endoplasmic reticulum calcium signals, enhancing cytochrome c release to the cytosol. J Cell Biol 2003;160:1115-1127.

95 Chaudhari N, Talwar P, Parimisetty A, Lefebvre dC, Ravanan P: A molecular web: endoplasmic reticulum stress, inflammation, and oxidative stress. Front Cell Neurosci 2014;8:213.

96 Zito E: ERO1: A protein disulfide oxidase and H2O2 producer. Free Radic Biol Med 2015;83:299-304.

97 Tu BP, Weissman JS: Oxidative protein folding in eukaryotes: mechanisms and consequences. J Cell Biol 2004;164:341-346.

98 Zeeshan HM, Lee GH, Kim HR, Chae HJ: Endoplasmic Reticulum Stress and Associated ROS. Int J Mol Sci 2016;17:327.

99 Hsieh YH, Su IJ, Lei HY, Lai MD, Chang WW, Huang W: Differential endoplasmic reticulum stress signaling pathways mediated by iNOS. Biochem Biophys Res Commun 2007;359:643-648.

100 Feissner RF, Skalska J, Gaum WE, Sheu SS: Crosstalk signaling between mitochondrial Ca2+ and ROS. Front Biosci (Landmark Ed) 2009;14:1197-1218.

101 Shibata T: 15-Deoxy-Delta(1)(2),(1)(4)-prostaglandin J(2) as an electrophilic mediator. Biosci Biotechnol Biochem 2015;79:1044-1049.

102 Healy SJ, Gorman AM, Mousavi-Shafaei P, Gupta S, Samali A: Targeting the endoplasmic reticulum-stress response as an anticancer strategy. Eur J Pharmacol 2009;625:234-246.

103 Boyce M, Bryant KF, Jousse C, Long K, Harding HP, Scheuner D, Kaufman RJ, Ma D, Coen DM, Ron D, Yuan J: A selective inhibitor of eIF2alpha dephosphorylation protects cells from ER stress. Science 2005;307:935-939.

104 de Almeida SF, Picarote G, Fleming JV, Carmo-Fonseca M, Azevedo JE, de SM: Chemical chaperones reduce endoplasmic reticulum stress and prevent mutant HFE aggregate formation. J Biol Chem 2007;282:27905-27912.

105 Axten JM, Medina JR, Feng Y, Shu A, Romeril SP, Grant SW, Li WH, Heerding DA, Minthorn E, Mencken T, Atkins C, Liu Q, Rabindran S, Kumar R, Hong X, Goetz A, Stanley T, Taylor JD, Sigethy SD, Tomberlin GH, Hassell AM, Kahler KM, Shewchuk LM, Gampe RT: Discovery of 7-methyl-5-(1-{[3-(trifluoromethyl)phenyl]acetyl}-2,3-dihydro-1H-indol-5-yl)-7H-pyrrolo[2,3-d]pyrimidin-4-amine (GSK2606414), a potent and selective first-in-class inhibitor of protein kinase R (PKR)-like endoplasmic reticulum kinase (PERK). J Med Chem 2012;55:7193-7207.

106 Schuligoi R, Sturm E, Luschnig P, Konya V, Philipose S, Sedej M, Waldhoer M, Peskar BA, Heinemann A: CRTH2 and D-type prostanoid receptor antagonists as novel therapeutic agents for inflammatory diseases. Pharmacology 2010;85:372-382.

107 Crider JY, Griffin BW, Sharif NA: Prostaglandin DP receptors positively coupled to adenylyl cyclase in embryonic bovine tracheal (EBTr) cells: pharmacological characterization using agonists and antagonists. Br J Pharmacol 1999;127:204-210.

108 Hata AN, Zent R, Breyer MD, Breyer RM: Expression and molecular pharmacology of the mouse CRTH2 receptor. J Pharmacol Exp Ther 2003;306:463-470.

109 Kihara S, Ouchi N, Funahashi T, Shinohara E, Tamura R, Yamashita S, Matsuzawa Y: Troglitazone enhances glucose uptake and inhibits mitogen-activated protein kinase in human aortic smooth muscle cells. Atherosclerosis 1998;136:163-168.

110 Ristow M, Muller-Wieland D, Pfeiffer A, Krone W, Kahn CR: Obesity associated with a mutation in a genetic regulator of adipocyte differentiation. N Engl J Med 1998;339:953-959.

111 Kubota T, Koshizuka K, Williamson EA, Asou H, Said JW, Holden S, Miyoshi I, Koeffler HP: Ligand for peroxisome proliferator-activated receptor gamma (troglitazone) has potent antitumor effect against human prostate cancer both in vitro and in vivo. Cancer Res 1998;58:3344-3352.

112 Leesnitzer LM, Parks DJ, Bledsoe RK, Cobb JE, Collins JL, Consler TG, Davis RG, Hull-Ryde EA, Lenhard JM, Patel L, Plunket KD, Shenk JL, Stimmel JB, Therapontos C, Willson TM, Blanchard SG: Functional consequences of cysteine modification in the ligand binding sites of peroxisome proliferator activated receptors by GW9662. Biochemistry 2002;41:6640-6650.

113 Pinton P, Giorgi C, Siviero R, Zecchini E, Rizzuto R: Calcium and apoptosis: ER-mitochondria Ca2+ transfer in the control of apoptosis. Oncogene 2008;27:6407-6418.

114 Liang SH, Zhang W, McGrath BC, Zhang P, Cavener DR: PERK (eIF2alpha kinase) is required to activate the stress-activated MAPKs and induce the expression of immediate-early genes upon disruption of ER calcium homoeostasis. Biochem J 2006;393:201-209.

115 Luciani DS, Gwiazda KS, Yang TL, Kalynyak TB, Bychkivska Y, Frey MH, Jeffrey KD, Sampaio AV, Underhill TM, Johnson JD: Roles of IP3R and RyR Ca2+ channels in endoplasmic reticulum stress and beta-cell death. Diabetes 2009;58:422-432.

116 Conti M: Cyclopentenone: a special moiety for anticancer drug design. Anticancer Drugs 2006;17:1017-1022.

117 Brown-Endres L, Schoenfeld D, Tian F, Kim HG, Namba T, Munoz-Fontela C, Mandinova A, Aaronson SA, Lee SW: Expression of the p53 target CDIP correlates with sensitivity to TNFalpha-induced apoptosis in cancer cells. Cancer Res 2012;72:2373-2382.

118 Hitomi J, Katayama T, Eguchi Y, Kudo T, Taniguchi M, Koyama Y, Manabe T, Yamagishi S, Bando Y, Imaizumi K, Tsujimoto Y, Tohyama M: Involvement of caspase-4 in endoplasmic reticulum stress-induced apoptosis and Abeta-induced cell death. J Cell Biol 2004;165:347-356.

119 Kar R, Singha PK, Venkatachalam MA, Saikumar P: A novel role for MAP1 LC3 in nonautophagic cytoplasmic vacuolation death of cancer cells. Oncogene 2009;28:2556-2568.

120 Krysko DV, Garg AD, Kaczmarek A, Krysko O, Agostinis P, Vandenabeele P: Immunogenic cell death and DAMPs in cancer therapy. Nat Rev Cancer 2012;12:860-875.

121 Cho WH, Choi CH, Park JY, Kang SK, Kim YK: 15-deoxy-(Delta12,14)-prostaglandin J2 (15d-PGJ2) induces cell death through caspase-independent mechanism in A172 human glioma cells. Neurochem Res 2006;31:1247-1254.

122 Gorlach A, Bertram K, Hudecova S, Krizanova O: Calcium and ROS: A mutual interplay. Redox Biol 2015;6:260-271.

123 Soliman E, Van DR: Anandamide-induced endoplasmic reticulum stress and apoptosis are mediated by oxidative stress in non-melanoma skin cancer: Receptor-independent endocannabinoid signaling. Mol Carcinog 2016;55:1807-1821.

124 Ray DM, Akbiyik F, Phipps RP: The peroxisome proliferator-activated receptor gamma (PPARgamma) ligands 15-deoxy-Delta12,14-prostaglandin J2 and ciglitazone induce human B lymphocyte and B cell lymphoma apoptosis by PPARgamma-independent mechanisms. J Immunol 2006;177:5068-5076.

125 Yamamoto Y, Koma H, Hiramatsu H, Abe M, Murakami K, Ohya A, Yagami T: Treatment of etoposide combined with 15-deoxy-Delta12,14-prostaglandin J2 exerted synergistic antitumor effects against renal cell carcinoma via peroxisome proliferator-activated receptor-gamma-independent pathways. Mol Clin Oncol 2014;2:292-296.

126 Malki S, Bibeau F, Notarnicola C, Roques S, Berta P, Poulat F, Boizet-Bonhoure B: Expression and biological role of the prostaglandin D synthase/SOX9 pathway in human ovarian cancer cells. Cancer Lett 2007;255:182-193.

127 Gustafsson A, Hansson E, Kressner U, Nordgren S, Andersson M, Lonnroth C, Lundholm K: Prostanoid receptor expression in colorectal cancer related to tumor stage, differentiation and progression. Acta Oncol 2007;46:1107-1112.

128 Hawcroft G, Gardner SH, Hull MA: Expression of prostaglandin D2 receptors DP1 and DP2 by human colorectal cancer cells. Cancer Lett 2004;210:81-84.

129 Murata T, Lin MI, Aritake K, Matsumoto S, Narumiya S, Ozaki H, Urade Y, Hori M, Sessa WC: Role of prostaglandin D2 receptor DP as a suppressor of tumor hyperpermeability and angiogenesis in vivo. Proc Natl Acad Sci U S A 2008;105:20009-20014.

130 Su RY, Chi KH, Huang DY, Tai MH, Lin WW: 15-deoxy-Delta12,14-prostaglandin J2 up-regulates death receptor 5 gene expression in HCT116 cells: involvement of reactive oxygen species and C/EBP homologous transcription factor gene transcription. Mol Cancer Ther 2008;7:3429-3440.

131 Zanotto-Filho A, Masamsetti VP, Loranc E, Tonapi SS, Gorthi A, Bernard X, Goncalves RM, Moreira JC, Chen Y, Bishop AJ: Alkylating Agent-Induced NRF2 Blocks Endoplasmic Reticulum Stress-Mediated Apoptosis via Control of Glutathione Pools and Protein Thiol Homeostasis. Mol Cancer Ther 2016;15:3000-3014.

132 Takahashi S, Odani N, Tomokiyo K, Furuta K, Suzuki M, Ichikawa A, Negishi M: Localization of a cyclopentenone prostaglandin to the endoplasmic reticulum and induction of BiP mRNA. Biochem J 1998;335 (Pt 1):35-42.

133 Movsesyan VA, Stoica BA, Yakovlev AG, Knoblach SM, Lea PM, Cernak I, Vink R, Faden AI: Anandamide-induced cell death in primary neuronal cultures: role of calpain and caspase pathways. Cell Death Differ 2004;11:1121-1132.

East Carolina University

.imal Care and
use Commitee
212 Ed Warren Life
Sciences Building
East Carolina University
Greenville, NC 27834

252-744-2436 office
252-744-2355 fax

February 24, 2014

Rukiyah Van Dross, Ph.D.
Department of Pharmacology
Brody 6S-10
ECU Brody School of Medicine

Dear Dr. Van Dross:

Your Animal Use Protocol entitled, "Examination of the Chemotherapeutic Potential of AEA and 15dPGJ2-EA" (AUP #W239) was reviewed by this institution's Animal Care and Use Committee on 2/24/14. The following action was taken by the Committee:

"Approved as submitted"

Please contact Dale Aycock at 744-2997 prior to hazard use

A copy is enclosed for your laboratory files. Please be reminded that all animal procedures must be conducted as described in the approved Animal Use Protocol. Modifications of these procedures cannot be performed without prior approval of the ACUC. The Animal Welfare Act and Public Health Service Guidelines require the ACUC to suspend activities not in accordance with approved procedures and report such activities to the responsible University Official (Vice Chancellor for Health Sciences or Vice Chancellor for Academic Affairs) and appropriate federal Agencies. **Please ensure that all personnel associated with this protocol have access to this approved copy of the AUP and are familiar with its contents.**

Sincerely yours,

Susan McRae, Ph.D.
Chair, Animal Care and Use Committee

SM/jd

Enclosure

EAST CAROLINA UNIVERSITY
University & Medical Center Institutional Review Board Office
4N-70 Brody Medical Sciences Building· Mail Stop 682
600 Moye Boulevard · Greenville, NC 27834
Office **252-744-2914** · Fax **252-744-2284** · **www.ecu.edu/irb**

Notification of Approval

From: Biomedical IRB

To: Daniel Ladin

CC: Rukiyah Van Dross

Date: 2/7/2017

Re: Ame1_UMCIRB 16-001098
UMCIRB 16-001098
The Chemotherapeutic potential of 15d-PMJ2 on Patient Primary Skin Tumor Cells

Your Amendment has been reviewed and approved using expedited review for the period of 2/4/2017 to 8/22/2017. It was the determination of the UMCIRB Chairperson (or designee) that this revision does not impact the overall risk/benefit ratio of the study and is appropriate for the population and procedures proposed.

Please note that any further changes to this approved research may not be initiated without UMCIRB review except when necessary to eliminate an apparent immediate hazard to the participant. All unanticipated problems involving risks to participants and others must be promptly reported to the UMCIRB. A continuing or final review must be submitted to the UMCIRB prior to the date of study expiration.The investigator must adhere to all reporting requirements for this study.

Approved consent documents with the IRB approval date stamped on the document should be used to consent participants (consent documents with the IRB approval date stamp are found under the Documents tab in the study workspace).

The approval includes the following items:

Description

Changes to Study Team/Personnel

The Chairperson (or designee) does not have a potential for conflict of interest on this study.

IRB00000705 East Carolina U IRB #1 (Biomedical) IORG0000418
IRB00003781 East Carolina U IRB #2 (Behavioral/SS) IORG0000418